CHAPTER 1

INTRODUCTION

1.1. Coating process

Coating is a covering that is applied to the surface of an object, usually referred to as the **substrate**. The purpose of applying the coating may be decorative, functional, or both. The coating itself may be an all-over coating, completely covering the substrate, or it may only cover parts of the substrate. Functional coating may be applied to change the surface properties of the substrate, such as adhesion, wettability, corrosion resistance, or wear resistance. Coating may be applied as liquid, gases, or solid.

Now a days Coating technology is growing because of its important role in improving, e.g., corrosion resistance, conductivity, and other properties of material in order to decrease costs and increase service life and safety. Thermal spray processes, including flame, arc, plasma, **high velocity oxygen fuel** (HVOF) and cold spraying, are the techniques to produce coatings from powder or wire feedstock by spraying molten, semi-molten or solid particles on the substrate and forming the coating. Acceleration of particles can be done by several ways based on energy used: electrical (arc and plasma spraying), chemical (flame and HVOF spraying), or kinetic (cold spraying) energy.

Coatings are being increasingly used to obtain the required surface and tribological properties in engineering components. Such coatings are often applied using thermal-spray processes such as high velocity oxy-fuel, detonation gun, and plasma spray. In these processes, the coating material is heated to temperatures high enough to induce melting. Consequently, the high heat input to a part being coated accompanying these processes can be detrimental, if the material of the part degrades when subjected to high temperatures.

1.2. Surface engineering in India

In India *Surface Engineering Division* (SED) of CSIR-NAL devotes itself to develop surface modification technologies for aerospace and engineering applications. SED works on import substitution in sensitive and critical areas to provide self-reliance. SED is involved in the development of innovative technologies driven by user industries. SED also under takes research in niche areas such as Nano scale architecture and energy sector. Coating is also a part of Surface Engineering. For example:

Mirror coatings for satellites

Highly polishable mirror coatings have been developed for passive radiative cooler of INSAT class satellites (C2A, 2B, 2E, 3A, Kalpana-I). This reflective coating is required to maintain the IR detector temperature of the *Very High Resolution Radiometer* (VHRR) at 105°K. This work has resulted in huge foreign exchange saving. Nano crystalline Ni coatings have also been developed for EUTELSAT.

Pressure sensitive paint

A stable binary pressure sensitive paint coating (NALPSP) has been developed for surface pressure mapping of wind tunnel models. NALPSP coating has been validated for transonic and supersonic applications.

Wear resistant composite coating Nickel-silicon carbide coating (NALNISIC) for trochoid of Wankel engine for UAV has been developed. The coating has been flight tested successfully in the indigenous 55HP rotary engine of NISHANT. Other potential applications of this coating are rotary and reciprocating engines of light weight aircraft sand auto mobiles.

Anti-corrosion coatings

Eco-friendly conversion coating sand sol-gel coatings have been developed for the corrosion protection of aerospace aluminium alloy AA2024-T3 as a replacement for the hazardous chromate conversion coatings. Oxide conversion layers modified with Mo and V oxyanions have with stood several hours of salt spray test. Sol-gel coatings doped with cerium so have displayed good corrosion protection.

Expertise

- Functional coatings by chemical, electrochemical and plasma assisted processes
- Wear and corrosion resistant coatings for aerospace and engineering sectors
- Highly polishable mirror reflective coatings for satellites
- Pressure sensitive coatings and magnetic sensors for aerospace sector
- Solar selective coatings for energy sector
- Characterization of nanomaterial sand coatings [7].

1.3. Cold spray

Cold spraying is a coating process which enables production of metallic and metallic ceramic coating with dense (very low porosity level) and pure (low oxygen content) structures. Several coating applications such as corrosion resistance and electrical conductivity rely on these properties. Generally, cold spraying is based on higher particle velocities and lower process temperature than other thermal spray process.

Cold gas spraying is a relatively new coating process by which coatings can be produced without significant heating of the sprayed powder. In contrast to the well-known thermal spray processes such as flame, arc, and plasma spraying, in cold spraying there is no melting of particles prior to impact on the substrate. The adhesion of particles in this process is due solely to their kinetic energy upon impact. Experimental investigations show that successful bonding is achieved only above a critical particle velocity, whose value depends on the temperature and the thermo mechanical properties of the sprayed material [1].

Cold-Gas Dynamic Spray or simply Cold Spray is a process of applying coatings by exposing a metallic or dielectric substrate to a high velocity (300 to 1200 m/s) jet of small (1 to 50 μm) particles accelerated by a supersonic jet of compressed gas. This process is based on the selection of the combination of particle temperature, velocity, and size that allows spraying at the lowest temperature possible. In the Cold Spray process, powder particles are accelerated by the supersonic gas jet at a temperature that is always lower than the melting point of the material, resulting in coating formation from particles in the

solid state. As a consequence, the deleterious effects of high-temperature oxidation, evaporation, melting, crystallization, residual stresses, gas release, and other common problems for traditional thermal spray methods are minimized or eliminated.

Cold spraying is an emerging coating process in which in contrast to the well-known thermal spray processes such as flame, arc, and plasma spraying, the powders does not melt before impacting the substrate. This character makes cold spray process commendable for many different coating applications dealing with various materials, not only metals but also polymers, composites, etc. Bonding of the particles in this process occurs due to the high kinetic energy upon impact; therefore, the velocity of the particle plays the most important role in material deposition. During the process, powders are accelerated by injection into a high velocity stream of gas. The high velocity stream is generated through a converging–diverging nozzle. As the process continues, the particles impact the substrate and form bonds with it, resulting in a uniform almost porosity-free coating with high bonding strength [2]. Low temperature also aids in retaining the original powder chemistry and phases in the coating, with changes only due to deformation and cold-working. Bonding of particles in cold gas spraying is presumed to be the result of extensive plastic deformation and related phenomena at the interface [3]. It is to be underlined that the particles remain in the solid state and are relatively cold, so the bulk reaction on impact and the cohesion of the deposited material is accomplished in solid state. Schematic diagram of the cold spray equipment is shown in Fig. 1. As mentioned, it is well-recognized that particle velocity prior to impact is a key parameter in cold spray process [3].

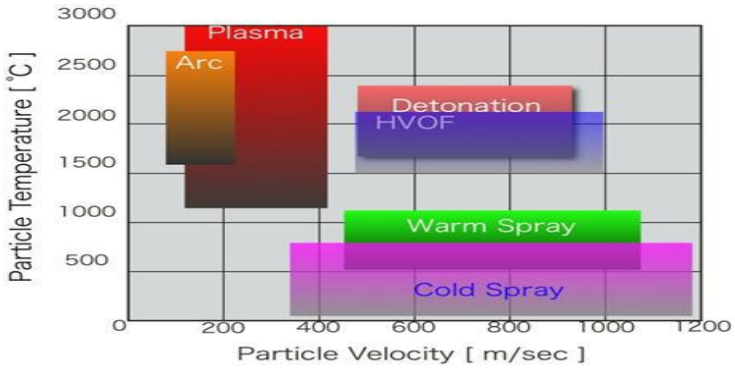

Fig.1. *Gas temperatures versus particle velocities in the thermal/cold spray processes*.

In cold spray process, a coating is deposited through the intensive plastic deformation of solid ductile particles impacting on a substrate at a temperature well below the melting point of spray material. As shown in figure 2, the supersonic jet is generated through a converging-diverging de-Laval nozzle. Spray particles are feed axially from the back of the spray gun. The operating temperature and the pressure of the accelerating gas are monitored by thermocouple and pressure gauge mounted on the spray gun. As a result, phenomena inherent to thermal spray at high temperatures, such as oxidation and phase transformation are avoided in cold spraying [4].

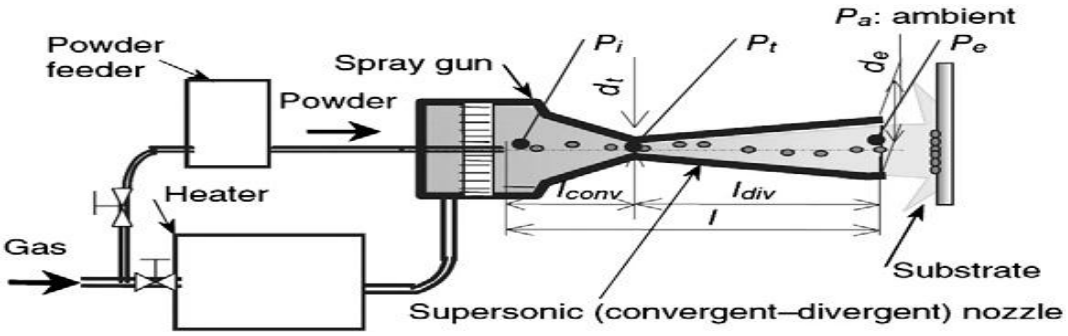

Fig.2. *Schematic view of the cold spray coating machine*

1.4. Advantage

- Avoid oxidation and undesirable phases in coatings.
- Retain properties of initial particle materials.
- Low thermally induced residual stresses.
- High thermal/electrical conductivity of coatings.
- High density, high hardness, cold-worked microstructure of coatings.
- Spray thermally sensitive materials.
- Spray powders with a particle size < 5 –50 μm.
- Work with highly dissimilar materials combinations.
- Minimum substrate surface preparation/masking, short standoff distance.
- High productivity due to high powder feed rate.
- High deposition rates and efficiencies for many materials.
- Collection and reuse of particles (powder utilization up to 100%with recycling).

- Minimal substrate heating.
- Increased operational safety because of the absence of high-temperature gas jets, radiation, explosive gases.

1.5. Evolution of cold spray

Mid 1980-s: Development of Cold Spray (ITAM of RAS, Russia)

***1994-199*5:** The first demonstration in the USA (Dr. Papyrin, National Center for Manufacturing Science)

2000–2002: R & D work on improvement and optimization of the process in framework of consortium (Sandia, Ford, Pratt & Whitney, Ktech, ASB Industries, Siemens, Praxair, and Alcoa)

2006: More than 30 companies around the world are involved in Cold Spray activity (Russia, USA, Germany, France, Belgium, England, Canada, Japan, Brazil, China, South Korea, Australia, and others

2006: More than 200 papers on various aspects of the Cold Spray process have been published

2006-2007: ***Three*** books on ***Cold Spray*** will be published:

a) Cold Spray Technology, by A. Papyrin, V. Kosarev, S. Klinkov, A. Alkhimov, and V. Fomin, Elsevier, 2006

b) Fundamentals of Cold-Gas Dynamics Spray, edited by V. Champagne, D. Helfritch, Wood head Publishing, 2007

c) Introduction to Low Pressure Gas Dynamic Spray, by R. Maev, V. Leshchynsky, WILEY-VCH, 2007

CHAPTER 2

LITERATURE REVIEW

2.1. Summary

Many works have been presented related to the performance of cold spray process. Various conventional methods have been proposed by different research scientists to make the design process of cold spray process more efficient and the product performance better. Below are presented the brief literature reviews of such works:

H. Fukanuma et al. [1]. A two-dimension asymmetrical model was employed in velocity and temperature of gas and particle simulation of a water-cooling and typical adiabatic cold spray gun nozzle. In addition, particle velocity was measured using DPV-2000 system. The flow in the predicted profiles along both particle velocity and temperature match well with the experimental results. Based on the validity of the calculations, the effect of water-cooling process is simulated and it was found that it has no significant diverse effect on particle velocity which is considered to be the most important parameter in particle deposition.

A. Papyinyrin [2]. Cold Spray looks promising for many applications because of its advantages; however, comprehensive R&D work is required to better understand the process and to eliminate its restrictions.

R. Ghelichi [3]. A 3D finite element model is developed in order to calculate the CV in the cold spray coating process. Regarding the mesh convergence, the "zero elements" method has been used to find the element size independent results. The obtained results from the software are converted to Wavelet parameters in order to calculate the second derivative of the physical parameters in Sobolev space.

Hamid Assadi et al. [4]. In this paper work demonstrates that plastic deformation phenomena in cold gas spraying can be modelled appropriately through finite element

analysis. The results of the Modelling provide a basis for understanding the bonding process. Based on these results, the bonding of particles can be attributed to adiabatic shear instabilities which occur at the particle/substrate or particle/particle interfaces at high velocities. The Modelling also shows a very non-uniform development of strain and temperature at the interface, suggesting that this bonding is confined to a fraction of the interacting surfaces. This result is consistent with the relatively low strength of the copper coatings as determined experimentally. The analysis also suggests that density and particle temperature have significant effects on the critical velocity and are thus two of the most influential parameters in cold gas spraying. Overall, the analysis supplies a tool to predict critical velocities and to optimise spray parameters for different materials.

R.C. Dykhuizen et al. [5] this article provides analytical equations that can be used to estimate the gas dynamics of the cold-spray process. Equations are also presented that allow calculation of the particle velocity. It is shown how the spray particle velocity depends on particle size and density, gas stagnation pressure, total gas temperature, gas molecular weight, and nozzle shape. Use of the equations derived in this article allows determination of an optimal nozzle shape given the gas conditions, particle properties, and nozzle length. However, it is shown that the spray particle velocity is relatively insensitive to the nozzle shape. Thus, a single nozzle can be used for a variety of operational conditions.

Xiaoqian Guo et al. [6]. The TiC-Mo composite coating was fabricated by VPS technique successfully, and the microstructures as well as tribological properties of the TiC-Mo were investigated. It is found that the composite coating was mainly composed of TiC (FCC) and Mo (BCC) phases. The protective environment of VPS process efficiently inhibited the formation of titanium oxides.

Sung Hwan Jang et al. [7]. In order to ensure a critical velocity, several nozzle designs based on converging and diverging type was suggested and their fluid flow fields were calculated. It was found that as the diameter of nozzle throat increase from 1.8 mm to 3.9 mm, gas velocity decreased from 982 m/se to 891 m/sec. On the other hand, unlike gas

velocity, particle velocity increased from 585 m/s to 633 m/s. As the nozzle length increases from 66 mm to 199 mm, particle velocities increased from 567.5 to 701.7 m/s by more than 130 m/s, and particle temperature was increased from 341.2 to 365.4 K.

S.V. Klinkov et al. [8]. It can be seen that powder mixture components with similar spraying parameters may be injected in the stream at the same point. Hard-sprayable components should be injected into the subsonic part of the nozzle while easy-sprayable ones may be injected into the supersonic one. As the components mixing takes place in the gas-dynamic channel, the components ratio in the coating may be set by changing the powder feed parameters. Compositionally graded coatings with varying through-thickness concentration of one of the components can be obtained using well controlled powder feeders. Two-component mixtures consisting of hard-sprayable and easysprayable components may be sprayed under the following scheme. The hard-sprayable component is injected into the subsonic part of the nozzle at a gas stagnation temperature favourable for this material to start the coating formation alone. The point of injection of the easysprayable component is determined in such a way that the particles of this material reach in-flight temperature and velocity sufficient for the coating formation at the selected gas stagnation temperature.

Wen Ya Li et al. [9]. Based on the simulation results, it was found that the main factors influencing significantly the particle velocity and temperature include the length and diameter of the barrel section, the nature of the accelerating gas and its operating pressure and temperature, and the particle size when using a CB nozzle. Particles achieve a relatively lower velocity but a higher temperature using the CB nozzle than a CD nozzle under the same gas inlet pressure. The experimental results with a Cu powder using a designed CB nozzle confirmed the feasibility to deposit a thick dense coating under a low gas inlet pressure.

Wen Ya Li et al. [10]. the optimization of nozzle exit diameter is influenced by the gas conditions, particle size, and nozzle divergent section length and throat diameter. The findings indicate that the optimal expansion ratio increases with the increases in gas pressure and nozzle divergent length. It decreases with the increases in gas temperature,

particle size and nozzle throat diameter. The optimal expansion ratio using Helium is less than that using N_2 under the same operating conditions.

2.2. Research gap

While a lot of work has been done in this field of coating processes cold spray, there is very little information in the area of cold spray process. The works of H. Fukanuma *et al.*, A. Papyinyrin *et al.*, Sung-Hwan *et al.*, and Wen-Ya-Li *et al.* [1, 2, 7, 8, 9 and 10] respectively involve analysis of simple models cold spray process. These models involve certain assumptions which may predictions from practical results. Some factors such as consideration of the two dimensional Nozzle Inlet, Nozzle Outlet, nozzle throat, Convergent length, and divergent length, Temperature distribution at outlet of nozzle and Solid Particles and finally Critical Velocity of the Solid particles.

2.3. Objectives of the present work

The objective of the present work is to develop & simulate a simple convergent divergent Nozzle which has different lengths of powder Injector with reference to the papers and my work then will simulate and compare with the existing work.

CHAPTER 3

FLOW MODELS

Introduction

In the flow models there are many flow models under this section. Mainly Turbulent Flows are characterized by fluctuating velocity fields. These fluctuations mix transported quantities such as momentum, energy, and species concentration, and cause the transported quantities to fluctuate as well. Since these fluctuations can be of small scale and high frequency, they are too computationally expensive to simulate directly in practical engineering calculations. Instead, the instantaneous (exact) governing equations can be time-averaged, ensemble-averaged, or otherwise manipulated to remove the small scales, resulting in a modified set of equations that are computationally less expensive to solve. However, the modified equations contain additional unknown variables, and turbulence models are needed to determine these variables in terms of known quantities.
FLUENT provides the following choices of turbulence models [14]:

- Spalart-Allmaras model

- k-ε models
  - ✓ Standard k-ε model
  - ✓ Renormalization-group (RNG) k-ε model
  - ✓ Realizable k- ε model

- k-ε models
  - ✓ Standard k- ε model
  - ✓ Shear-stress transport (SST) k- ε model

- v^2-f model (addon)

- Reynolds stress model (RSM)
  - ✓ Linear pressure-strain RSM model

- ✓ Quadratic pressure-strain RSM model
- ✓ Low-Re stress-omega RSM model

- Detached eddy simulation (DES) model
  - ✓ Spalart-Allmaras RANS model
  - ✓ Realizable k-ε RANS model
  - ✓ SST k-ε RANS model

- Large eddy simulation (LES) model
  - ✓ Smagorinsky-Lilly subgrid-scale model
  - ✓ WALE subgrid-scale model
  - ✓ Kinetic-energy transport subgrid-scale model

➢ In my project problem realizable k-ε model theory is used for simulate the problem by this model.

K-ε Models theory

This section presents the standard, RNG, and realizable k-ε models. All three models have similar forms, with transport equations for k and ε. The major differences in the models are as follows:

- the method of calculating turbulent viscosity
- the turbulent Prandtl numbers governing the turbulent diffusion of k and ε
- the generation and destruction terms in the ε equation

The transport equations, methods of calculating turbulent viscosity, and model constants are presented separately for each model. The features that are essentially common to all models follow, including turbulent production, generation due to buoyancy, accounting for the effects of compressibility, and modeling heat and mass transfer [14].

3.1. Standard k-ε Model

Overview

The simplest "complete models" of turbulence are two-equation models in which the solution of two separate transport equations allows the turbulent velocity and length

scales to be independently determined. The standard k-ε model in FLUENT falls within this class of turbulence model and has become the workhorse of practical engineering flow calculations in the time since it was proposed by Launder and Spalding. Robustness, economy, and reasonable accuracy for a wide range of turbulent flows explain its popularity in industrial flow and heat transfer simulations. It is a semi-empirical model, and the derivation of the model equations relies on phenomenological considerations and empiricism. As the strengths and weaknesses of the standard k- ε model have become known, improvements have been made to the model to improve its performance. Two of these variants are available in FLUENT: the RNG k- ε model and the realizable k- ε model [14].

The standard k- ε model is a semi-empirical model based on model transport equations for ***the turbulence kinetic energy (k)*** and ***its dissipation rate (ε)***. The model transport equation for k is derived from the exact equation, while the model transport equation for ε was obtained using physical reasoning and bears little resemblance to its mathematically exact counterpart. In the derivation of the k- ε model, the assumption is that the flow is fully turbulent, and the effects of molecular viscosity are negligible. The standard k- ε model is therefore valid only for fully turbulent flows [14].

3.2. RNG k-ε Model

Overview

The **RNG** k-ε model was derived using a rigorous statistical technique ***(called Renormalization group theory)*** [14]. It is similar in form to the standard k-ε model, but includes the following refinements:

- ✓ The RNG model has an ***additional term in its ε*** equation that significantly improves the accuracy for rapidly strained flows.
- ✓ The effect of swirl on turbulence is included in the RNG model, enhancing accuracy for swirling flows.
- ✓ The RNG theory provides an analytical formula for turbulent Prandtl numbers, while the standard k-ε model uses user-specified, constant values.

- ✓ While the standard k-ε model is a high-Reynolds-number model, the RNG theory provides an analytically-derived differential formula for effective viscosity that accounts for low-Reynolds-number effects. Effective use of this feature does, however, depend on an appropriate treatment of the near-wall region.

These features make the RNG k-ε model more accurate and reliable for a wider class of flows than the standard k-ε model.

The RNG-based k-ε turbulence model is derived from the instantaneous Navier-Stokes equations, using a mathematical technique called "renormalization group" (RNG) methods.

The analytical derivation results in a model with constants different from those in the standard k-ε model, and additional terms and functions in the transport equations for k and ε.

3.3. Realizable k-ε Model

Overview

The realizable k-ε model is a relatively recent development and differs from the standard k-ε model in two important ways:

- ✓ The realizable k-ε model contains a new formulation for the turbulent viscosity.
- ✓ A new transport equation for the dissipation rate, ε, has been derived from an exact equation for the transport of the mean-square vorticity fluctuation.

The term **"Realizable**" means that the model satisfies certain mathematical constraints on the Reynolds stresses, consistent with the physics of turbulent flows. Neither the standard k-ε model nor the RNG k-ε model is realizable.

An immediate benefit of the realizable k-ε model is that it more accurately predicts the spreading rate of both planar and round jets. It is also likely to provide superior performance for flows involving rotation, boundary layers under strong adverse pressure gradients, separation, and recirculation [14].

To understand the mathematics behind the realizable k-ε model, consider combining the Boussinesq relationship and the eddy viscosity definition to obtain the following expression for the normal Reynolds stress in an incompressible strained mean flow:

$$\overline{u^2} = \frac{2}{3}k - 2v_t\frac{\partial U}{\partial x} \tag{3.7}$$

For $v_t = \frac{\mu}{\rho}$ one obtains the result that the normal stress, $\overline{u^2}$, which by definition is a positive quantity, becomes negative, i.e., "non-realizable", when the strain is large enough to satisfy

$$\frac{k}{3\epsilon}\frac{\partial U}{\partial x} > \frac{1}{3C_\mu} \approx 3.7 \tag{3.8}$$

Both the realizable and RNG k-ε models have shown substantial improvements over the standard k-ε model where the flow features include strong streamline curvature, vortices, and rotation. Since the model is still relatively new, it is not clear in exactly which instances the realizable k-ε model consistently outperforms the RNG model. However, initial studies have shown that the realizable model provides the best performance of all the k-ε model versions for several validations of separated flows and flows with complex secondary flow features [14].

One of the weaknesses of the standard k-ε model or other traditional k-ε models lies with the modeled equation for the dissipation rate (ε). The well-known round-jet anomaly (named based on the finding that the spreading rate in planar jets is predicted reasonably well, but prediction of the spreading rate for axisymmetric jets is unexpectedly poor) is considered to be mainly due to the modeled dissipation equation.

The realizable k-ε model proposed by Shih et al. [15] was intended to address these deficiencies of traditional k-ε models by adopting the following:

- A new eddy-viscosity formula involving a variable C_μ originally proposed by Reynolds [15].
- A new model equation for dissipation (ε) based on the dynamic equation of the mean-square vorticity fluctuation.

One limitation of the realizable k-ε model is that it produces non-physical turbulent viscosities in situations when the computational domain contains both rotating and stationary fluid zones (e.g., multiple reference frames, rotating sliding meshes). This is due to the fact that the realizable k-ε model includes the effects of mean rotation in the definition of the turbulent viscosity. This extra rotation effect has been tested on single rotating reference frame systems and showed superior behavior over the standard k-ε

model. However, due to the nature of this modification, its application to multiple reference frame systems should be taken with some caution.

3.3.1. Transport Equations for the Realizable k-ε Model

The modeled transport equations for k and ε in the realizable k- ε model are:

$$\frac{\partial}{\partial t}(\rho k) + \frac{\partial}{\partial x_j}(\rho k u_j) = \frac{\partial}{\partial x_j}\left[\left(\mu + \frac{\mu_t}{\sigma_k}\right)\frac{\partial k}{\partial x_j}\right] + G_k + G_b - \rho\epsilon - Y_M + S_K \quad (3.9)$$

And

$$\frac{\partial}{\partial t}(\rho\epsilon) + \frac{\partial}{\partial x_j}(\rho\epsilon u_j) = \frac{\partial}{\partial x_j}\left[\left(\mu + \frac{\mu_t}{\sigma_\epsilon}\right)\frac{\partial \epsilon}{\partial x_j}\right] + \rho C_1 S_\epsilon + \rho C_2 \frac{\epsilon^2}{k+\sqrt{\nu\epsilon}} + C_{2\epsilon}\frac{\epsilon}{k} C_{3\epsilon} G_b + S_\epsilon \quad (3.10)$$

Where

$$C_1 = max\left[0.43, \frac{\eta}{\eta+5}\right] \;\; ; \eta = S\frac{k}{\varepsilon} \;\; ; \;\; S = \sqrt{2S_{ij}S_{ij}}$$

In these equations,

G_k- represents the generation of turbulence kinetic energy due to the mean velocity gradients, calculated as Modeling Turbulent Production in the k- ϵ Models.

G_b- is the generation of turbulence kinetic energy due to buoyancy, calculated as Effects of Buoyancy on Turbulence in the k- ϵ Models.

Y_M - represents the contribution of the fluctuating dilatation in compressible turbulence to the overall dissipation rate, calculated as Effects of Compressibility on Turbulence in the k- ϵ Models.

$C_{1\epsilon}$, $C_{2\epsilon}$ and $C_{3\epsilon}$ are constants. α_k and α_ϵ are the inverse effective Prandtl numbers for k and ϵ, respectively. S_K and S_ϵ are user-defined source terms.

Note that the k equation is the same as that in the standard k- ϵ model and the RNG k- ϵ model, except for the model constants [14].

3.3.2. Modeling the Turbulent Viscosity

As in other k- ϵ models, the eddy viscosity is computed from

$$\left[\mu_t = \rho C_\mu \frac{k^2}{\varepsilon}\right] \tag{3.11}$$

The difference between the realizable k- ϵ model and the standard and RNG k- ϵ models is that C_μ is no longer constant. It is computed from

$$\left[C_\mu = \frac{1}{A_0 + A_s \frac{kU^*}{\epsilon}}\right] \tag{3.12}$$

$$U^* = \sqrt{S_{ij}S_{ij} + \widetilde{\Omega_{ij}}\widetilde{\Omega_{ij}}} \tag{3.13}$$

$$\widetilde{\Omega_{ij}} = \Omega_{ij} - 2\epsilon_{ijk}\omega_k \tag{3.14}$$

$$\Omega_{ij} = \overline{\Omega_{ij}} - \epsilon_{ijk}\omega_k \tag{3.15}$$

Where $\overline{\Omega_{ij}}$ is the mean rate of rotation tensor viewed in a rotating reference frame with the angular velocity(ω_k). The model constants and A_s are given by [14]:

$A_0 = 4.04$; $A_s = \sqrt{6}\cos\varphi$

Where

$\varphi = \frac{1}{3}\cos^{-1}(\sqrt{6}\,W)$ and $W = \frac{S_{ij}S_{ij}S_{ij}}{\tilde{S}^3}$

CHAPTER 4

CFD

4.1. Introduction

Computational Fluid dynamics (CFD) is the branch of fluid dynamics providing a cost-effective means of simulating real flows by the numerical solution of the governing equation. Computational fluid dynamics (CFD) is the science of predicting fluid flow, heat transfer, mass transfer, chemical reactions, and related phenomena by solving the mathematical equations which govern these processes using a numerical process [16].

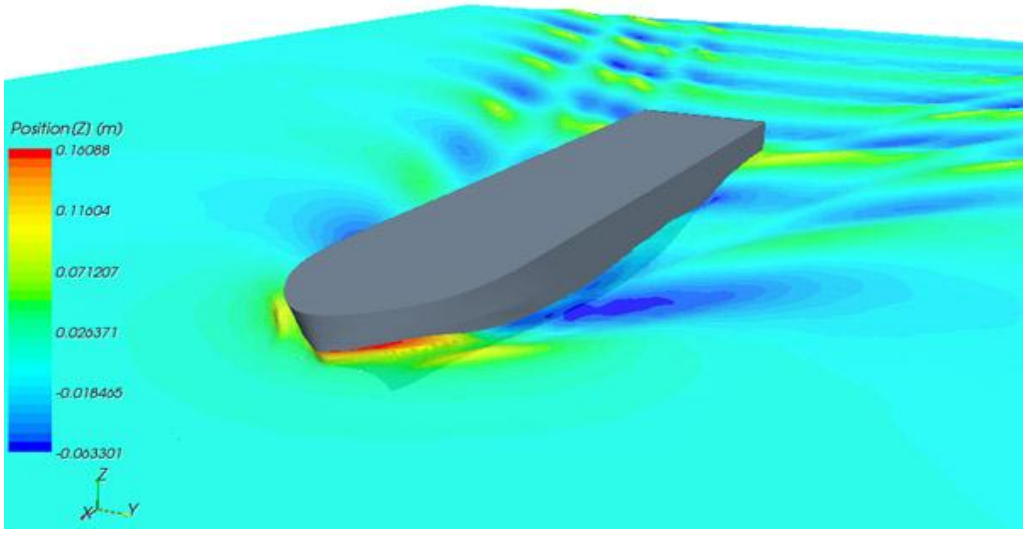

Fig.3. *3D view of ship in CFD*

Computational Fluid Dynamics (CFD) provides a qualitative (and sometimes even quantitative) prediction of fluid flows by means of

- mathematical modeling (partial differential equations)
- numerical methods (discretization and solution techniques)
- software tools (solvers, pre- and post-processing utilities)

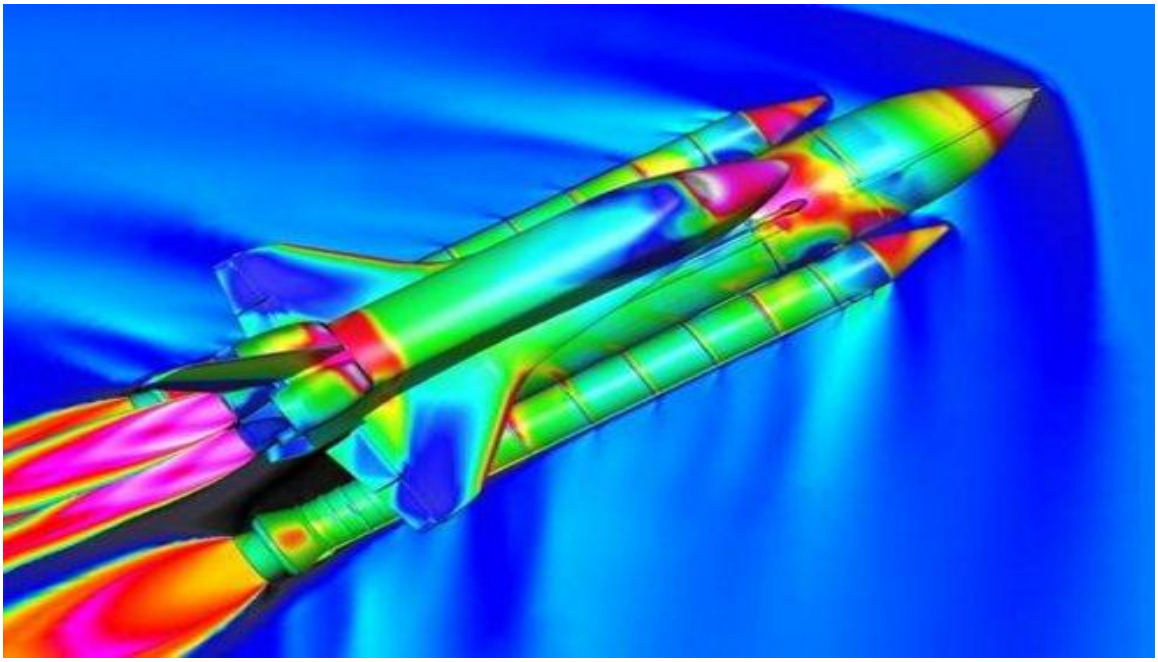

Fig.4. *3D view of Space settles*

4.2. Need of CFD

Numerical simulations of fluid flow (will) enable

- Architects to design comfortable and safe living environments
- Designers of vehicles to improve the aerodynamic characteristics
- Chemical engineers to maximize the yield from their equipment
- Petroleum engineers to devise optimal oil recovery strategies
- Surgeons to cure arterial diseases (computational hemodynamics)
- Meteorologists to forecast the weather and warn of natural disasters
- Safety experts to reduce health risks from radiation and other hazards
- Military organizations to develop weapons and estimate the damage
- CFD practitioners to make big bucks by selling colorful pictures
- Heating, ventilation and air conditioning of buildings, cars etc.
- Combustion in automobile engines and other propulsion systems
- Complex flows in furnaces, heat exchangers, chemical reactors etc.

Applying the fundamental laws of mechanics to a fluid gives the governing equations for a fluid. The conservation of mass equation is

$$\frac{\partial \rho}{\partial t} + \nabla.\left(\rho \vec{V}\right) = 0 \tag{2.1}$$

And the conservation of momentum equation is

$$\rho \frac{\partial \vec{V}}{\partial t} + \rho\left(\vec{V}.\ \nabla\right)\vec{V} = -\nabla p + \rho \vec{g} + \nabla.\tau_{ij} \tag{2.2}$$

These equations along with the conservation of energy equation form a set of coupled, nonlinear partial differential equations. It is not possible to solve these equations analytically for most engineering problems [16].

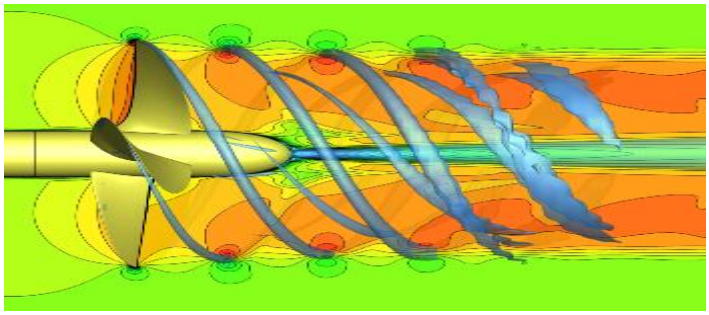

Fig.5. *Contours of Propeller in CFD*

However, it is possible to obtain approximate computer-based solutions to the governing equations for a variety of engineering problems. This is the subject matter of Computational Fluid Dynamics (CFD).

4.2.1. Applications of CFD

CFD is useful in a wide variety of applications and here we note a few to give you an idea of its use in industry. The simulations shown below have been performed using the FLUENT software [17].

CFD can be used to simulate the flow over a vehicle. For instance, it can be used to study the interaction of propellers or rotors with the aircraft fuselage.

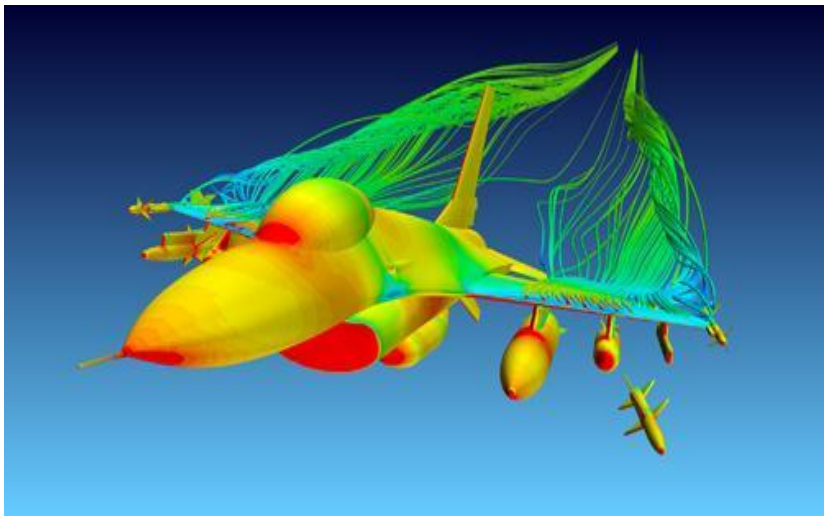

Fig.6. *Air flow over the fighter jet in CFD*

4.2.2. Difference between Experiments and Simulation

Quantitative description of flow phenomena using measurements

- for one quantity at a time
- at a limited number of points and time instants
- for a laboratory-scale model
- for a limited range of problems and operating conditions
- it is expensive, slow, sequential, single-purpose

Error sources: measurement errors; flow disturbances by the probes

Quantitative prediction of flow phenomena using CFD software

- for all desired quantities
- with high resolution in space and time
- for the actual flow domain
- for virtually any problem and realistic operating conditions
- It is cheaper, faster, parallel, and multiple-purpose

Error sources: modeling, discretization, iteration, implementation [17].

4.3. Finite Volume Method

Finite Volume Methods (FVM) many times also called box methods and these are mainly employed for the numerical solution of problems in fluid mechanics, where they were introduced in the 1970s by McDonald, MacCormack, and Paullay. However, the application of the FVM is not limited to flow problems.

An important property of finite volume methods is that the balance principles, which are the basis for the mathematical Modelling of continuum mechanical problems, per definition, also are fulfilled for the discrete equations (conservatively). In this chapter we will discuss the most important basics of finite-volume discretization applied to continuum mechanical problems. For clarity in the presentation of the essential principles we will restrict ourselves mainly to the 2D case [19].

In general, the FVM involves the following steps:

(1) Decomposition of the problem domain into control volumes.

(2) Formulation of integral balance equations for each control volume.

(3) Approximation of integrals by numerical integration.

(4) Approximation of function values and derivatives by interpolation with nodal values.

(5) Assembling and solution of discrete algebraic system.

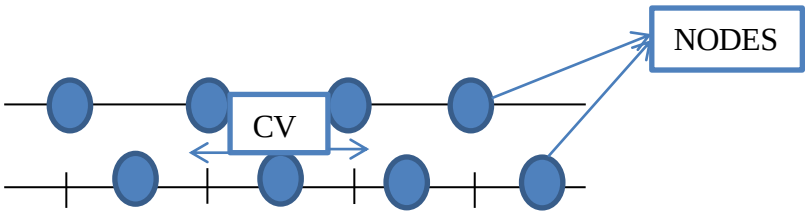

Fig.7. *Definitions of CVs and edge (top) and cell-oriented (bottom) arrangement of nodes for one-dimensional grids*

The starting point for a finite-volume discretization is a decomposition of the problem domain Ω into a finite number of subdomains V_i (i = 1..... N), called ***control volumes***

(CVs), and related nodes where the unknown variables are to be computed. The union of all CVs should cover the whole problem domain. In general, the CVs also may overlap, but since this result in unnecessary complications we consider here the non-overlapping case only. Since finally each CV gives one equation for computing the nodal values, their final number (i.e., after the incorporation of boundary conditions) should be equal to the number of CVs.

In order to keep the usual terminology of the FVM, we always talk of volumes (and their surfaces), although strictly speaking this is only correct for the three-dimensional case.

For one-dimensional problems the CVs are subintervals of the problem interval and the nodes can be the midpoints or the edges of the subintervals (see Fig. 4.3.1).

4.4. Isentropic gas flow model

This section presents the model equations. First, the gas flow model is introduced. It is assumed that the gas flow conditions can be calculated without consideration to feedback from the powder flux. Then the powder flow model is introduced. From the powder flow solution, optimal conditions are identified that yield maximum powder acceleration. Next, equations are introduced that describe the nozzle shape that yields the optimal condition.

Finally, the particle velocity for the optimal nozzle is analytically determined [5].

The spray particle velocity that can be obtained via a cold spray device is limited only by the gas velocity. Use of a high pressure gas flow, long nozzles and small particles result in particles traveling at the gas velocity. The gas velocity can be increased by using low molecular weight gases, high temperatures, and large expansion ratio nozzles. However, practical limits exist for all of the process variables. Thus, it is desirable to produce a sufficient spray particle velocity, with an optimal design, so that the guns can be compact and the gas use minimized.

It is also desirable to avoid using high gas pressures and temperatures. The analytic equations presented in this article allow the design of such a device. The typical cold-spray geometry includes a converging/diverging nozzle, which is shown schematically in Fig. 3. It is assumed that the gas flow is isentropic (adiabatic and frictionless) and one dimensional the one-dimensional analysis ignores the small gas flow boundary layers

along the nozzle walls, where the gas is traveling slower than the mean. Thus, the gas flow rates calculated by the model are slightly higher than those obtained in practice. Also, the one-dimensional assumptions limit the application of the model to regions away from the jet impingement on the substrate.

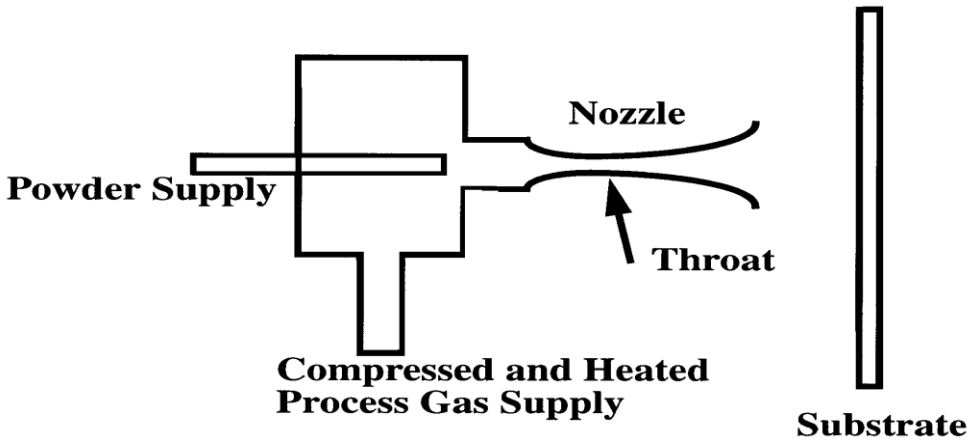

Fig.8. *Typical cold-spray system geometry*

The above assumptions yield gas conditions that are a function of the nozzle geometry, total gas temperature, and stagnation pressure. The flow is accelerated or decelerated by changing flow areas. The total gas temperature and stagnation pressure are those that would be measured at the source of the gas, where it is stagnant. As the gas is accelerated through the nozzle, the temperature and pressure decrease from these values while the velocity increases (although the stagnation values would be reestablished if the gas were isentropically decelerated to zero velocity) [5].

The gas conditions for this type of problem are typically written as a function of the local Mach number (the velocity of the gas divided by the local sound speed). However, the local flow area and the local Mach number can be related. The optimal variation of the local flow area with axial distance (the shape of the nozzle) is one of the outputs that can be obtained from the analysis presented here.

It is interesting to examine briefly the thermal aspects of the cold-spray process. Typically, the total temperature of a cold spray gas is hotter than ambient. This produces improved performance via greater gas velocities. The higher-temperature gas causes the spray particles to heat up as they encounter the gas stream. However, as the gas gains kinetic energy, it cools. If the spray particle does not accelerate quickly, the gas

temperature it experiences will remain constant because the gas has to slow back down to interact with the static particle. However, as the particle approaches the gas velocity, the thermal energy transfer is now with a cool gas and often results in cooling the spray particle [8].

Numerical simulation of this process shows that the particle interacts with the slow warm gas for greater time periods and with higher heat transfer coefficients than with the fast cool gas, so the net effect is a slightly elevated-temperature spray particle upon impact. No further discussion of the thermal aspects of cold spray is provided in this article. However, it is noted here that the particle flux is assumed to be dilute so that any heat transfer between the particles and gas does not violate the adiabatic gas flow assumption.

The process gas flow is assumed to originate from a large chamber or duct where the pressure is equal to the stagnation pressure (*P*o), the temperature is the total temperature (*T*o), and the velocity is zero. For practical purposes, this matches the conditions upstream of the nozzle throat where the flow area is greater than three times the throat area. It is assumed that the total temperature and the mass flow rate (not the stagnation pressure) is set by the user. The mass flow rate is frequently set in thermal spray devices by setting a pressure level upstream of a critical flow orifice in the gas supply line. Note that this pressure is not equal to the stagnation pressure of the flow through the nozzle because of the frictional losses associated with the gas traversing the orifice [5].

The following equation relates the gas temperature at the throat (*T**) to the total gas temperature (note all quantities given with an * is throat or sonic conditions):

$$\frac{T_0}{T^*} = 1 + \frac{\gamma - 1}{2} \qquad (4.3.1)$$

Where γ is the ratio of specific heats. For monatomic gases, γ is 1.66, and for diatomic gases γ is typically 1.4 (Air is typically modeled as a diatomic gas because it is a mixture of nitrogen and oxygen.) Larger molecules have even lower specific heat ratios, but are typically not used in thermal spray applications. Equation (4.3.1) assumes that the throat condition is sonic. Sonic conditions are only obtained for sufficient stagnation gas pressures, but this condition is usually obtained for all thermal spray applications.

At the throat, the Mach number is unity, and the local velocity can be obtained from

$$V^* = \sqrt{\gamma R T^*} \tag{4.3.2}$$

Where R is the specific gas constant (the universal gas constant divided by the gas molecular weight) . Equation 2 illustrates why it is often found that helium makes a better carrier gas due to its smaller molecular weight and higher specific heat ratio.

A mass balance yields the throat density:

$$\rho^* = \frac{\dot{m}}{V^* A^*} \tag{4.3.3}$$

At this point, the throat area (A*) can be set to unity and the mass flow rate $(\dot{m})$ specified as a flux per unit throat area. This allows obtaining a single solution that can then be easily scaled by the throat area if desired.
Using the perfect gas law, the throat pressure P^* is obtained:

$$P^* = \rho^* R T^* \tag{4.3.4}$$

From the throat pressure, the stagnation pressure P_0 can be calculated:

$$\frac{P_0}{P^*} = \left(1 + \frac{\gamma - 1}{2}\right)^{\frac{\gamma}{\gamma - 1}} \tag{4.3.5}$$

If sonic conditions are to be maintained at the throat, the throat pressure must be above the ambient, or spray chamber, pressure. To complete the gas dynamic calculation, a single nozzle exit condition needs to be specified. This could be the exit pressure, exit velocity, exit Mach number, or exit area. The gas exit pressure need not match the ambient pressure. Current cold-spray gun operating conditions have an exit pressure well below ambient to obtain maximum spray particle velocities. Thus, the gas flow is said to be over expanded. This results in a flow outside of the nozzle that cannot be solved by simple one-dimensional gas dynamic equations. However, the one-dimensional results

presented here still apply inside the nozzle as long as the overexpansion is not so great as to cause a normal shock inside the gun. Shocks inside the gun have not been predicted in operational conditions tested at Sandia to this point [5].

It is assumed here that the exit area is specified. The following equation is used to obtain the exit Mach number when the exit area is specified:

$$\frac{A}{A^*} = \left(\frac{1}{M}\right)\left[\left(\frac{2}{\gamma+1}\right)\left(1+\frac{\gamma-1}{2}M^2\right)\right]^{\frac{\gamma+1}{(2\gamma-1)}} \tag{4.3.6}$$

With the exit Mach number known, the other gas conditions can be obtained from the following isentropic relationships:

$$\frac{P}{P^*} = \left[\left(\frac{\gamma+1}{2+(\gamma-1)M^2}\right)\right]^{\frac{\gamma}{(\gamma-1)}} \tag{4.3.7}$$

$$\frac{T_0}{T} = 1+\frac{\gamma-1}{2}M^2 \tag{4.3.8}$$

$$V = \sqrt{\gamma RT} \tag{4.3.9}$$

$$\frac{\rho_0}{\rho} = \left(1+\frac{\gamma-1}{2}M^2\right)^{\frac{\gamma}{(\gamma-1)}} \tag{4.3.10}$$

Because the exit pressure calculated is typically less than ambient, a simple check is required to make sure the given solution is possible. The following calculation yields a trial pressure for the design. *P*s is the downstream shock pressure that would be obtained if a shock occurred at the nozzle exit:

$$\frac{P_s}{P_c} = \left(\frac{2\gamma}{\gamma+1}M_c^2 - \frac{\gamma-1}{\gamma+1}\right) \tag{4.3.11}$$

If this pressure (*P*s) is equal to the ambient pressure, a shock occurs at the nozzle exit. If this pressure is less than the ambient pressure, a shock occurs somewhere inside the

nozzle and subsequent subsonic flow occurs past the shock location so that the exit pressure is equal to the ambient pressure. The normal operating condition for cold-spray nozzles results in the exit pressure being less than the ambient pressure, and *P*s being greater than the ambient pressure. When this is the case, the flow is over expanded and all conditions calculated represent real conditions inside of the nozzle. The gas stream then slows down outside of the nozzle exit as the pressure adjusts to the ambient. This gas deceleration upon exiting is not as significant in cold-spray applications as in other thermal spray processes due to the short standoff distances [5].

Equations (4.3.1) through (4.3.4) and (4.3.6) through (4.3.10) can also be used to simulate plasma or HVOF spray systems by assuming an isentropic expansion from the throat to the exit of a diverging nozzle.

However, the total gas temperature must be obtained through an energy balance. The total gas temperature is greater than the incoming gas temperature due to the energy additions. So, in place of (Eq. 4.3.5) (to calculate the stagnation pressure), another relation must be substituted. Reasonable agreement with experimental data has been obtained using a Rayleigh Line calculation instead of the isentropic assumption. The Rayleigh Line calculation assumes a constant area energy addition [5].

4.5. Discrete phase Modelling

The solid copper particles were treated as discrete phase and air as primary phase. The two ways turbulence coupling is used because there is a strong dependency between the phases presents i.e. copper and air. But this dependency is less than the water and air dependency. The discrete phase copper particle was made to interact with the air, which is the continuous phase. The discrete phase was updated after 10 iterations for the air (continuous phase).The copper particles were treated in unsteady manner. The time step used was 1 second. To take into account the variation of turbulent quantities two way turbulence coupling was used.

To ensure the uniform distribution of copper particles the surface injection was used. The droplet collision and droplet breakup was considered to realize the problem in a practical

way. The discrete phase droplets were injected at a constant mass flux. For modeling of the particle turbulent dispersion stochastic tracking approach was used.

The trajectory of a discrete phase particle is in a Lagrangian reference frame. The different forces on discrete phase can be written (for the *x* direction in Cartesian coordinates) as: [16]

$$\frac{du_p}{dt} = F_D\left(u - u_p\right) + \frac{g_x(\rho_p - \rho)}{\rho_p} + F_x + F_y \qquad (3.4.1)$$

Where, the drag force per unit particle mass is $F_D\left(u - u_p\right)$

And

$$F_D = \frac{18\mu}{\rho_p d_p^2} * \frac{C_D Re}{24} \qquad (3.4.2)$$

Where, u is the fluid phase velocity, $u_p$is the particle velocity, μ is the molecular viscosity of the fluid, ρ is the fluid density, ρ_p is the density of the particle, d_p is the particle diameter and C_D Is discharge coefficient and Re is the Reynolds number.

$$F_x = -D_{T,P}\frac{1}{m_p T}\frac{\partial T}{\partial x} \qquad (3.4.3)$$

Where

$VD_{T,P}$ is thermophoretic coefficient; F_y is Saffman's lift force or lift force due to shear that is applied lift force due to shear that is applied on copper particle Reynolds numbers.

4.6. Flow Solvers

In this respect of FLUENT there are mainly two numerical methods for solve the problem.

- Pressure Based Solver
- Density Based Solver

The pressure-based approach was developed for low-speed incompressible flows, while the density-based approach was mainly used for high-speed compressible flows. However, recently both methods have been extended and reformulated to solve and operate for a wide range of flow conditions beyond their traditional or original intent.

In both methods the velocity field is obtained from the momentum equations. In the density-based approach, the continuity equation is used to obtain the density field while the pressure field is determined from the equation of state [14].

On the other hand, in the pressure-based approach, the pressure field is extracted by solving a pressure or pressure correction equation which is obtained by manipulating continuity and momentum equations.

Using either method, FLUENT will solve the governing integral equations for the conservation of mass and momentum, and (when appropriate) for energy and other scalars such as turbulence and chemical species. In both cases a control-volume-based technique is used that consists of:

- Division of the domain into discrete control volumes using a computational grid.
- Integration of the governing equations on the individual control volumes to construct algebraic equations for the discrete dependent variables (\unknowns") such as velocities, pressure, temperature, and conserved scalars.
- Linearization of the discretized equations and solution of the resultant linear equation system to yield updated values of the dependent variables.

The two numerical methods employ a similar discretization process (finite-volume), but the approach used to linearize and solve the discretized equations is different.

4.5.1. Pressure Based Solver

In this, solver employs an algorithm which belongs to a general class of methods called the projection method. In the projection method, wherein the constraint of mass conservation (continuity) of the velocity field is achieved by solving a pressure (or pressure correction) equation. The pressure equation is derived from the continuity and the momentum equations in such a way that the velocity field, corrected by the pressure, satisfies the continuity. Since the governing equations are nonlinear and coupled to one another, the solution process involves iterations wherein the entire set of governing

equations is solved repeatedly until the solution converges. Two pressure-based solver algorithms are available in FLUENT. A segregated algorithm and a coupled algorithm. These two approaches are discussed in the sections below.

4.5.2. The Pressure-Based Segregated Algorithm

The pressure-based solver uses a solution algorithm where the governing equations are solved sequentially (i.e., segregated from one another). Because the governing equations are non-linear and coupled, the solution loop must be carried out iteratively in order to obtain a converged numerical solution. In the segregated algorithm, the individual governing equations for the solution variables (e.g., u, v, w, p, T, k, etc.) are solved one after another. Each governing equation, while being solved, is "decoupled" or "segregated" from other equations, hence its name.

The segregated algorithm is memory-efficient, since the discretized equations need only be stored in the memory one at a time. However, the solution convergence is relatively slow, inasmuch as the equations are solved in a decoupled manner.

With the segregated algorithm, each iteration consists of the steps illustrated outlined below:

- Update fluid properties (e.g., density, viscosity, specific heat) including turbulent viscosity (diffusivity) based on the current solution.
- Solve the momentum equations, one after another, using the recently updated values of pressure and face mass fluxes.
- Solve the pressure correction equation using the recently obtained velocity field and the mass-flux.
- Correct face mass fluxes, pressure, and the velocity field using the pressure correction obtained from Step 3 in this section.
- Solve the equations for additional scalars, if any, such as turbulent quantities, energy, species, and radiation intensity using the current values of the solution variables.
- Update the source terms arising from the interactions among different phases (e.g., source term for the carrier phase due to discrete particles).
- Check for the convergence of the equations.

CHAPTER 5

SIMULATION STUDIES AND DISCUSSIONS

5. Simulation studies for convergent divergent Nozzle

In this respect for the purpose of numerical integration of the differential equations, k-ε method of is employed. A set of initial values are supplied as input by the user. In the project problem RNG k- ε model for simulating the problem have used because of its inherent advantages.

5.1. Boundary Conditions

The input is boundary conditions which for parallel downward flow are:

a) Nozzle geometry: Inlet, Throat, Outlet, cross section area and Injector of the nozzle.
b) Spray characteristics: Particles velocity, angle of projection, mean diameter of Particles model and diameter range (5-50) μm.
c) Inlet air conditions: Air or Nitrogen velocity, Pressure.
d) Particles Inlet condition: Mass flow rate and its temperature at inlet and Pressure.

5.2. Simulation Procedure

The first step in the approach towards solution procedure is to divide the nozzle Length L, into a number of divisions (div), the numerical integration is carried out in each division to find the variation of the main parameters with length. The main parameters are those parameters that change during the course of the integration seven main parameters are used in this analysis. These parameters are

$\boldsymbol{T_{air,in}}$ – Temperature of inlet, $\boldsymbol{T_{air,outlet}}$ – Temperature of outlet, $\boldsymbol{V_{air,in}}$- velocity of air at inlet, $\boldsymbol{P_{in}}$ - Pressure at inlet of Injector, $\boldsymbol{D_p}$ - Diameter of Particles, $\boldsymbol{V_{p,in}}$ - Inlet Velocity of particles, $\boldsymbol{V_{p,o}}$ - Outlet Velocity of particles.

The lagging parameters on the other hand are assumed to be constant during the individual elements of integration. These parameters include kinematic viscosity, density of air, heat transfer coefficient, Lewis factor etc. The lagging parameters are recalculated using the main parameters at every division. These parameters along with the main parameters serve as a fresh input to the solver for the subsequent interval or division. The above discussion holds good for single as well as multi-diameter droplets model. In multi-diameter droplets model, the different equations of main parameters for different droplets are numerically integrated separately.

5.3. Systematic Plan of Problem

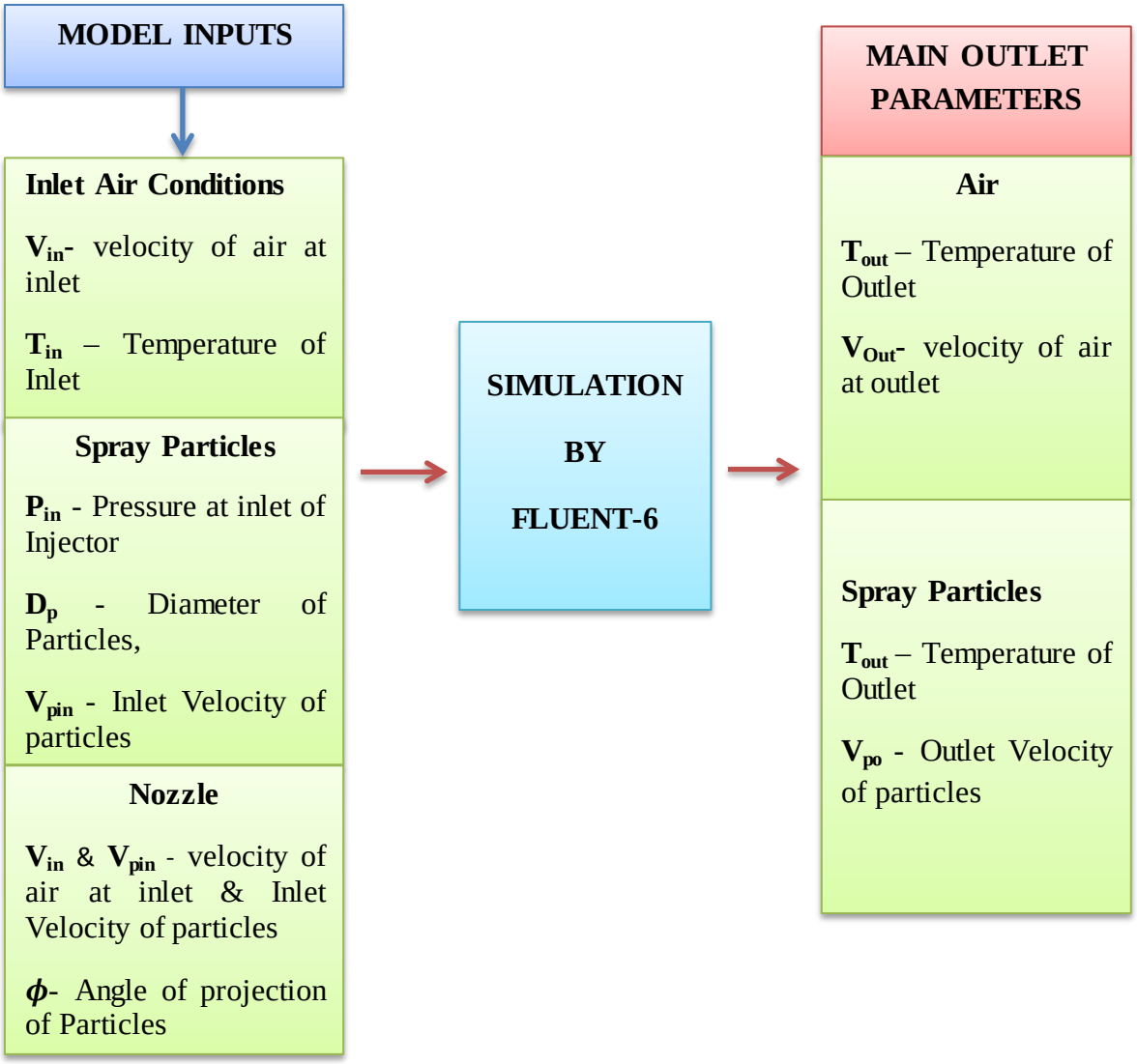

Input Data

Parameters of Copper

TABLE 1

Parameters	Cu	Ni	SS316
Density (kg./m3)	8960	8900	8031
Conductivity (W/km2)	386	90.9	16
Specific Heat (J/KgK)	383	435-446	457
Melting Point (K)	1356	1727	1643
C.V. (m/s)	420	520	470
Poisson ratio	0.34	0.31	0.3
Module of elasticity (GPa)	124	200	193

Resource: R. Ghelichi [3].

Data collected through above table 1 consider the Copper as the Injector Powder for the project because in the FLUENT-6 Copper is more easy to use compare to other materials.

Input Parameters of Nozzle

TABLE 2

Parameters	Cold Spray Machine
Nozzle Mach	1.5-2.6
Working Pressure	1.5, 2.5& 3.0 MPa
Gas Temperature	30-500˚C
Working Gas (Ideal-Gas)	Air
Gas flow Rate	18-20 gm/sec
Particle Diameter (Uniform)	20 μm
Diameter of Throat	2.7 mm
Stand Off Distance	25mm
Inlet Diameter of Nozzle	18.2 & 18 mm
Throat Diameter	2.7 mm
Exit Diameter	8.35 mm
Convergent Length	54 & 48mm
Divergent Length	67.6 & 101 mm
Powder Injector Diameter	2 mm
Powder Injector Length	10,20,25 & 30 mm
Particle Powder	Copper
Intake Particles Velocity	20-30 m/sec
Mass Flow rate	10 gm/sec

Resource: *Sung Hwan Jang et al.*, [7].
Resource: *T.Van steenkiste et al.*, [12].

5.4. Flow Chart of Cold spray Modelling with Discrete phase

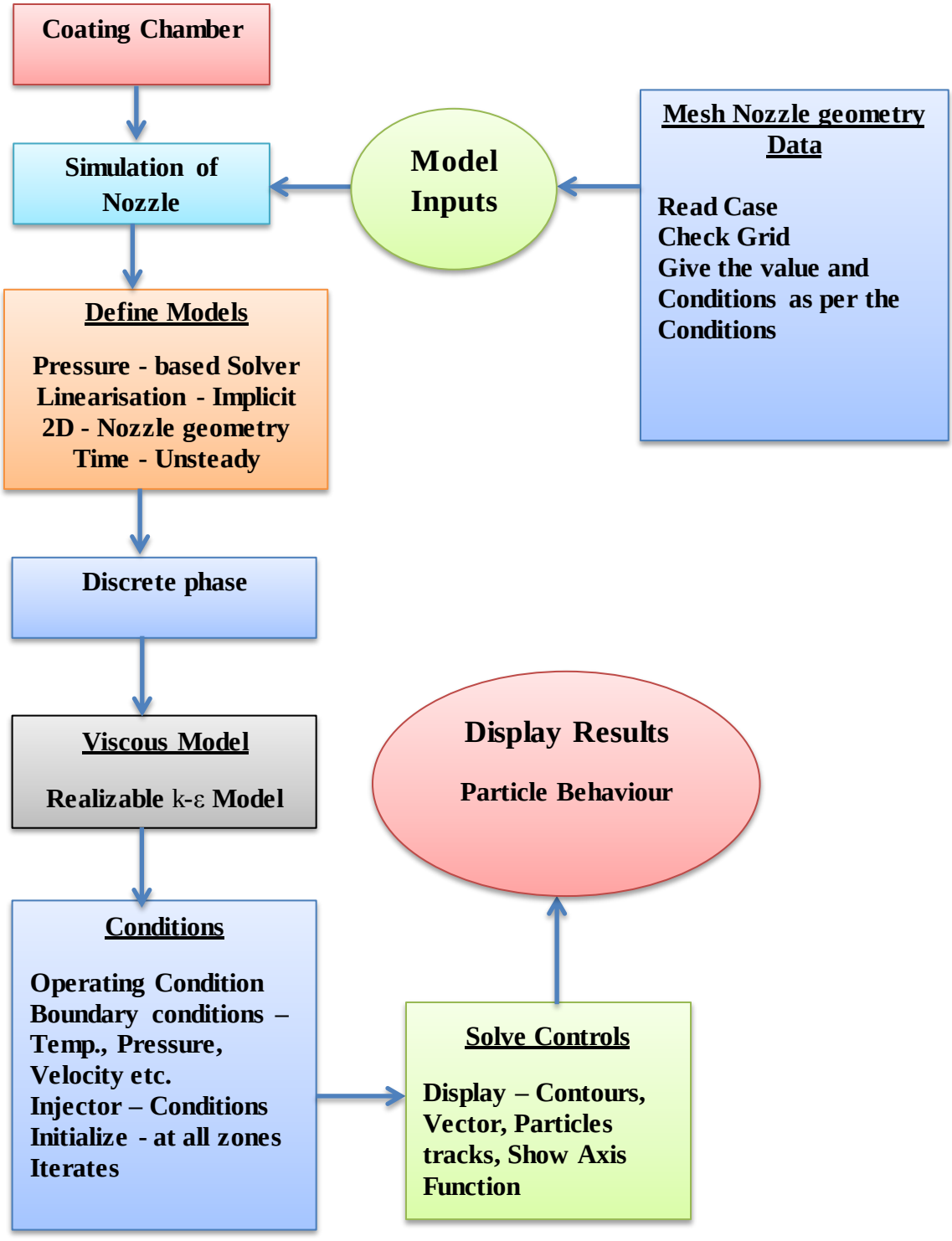

Fig.9. *Flow chart of Simulation process for the project*

5.5. Make Nozzle geometry by GAMBIT

STEP 1: Open the exceed software after that open GAMBIT 2.4.6.

STEP 2: Open the operation geometry command after that opens tool pads that allow me to create and modify model geometry.

STEP 3: After that in the geometry function (vortex command) opens a sub-pad, related to operations involves vertices.

STEP 4: Now by co-ordinate system draw geometry of nozzle by point's co-ordinate.

STEP 5: Now go to the edge command open a sub-pad related to operation involving edges first main geometry of nozzle. *Fig.10*.

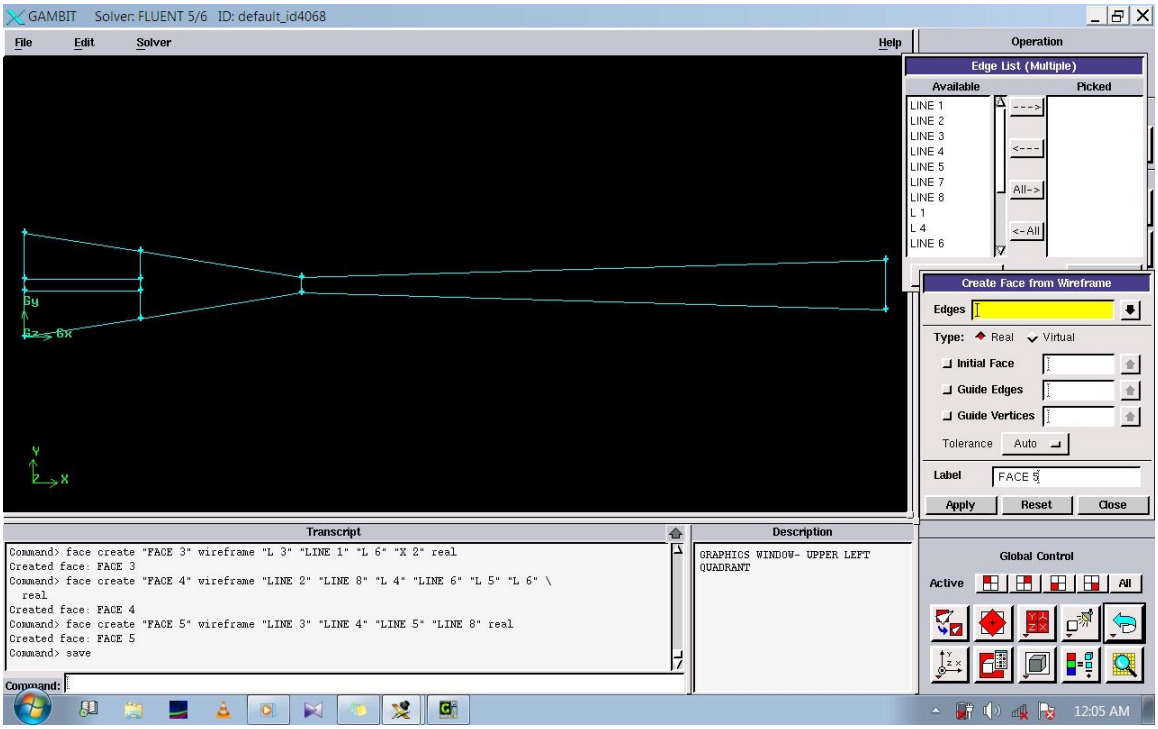

Fig.10. *Show First main nozzle geometry*

STEP 6: Now go face geometry select all edges for make face. Face forms a real or virtual face from existing topological entities.

STEP 7: After that go to on the command of operation-mesh-edge command, open a sub-pad related to operation involving edges. After that generate the mesh with give the spacing according to the need interval count. Fig.11.

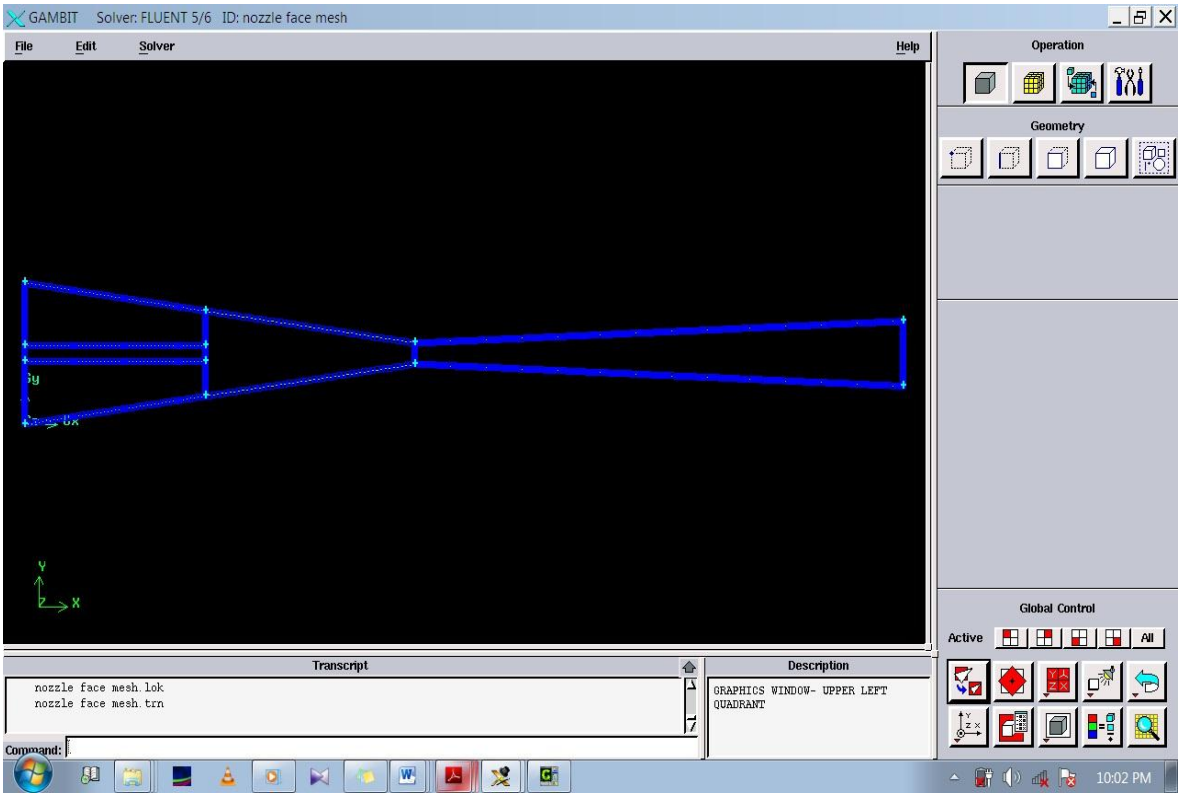

Fig.11. *Show Nozzle with interval count and spacing*

STEP 8: for finalized the nozzle must give the boundary condition like inlet, outlet, wall etc. After that save as the file with some name and finally Export file as (.msh) format to read in FLUENT 6.

5.6. Nozzle with meshing And boundary conditions

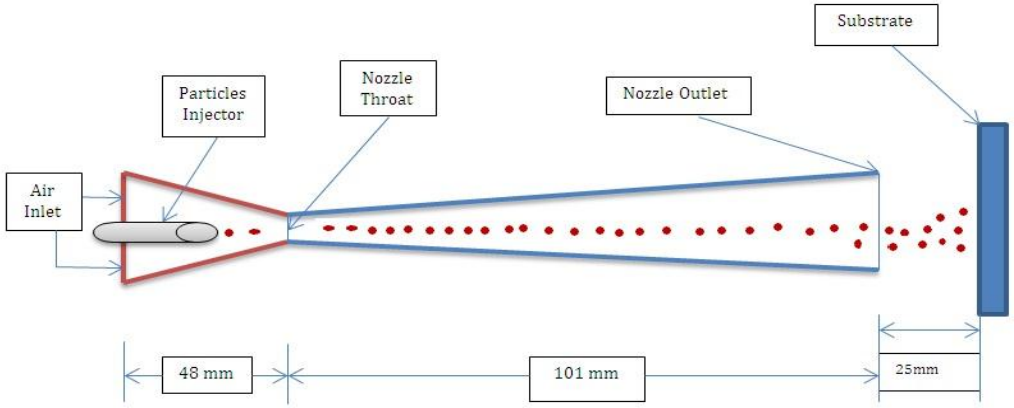

Fig.12a. *Shows main parts of Nozzle*

Fig.12a. Show main parts of the nozzle with dimensions, D_{inlet} = 18 mm; D_{outlet} = 8.35 mm; D_{throat} = 2.7 mm; $L_{conv.}$= 48 mm; $L_{div.}$ = 101 mm, Stand-off Distance = 25 mm, which are always fixed during the project work.

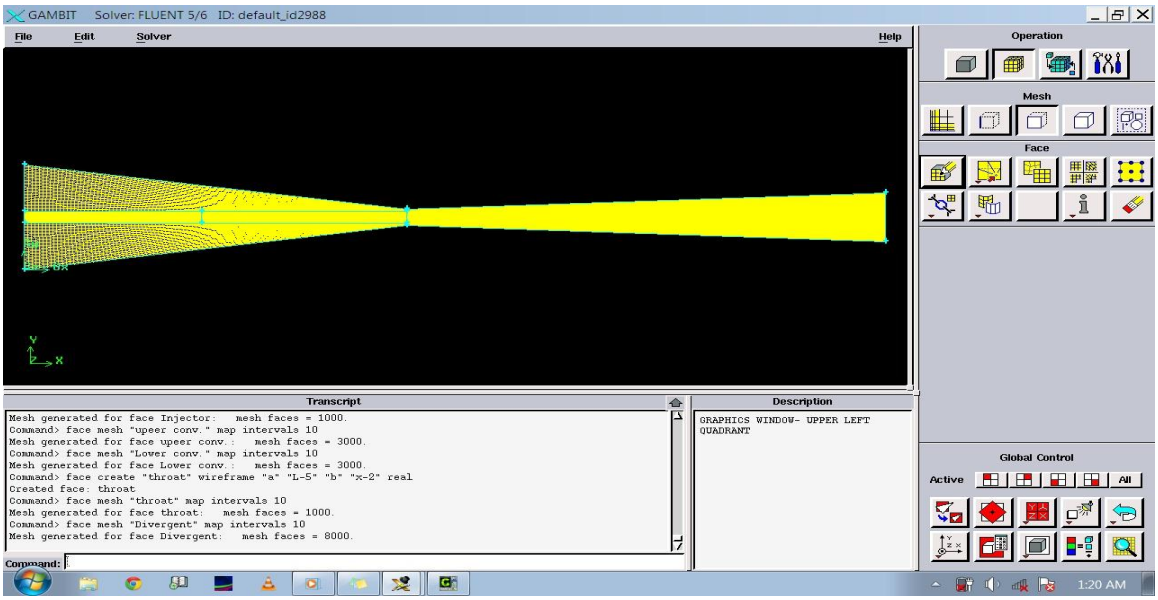

Fig.12b. *Final Nozzle with boundary conditions*

Fig.12b. show the meshing of nozzle with boundary conditions, which are like air inlet velocity; air inlet temp.; mass flow rate of particles; Particle temp. and velocity at Outlet.

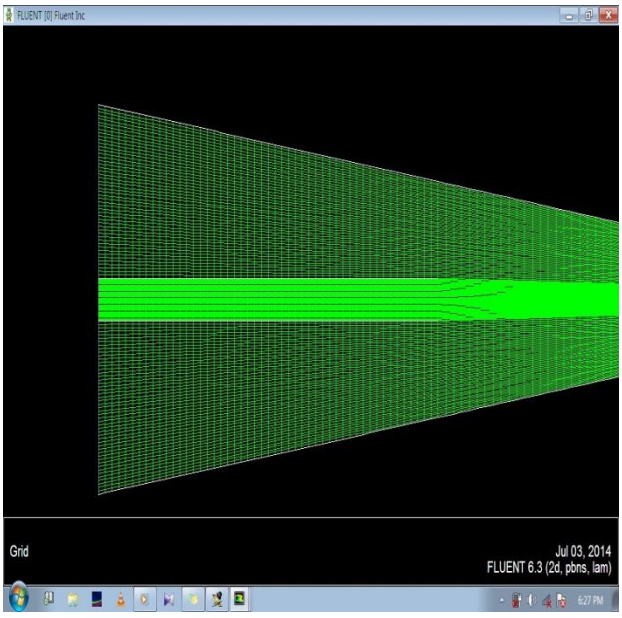

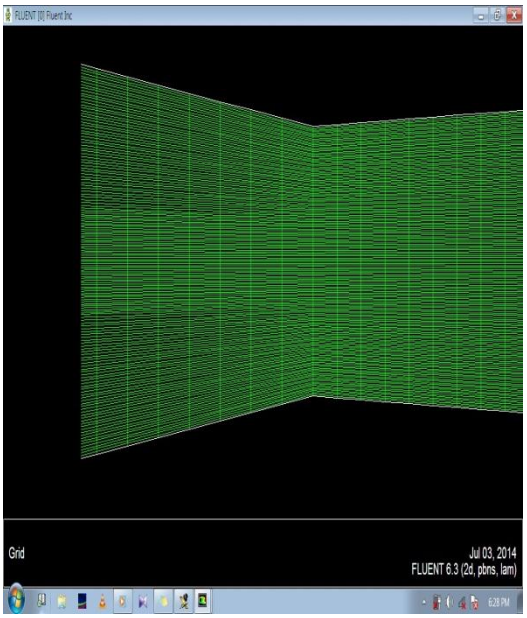

Fig.12c. ***Fig.12d.***

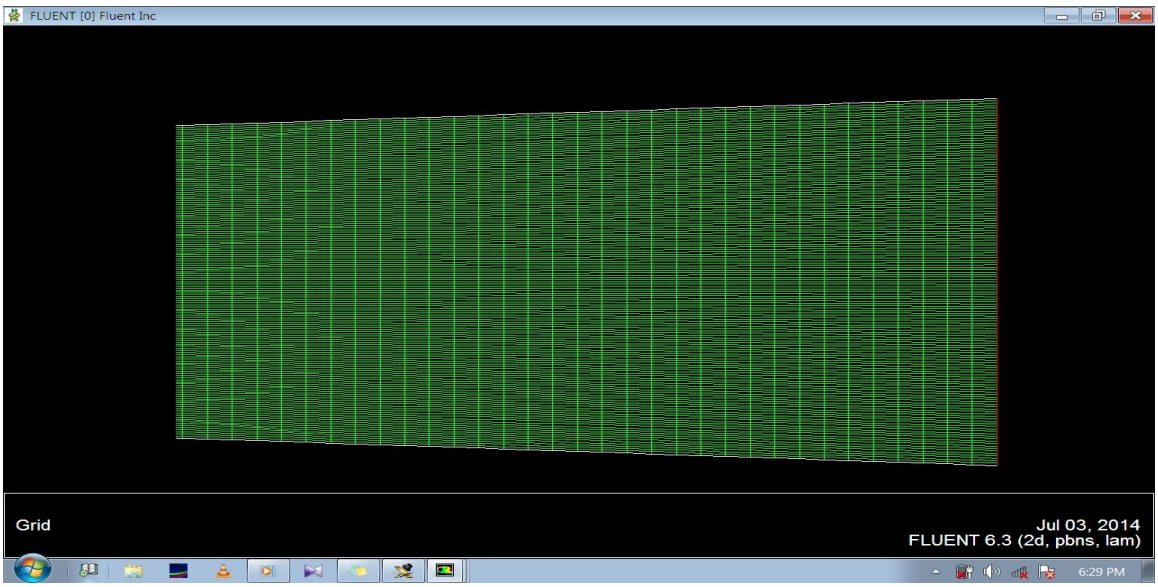

Fig.12e. *Above three Figure shows Mesh faces at the convergent, throat and Divergent section of the nozzle.*

Fig.12c. Show the mesh at the all sections of the nozzle, in that nozzle inlet, throat and divergent sections have 150 interval counts, lower & upper part of convergent and divergent nozzle have 100 & 150 interval counts respectively with 10 spacing by each sections.

5.6.1. Check Back Flow at Injector, Inlet and Outlet

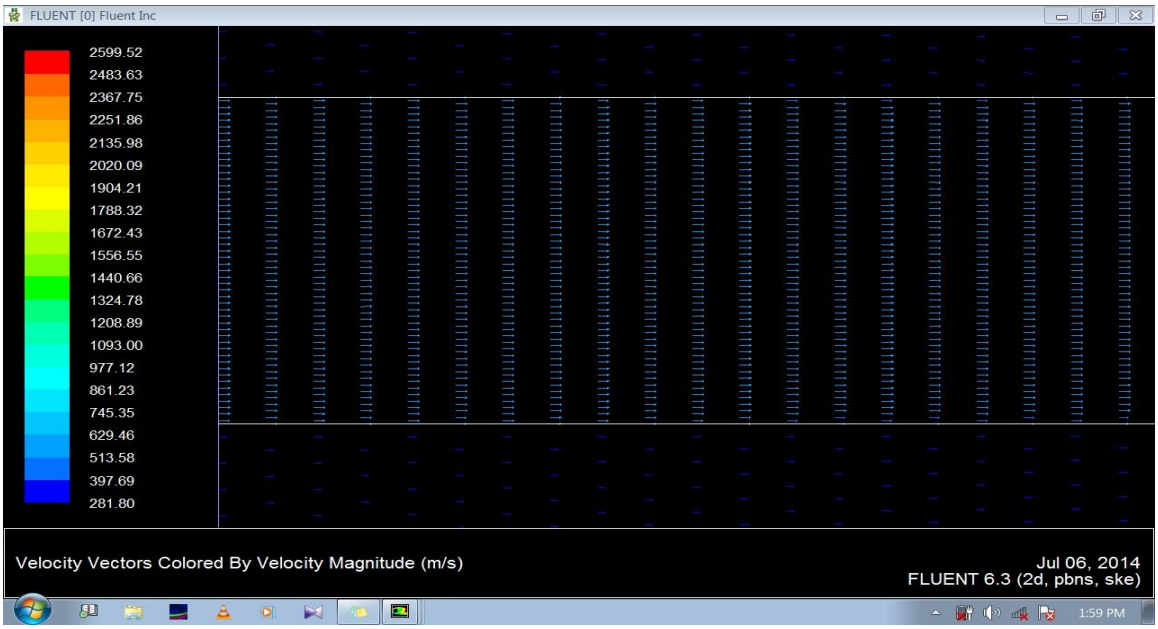

Fig.13a. *above Figure shows there is not any back flow at the Convergent and Injector Of the nozzle.*

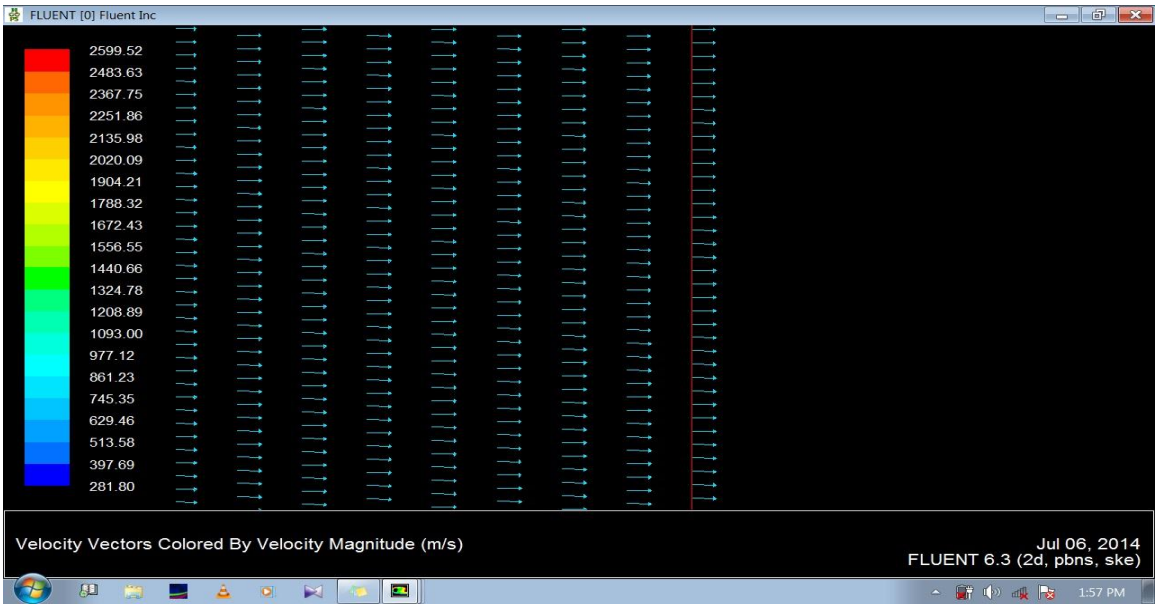

Fig.13b. *above Figure shows there is not any back flow at the Divergent Section of the nozzle.*

5.7. MODEL VALIDATION

The equations obtained in the chapter 3 & 4 the discussion on their simulation in the previous section seems a rational way of approaching the problem of finding the results for a cold spray process.

At Inlet

$V_{air,\ in}$ = 500 m/sec; $T_{air,\ in}$ = 733 ^{0}K ;

$V_{p,\ in}$ = 30 m/sec; $T_{p,in}$ = 300 ^{0}K

At outlet

$V_{p,\ out}$ = 680 m/sec

$T_{p,\ out}$ = 1002 ^{0}K

A first calculation was made by using the same diameters of nozzle throat while total length of nozzle was fixed [1]. Results obtain from these calculations were gas and particle velocity and particle temperature. It was found that particle velocity is 680 m/sec and the temperature of particles at the outlet if nozzle is 1002 ^{0}Kwhich is very close by the results of *H. Fukanuma et al.*

This result show that nozzle is properly works and result is very close to the previous results. So now we can use this nozzle for the further work of project.

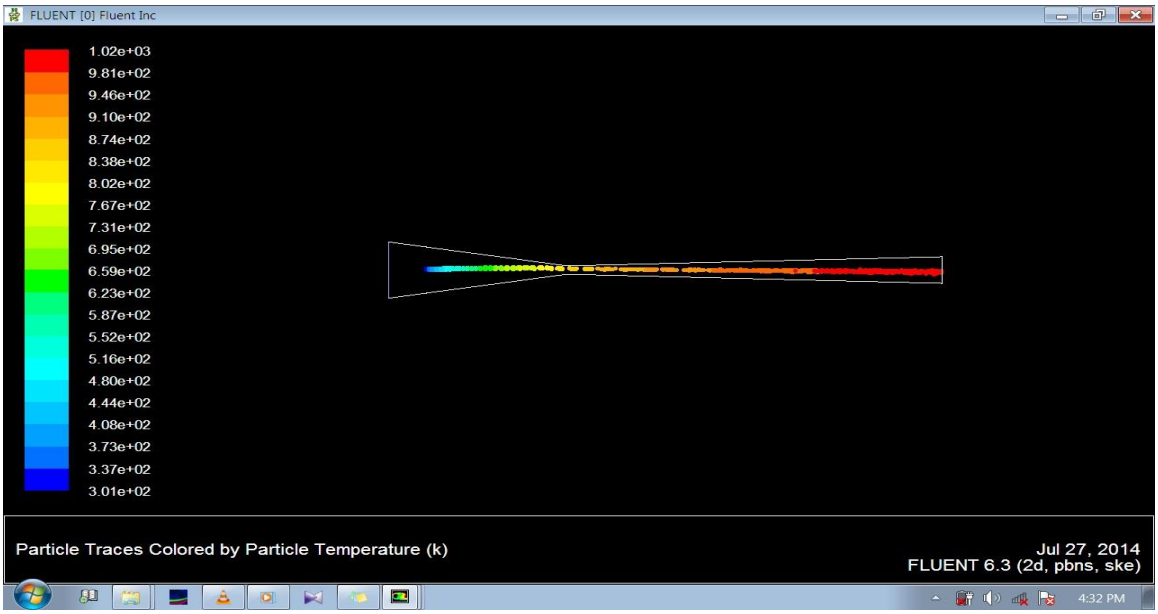

Fig.14a. *Figure shows that maximum Temp. of Particles at outlet of the nozzle is 1002 ^{0}K*

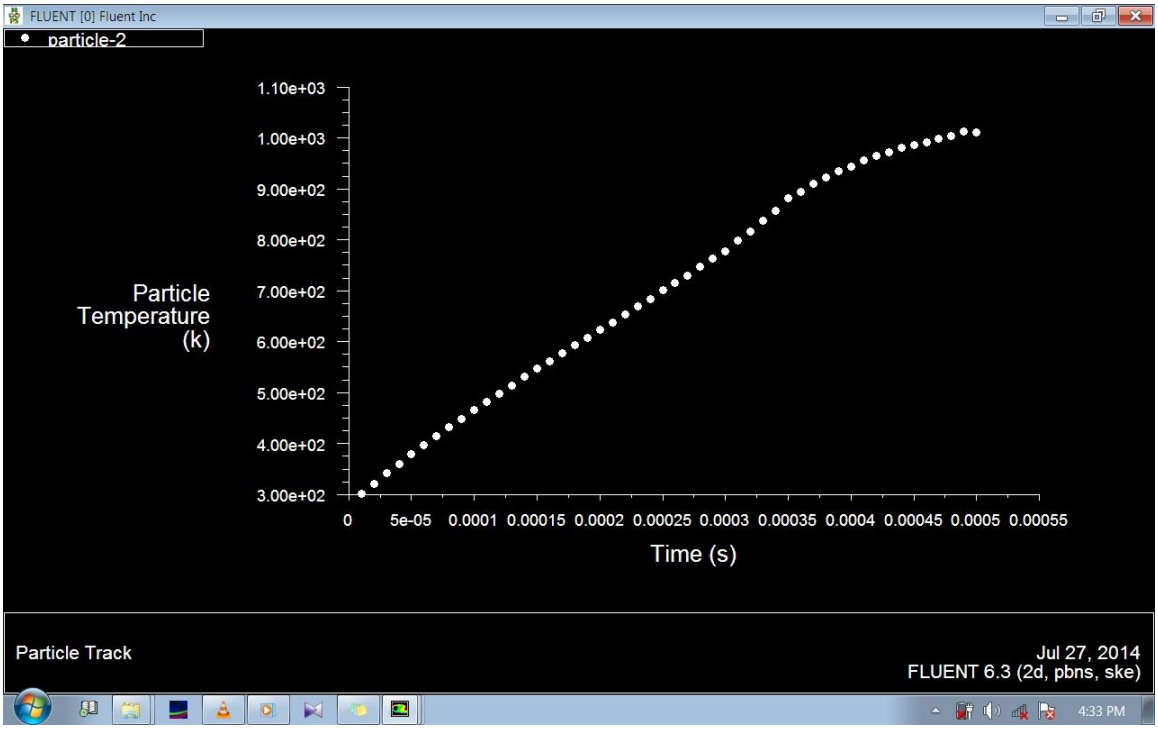

Fig.14b. *Graph shows that maximum Temp. of Particles at outlet of the nozzle is 1002 ^{0}K and the temp. is continuously increase with respect to Time as well as Length of Nozzle.*

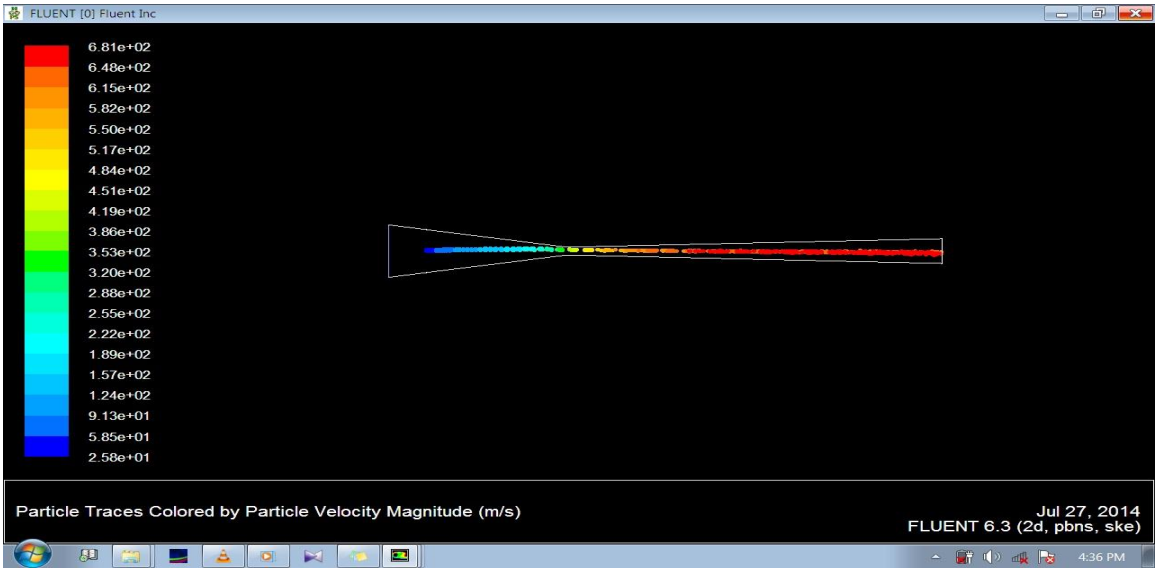

Fig.15a. *Figure shows that maximum Velocity of Particles at outlet of the nozzle is 680 m/sec*

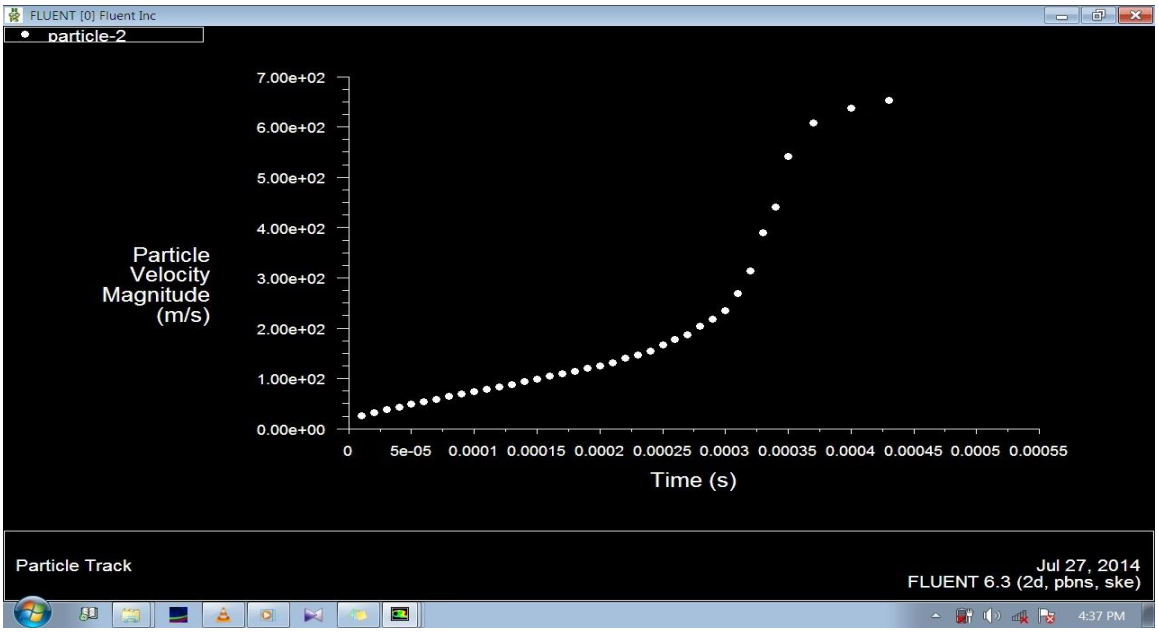

Fig.15b. *Graph shows Particle velocity vs. Time*

In above graph fig. 15.b. maximum Velocity of Particles at outlet of the nozzle is 680 m/sec, Velocity of particles firstly increase slowly and smoothly but after the throat it increase very rapidly and achieved 680 m/sec speed at the exit of nozzle.

CHAPTER 6

RESULTS & CONCLUSIONS

6.1. Simulation of nozzle at different Inlet air velocity & constant Pressure 2.5 MPa

TABLE -3 At 2.5 MPa

S.NO	V_{air} Inlet	V_p Inlet (m/sec)	T_{air} inlet (^{0}K)	V_p outlet (m/sec)	T_p Outlet (^{0}K)	Injection Length (mm)
1	350	30	400	560	348	10
2	350	30	400	566	343	20
3	350	30	400	544	337	30
4	370	30	400	545	350	10
5	370	30	400	575	344	20
6	370	30	400	571	335	30
7	390	30	400	627	448	10
8	390	30	400	652	342	20
9	390	30	400	622	334	30
10	410	30	400	691	347	10
11	410	30	400	655	342	20
12	410	30	400	652	334	30

The above table 3 show the data which have been taken by me to solve the project problem. By this data we have to find many other results with fixed dimensions of the nozzle instead of injector length. By the data of table this is clear that in this simulation we have to use three different types of injector which have same diameter 2 mm. In this simulation we have taken total four type of different velocity of Air at the inlet section of the nozzle; these are 350, 370, 390 and 410 m/sec. for the 10, 20 and 30 mm length of injector simultaneously at the 2.5 MPa pressure.

6.1.1. Simulation for 350 m/sec. at 10, 20 and 30 mm Injector length

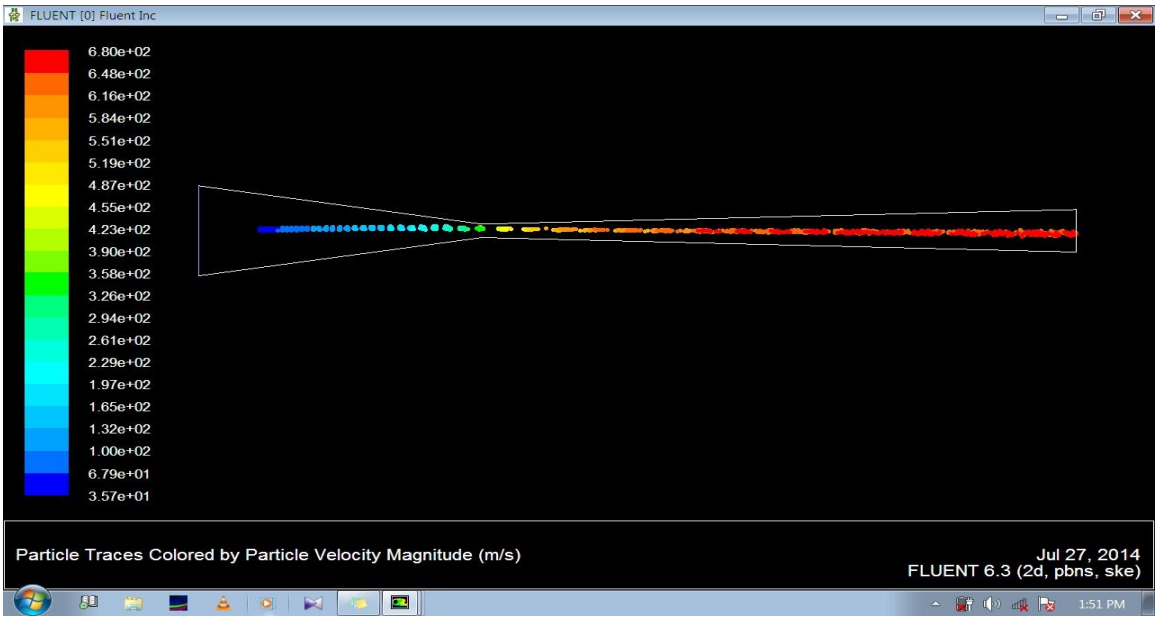

Fig.16a. *Velocity of Particle at outlet of nozzle for the fixed value of* $V_{air,\,in}$ *;*$V_{p,\,in}$ *;* $T_{air,\,in}$ and *Injection Length, which are 350; 30m/sec; 400K and 10 mm respectively.*

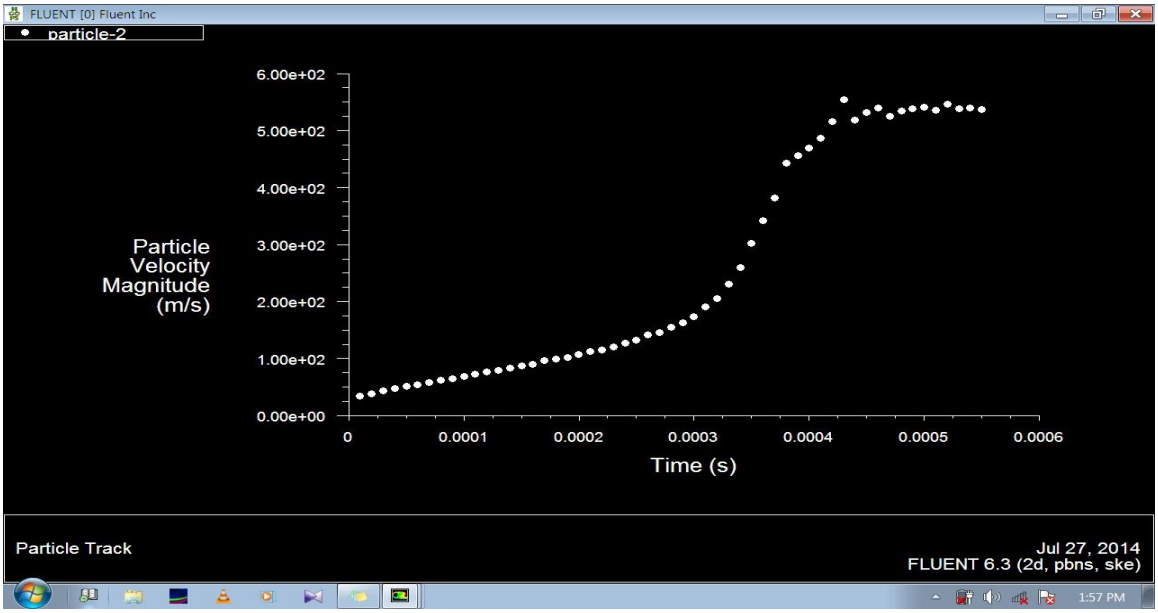

Fig.16b. *Velocity of Particle vs. Time for 10 mm Injector length.*

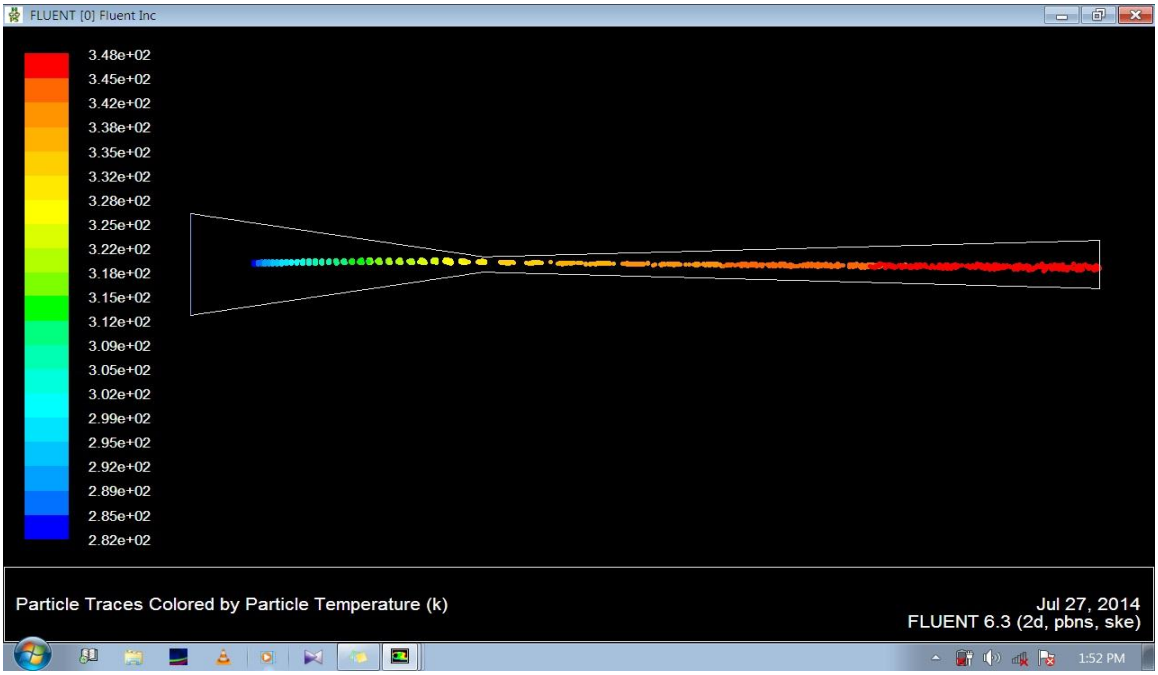

Fig.17a. *Temp. of Particle at outlet of nozzle for the fixed value of* $V_{air,\,in}$ *;* $V_{p,\,in}$ *;* $T_{air,\,in}$ and *Injection Length, which are 350; 30m/sec; 400K and 10 mm respectively.*

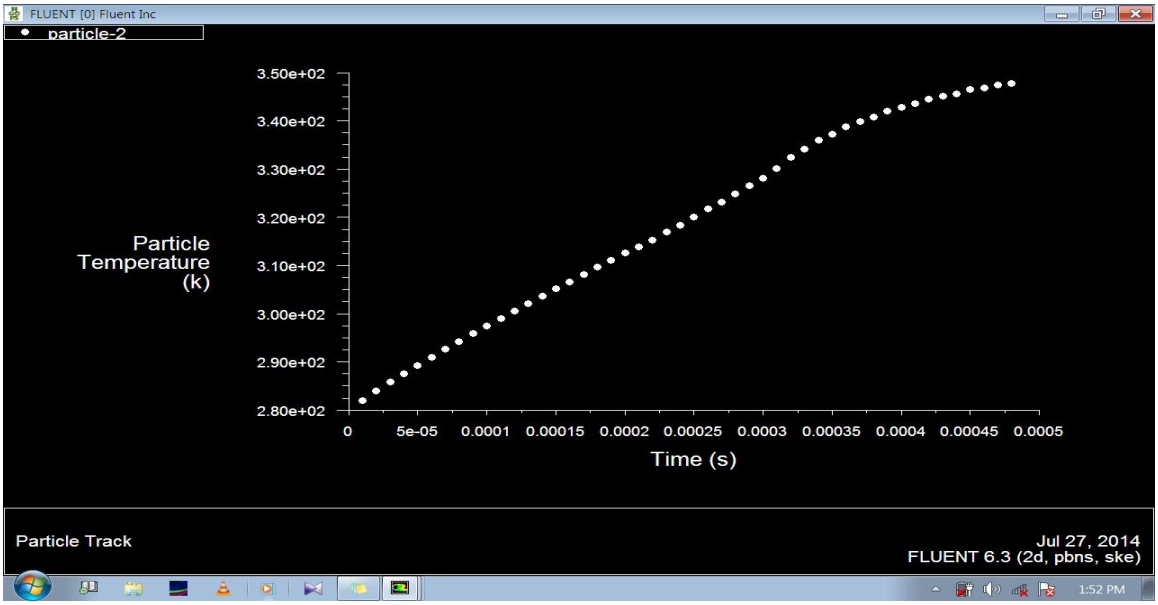

Fig.17b. *Temp. of Particle vs. Time for 10 mm Injector length.*

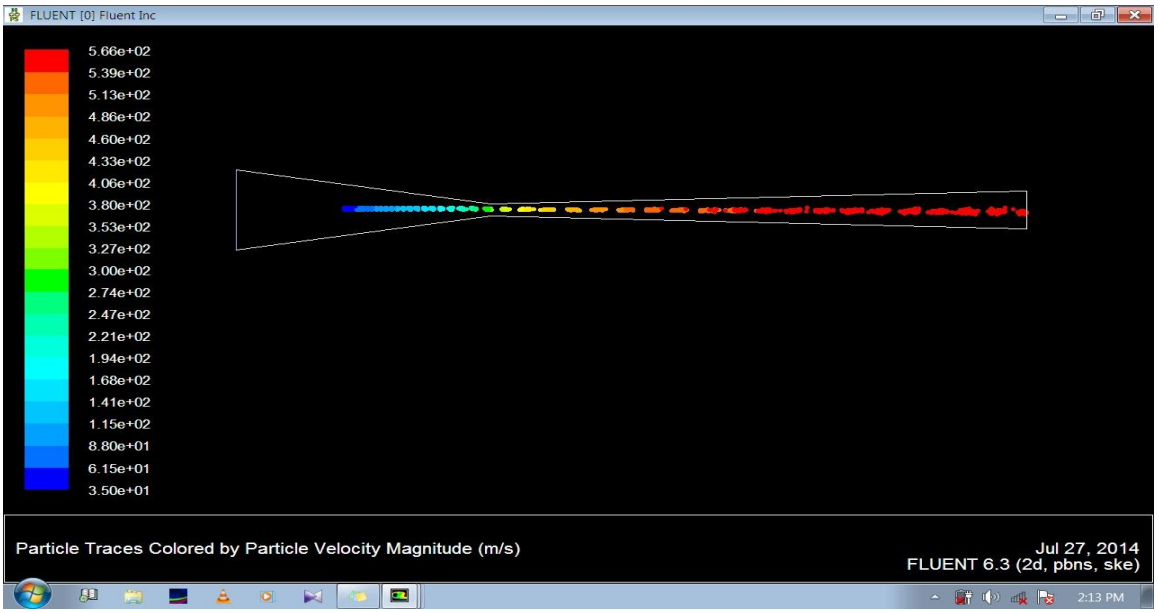

Fig.18a. *Velocity of Particle at outlet of nozzle for the fixed value of* $V_{air,\,in}$ *;*$V_{p,\,in}$ *;* $T_{air,\,in}$ and *Injection Length, which are 350; 30m/sec; 400K and 20 mm respectively.*

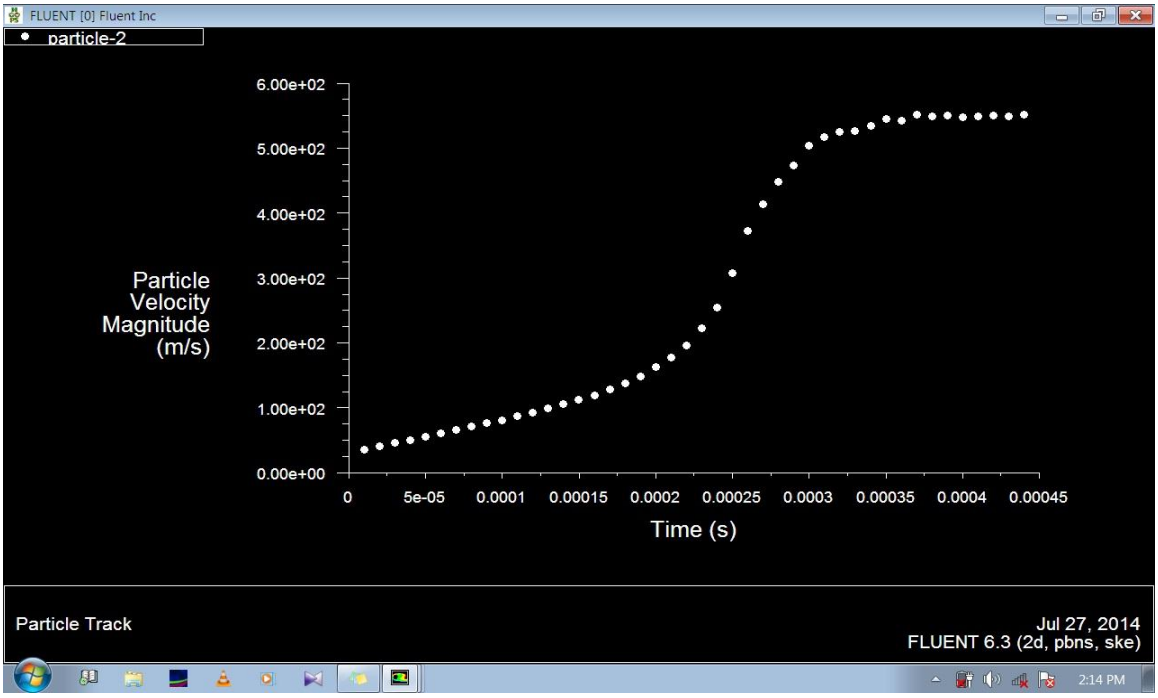

Fig.18b. *Velocity of Particle vs. Time for 20 mm Injector length.*

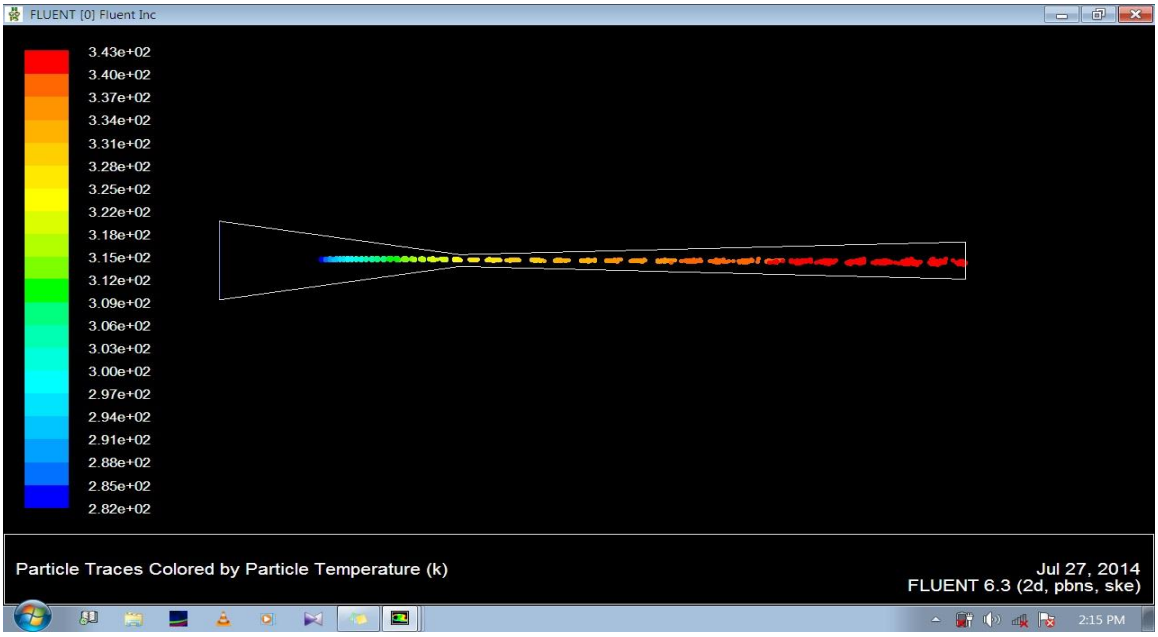

Fig.19a. *Temp. of Particle at outlet of nozzle for the fixed value of* $V_{air,\,in}$ *;*$V_{p,\,in}$ *;* $T_{air,\,in}$ and *Injection Length, which are 350; 30m/sec; 400K and 20 mm respectively.*

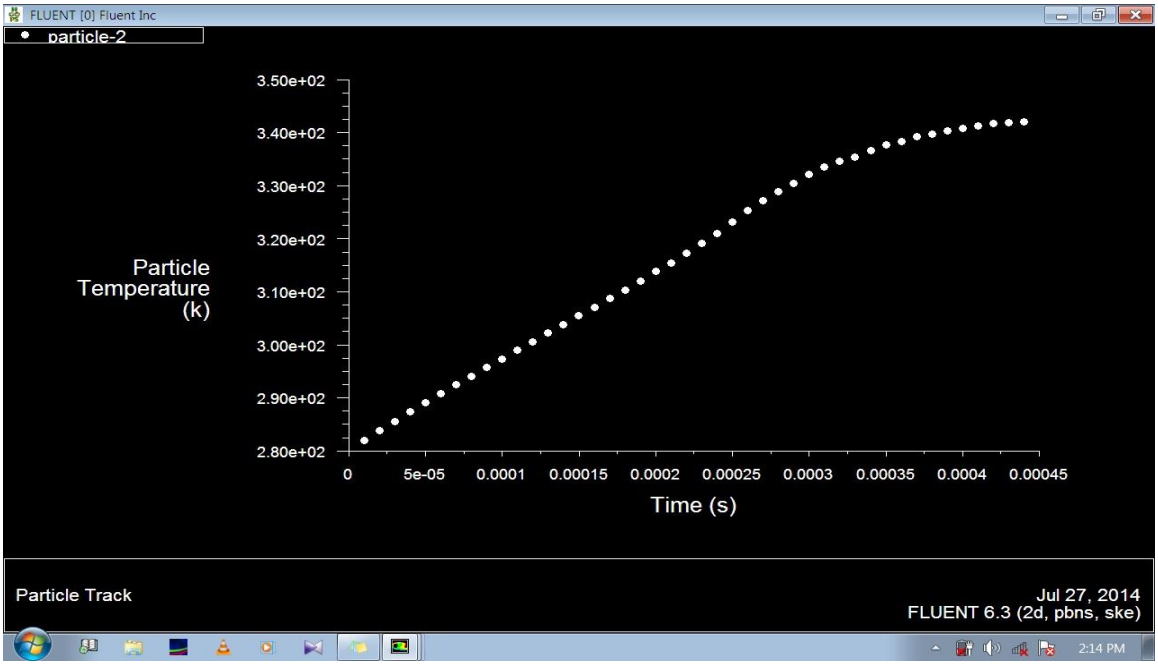

Fig.19b. *Temp. of Particle vs. Time for 20 mm Injector length*

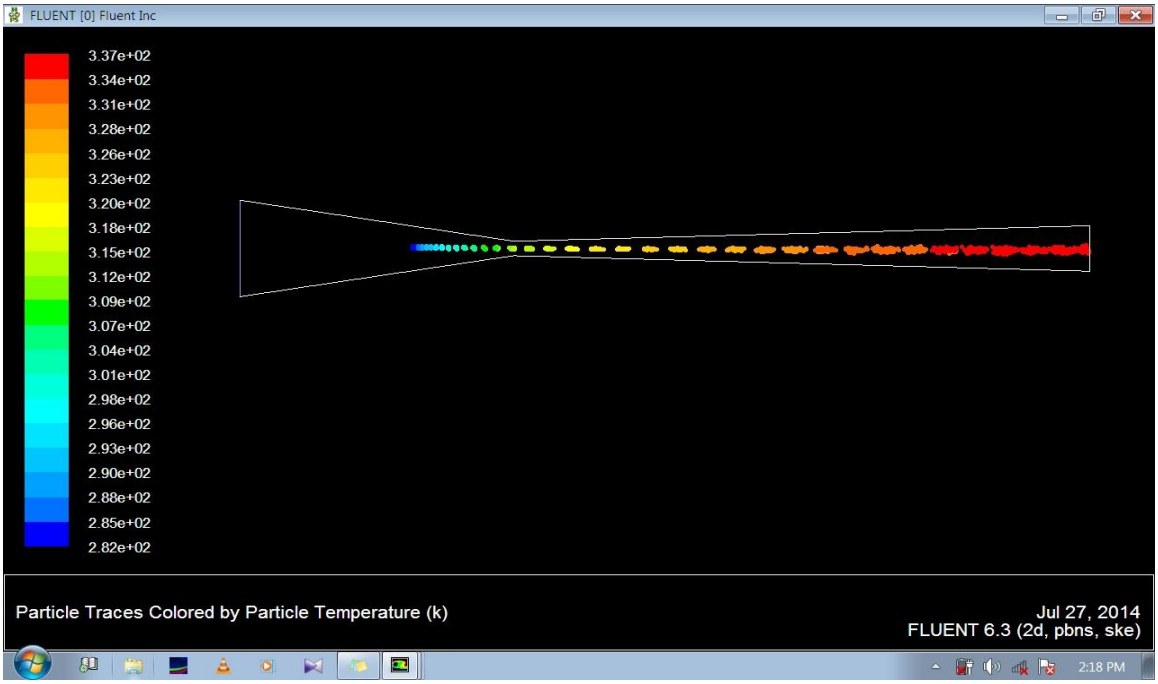

Fig.20a. *Temp. of Particle at outlet of nozzle for the fixed value of* $V_{air,\,in}$ *;* $V_{p,\,in}$ *;* $T_{air,\,in}$ and *Injection Length, which are 350; 30m/sec; 400K and 30 mm respectively.*

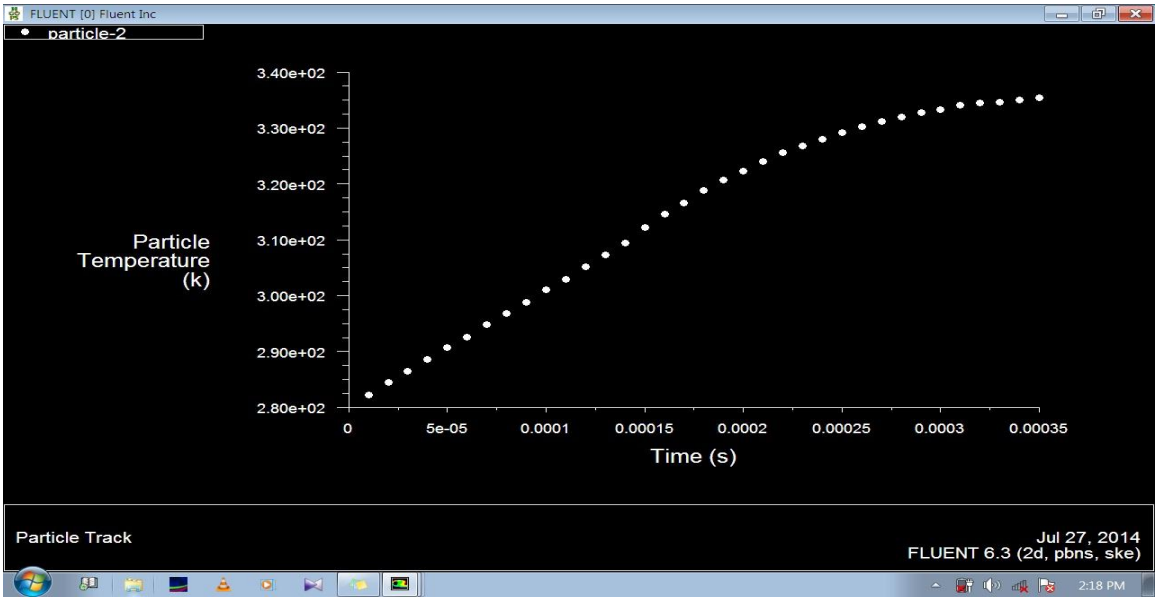

Fig.20b. *Temp. of Particle vs. Time for 30 mm Injector length*

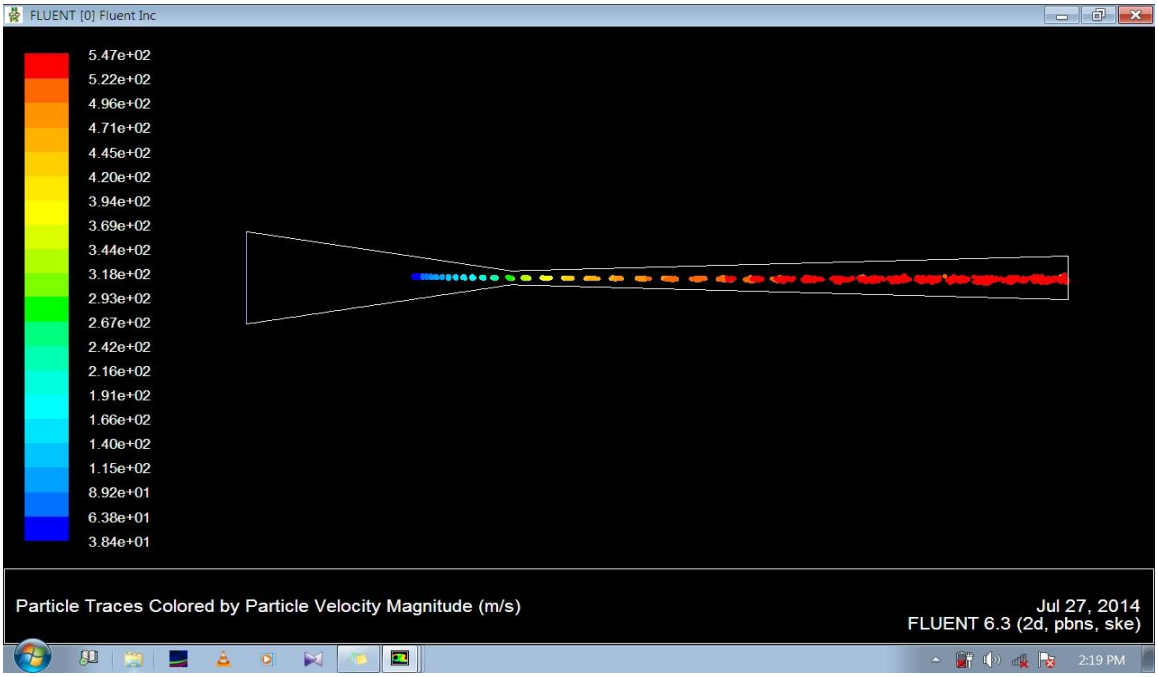

Fig.21a. *Velocity of Particle at outlet of nozzle for the fixed value of* $V_{air,\,in}$ *;*$V_{p,\,in}$ *;* $T_{air,\,in}$ and *Injection Length, which are 350; 30m/sec; 400K and 30 mm respectively*

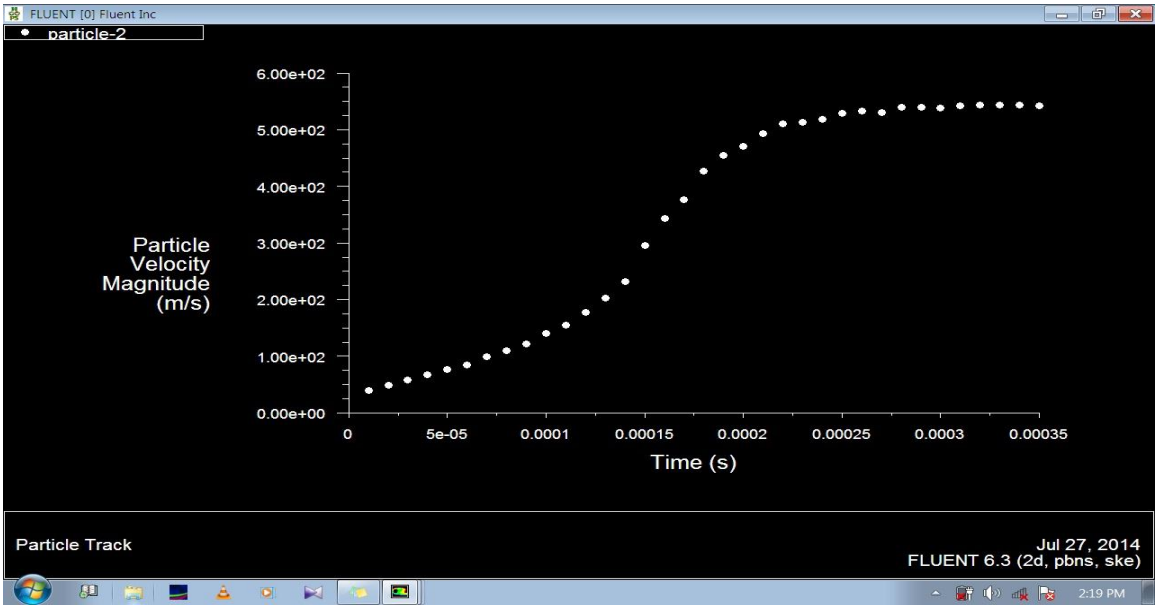

Fig.21b *Velocity of Particle vs. Time for 30 mm Injector length.*

6.1.2. Simulation for 370 m/sec. at 10, 20 and 30 mm Injector length

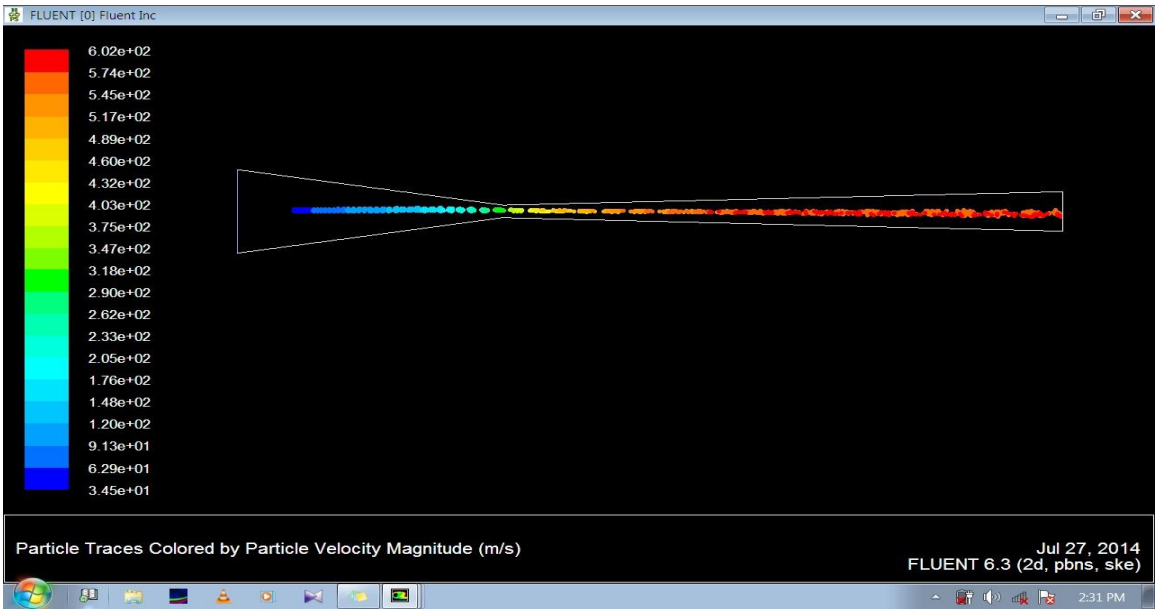

Fig.22a. *Velocity of Particle at outlet of nozzle for the fixed value of* $V_{air,\,in}$ *;*$V_{p,\,in}$ *;* $T_{air,\,in}$ and *Injection Length, which are 370; 30m/sec; 400K and 10 mm respectively*

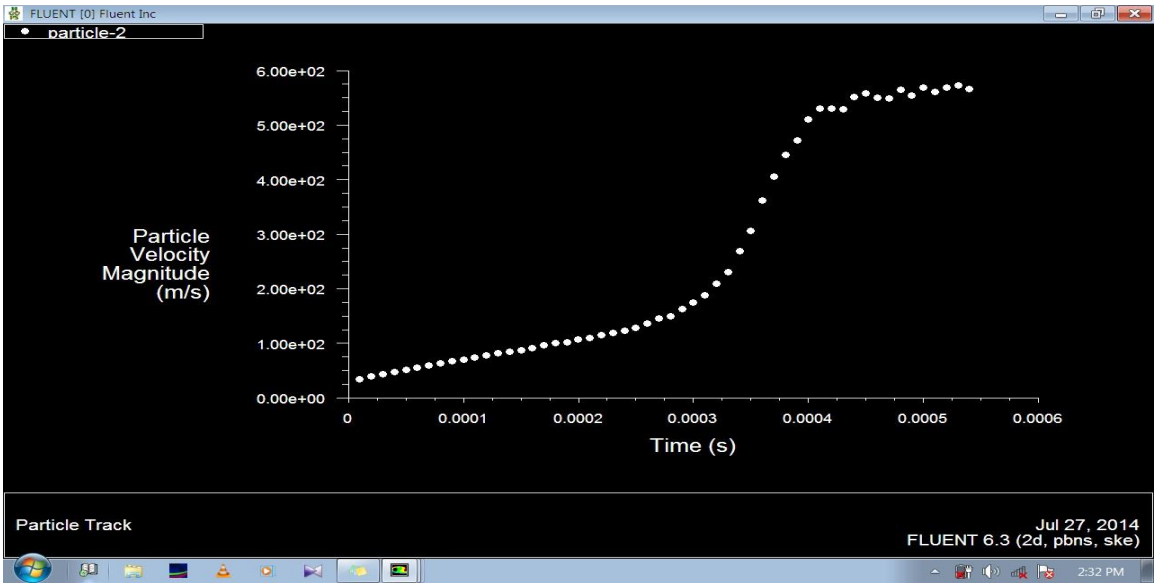

Fig.22b. *Velocity of Particle vs. Time for 10 mm Injector length*

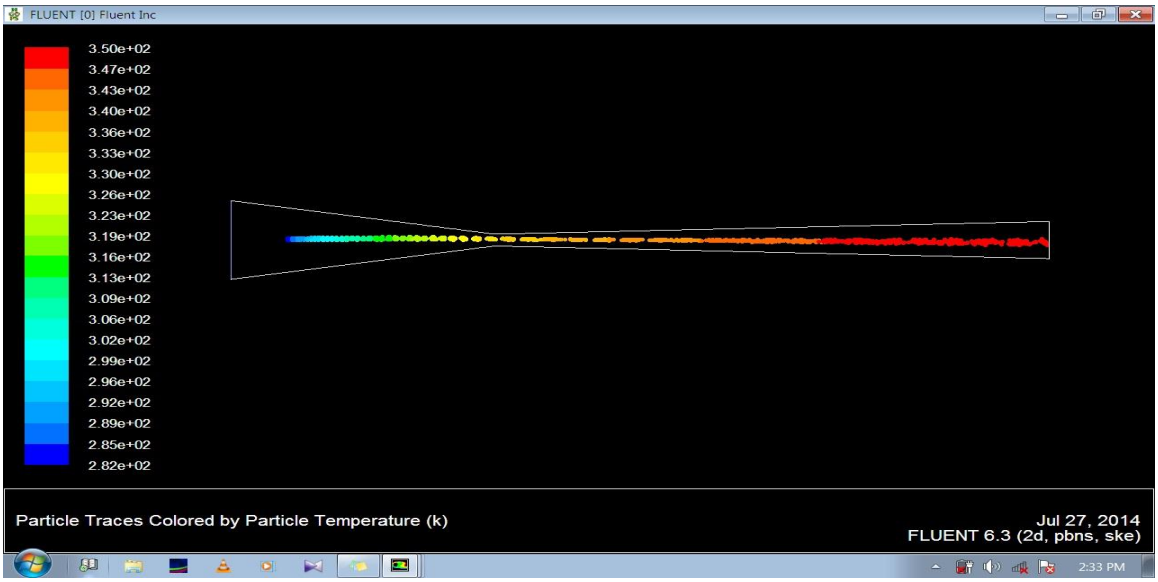

Fig.23a. *Temp. of Particle at outlet of nozzle for the fixed value of* $V_{air,\,in}$ *;* $V_{p,\,in}$ *;* $T_{air,\,in}$ and *Injection Length, which are 370; 30m/sec; 400K and 10 mm respectively*

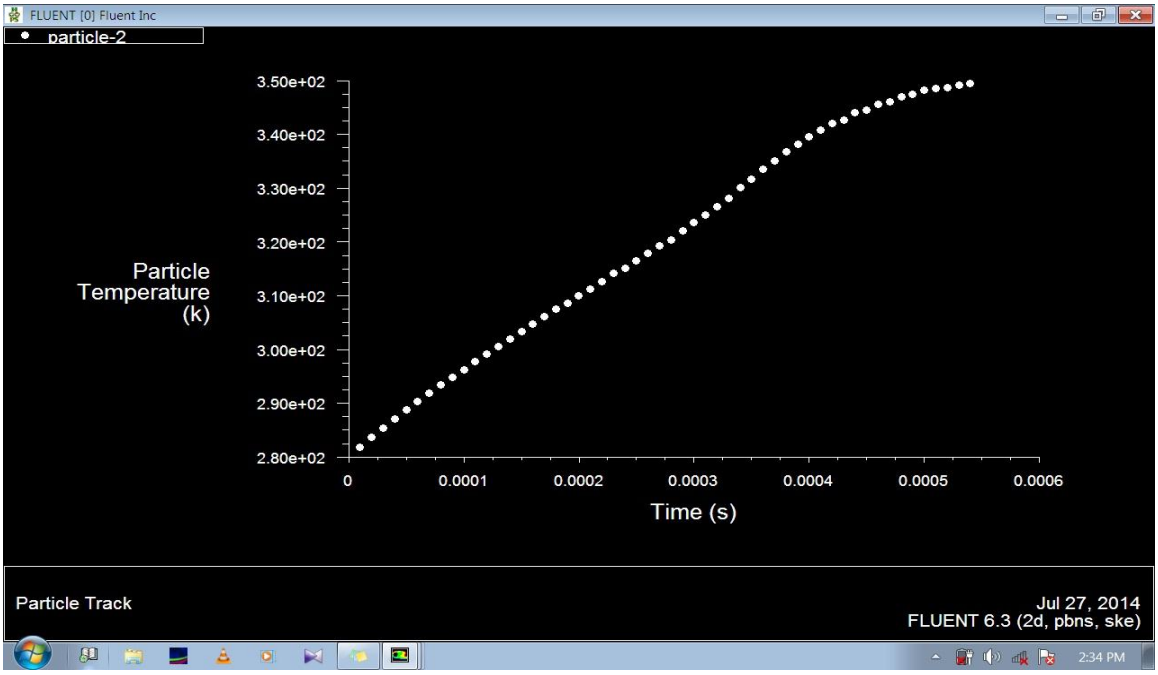

Fig.23b. *Temp. of Particle vs. Time for 10 mm Injector length*

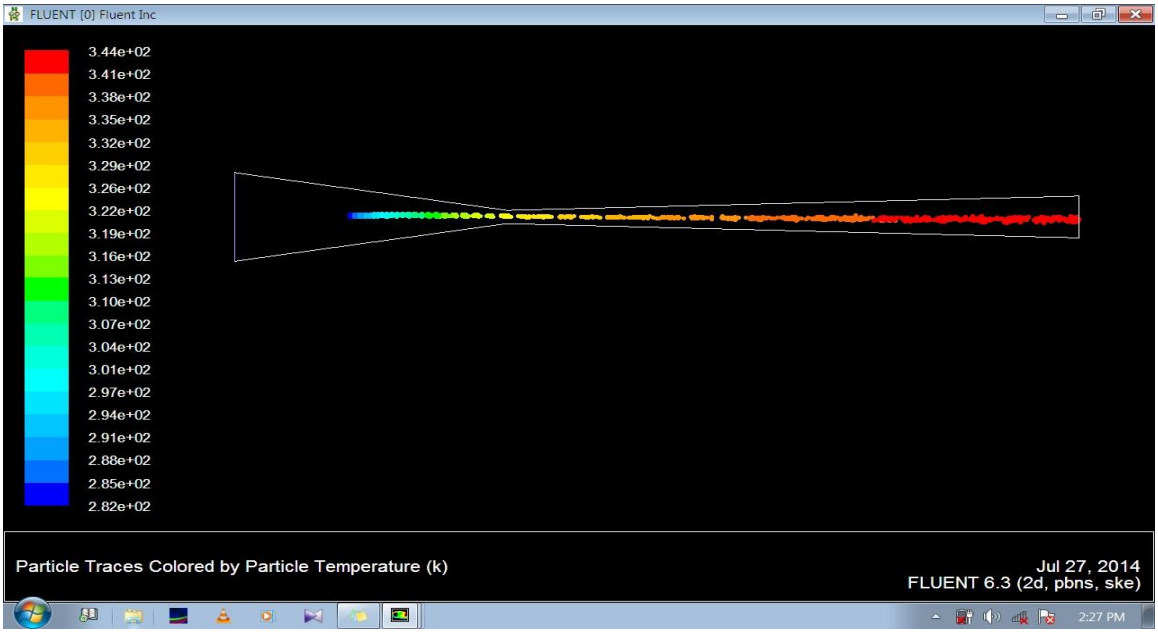

Fig.24a. *Show the Temp. of Particle at outlet of nozzle for the fixed value of* $V_{air,\,in}$ *;*$V_{p,\,in}$ *;* $T_{air,\,in}$ and *Injection Length, which are 370; 30m/sec; 400K and 20 mm respectively.*

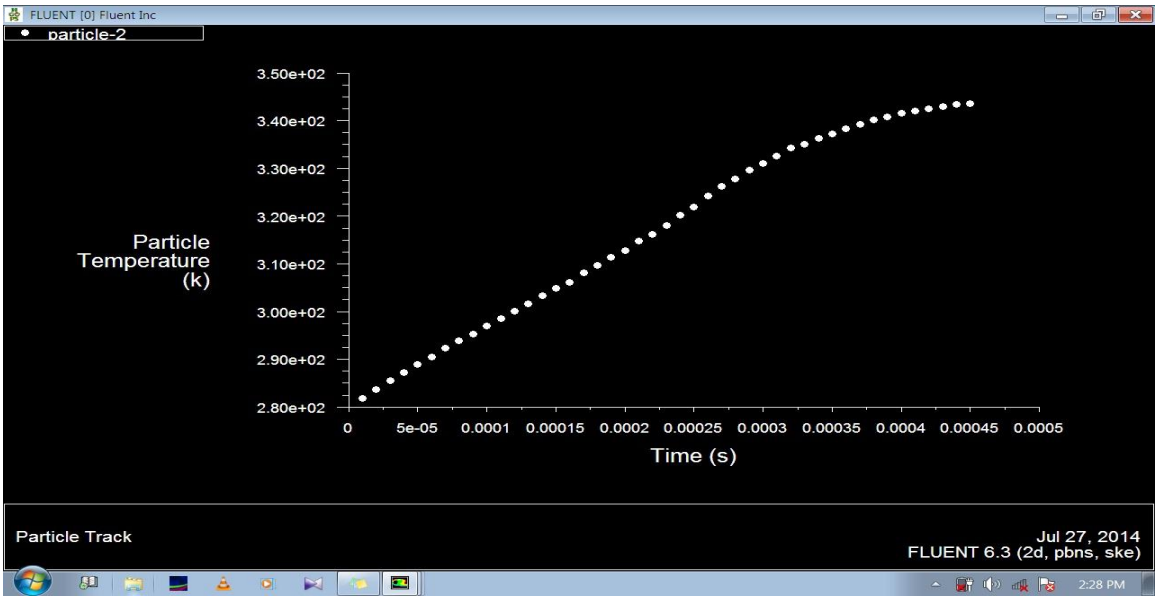

Fig.24b. *Temp. of Particle vs. Time for 20 mm Injector length*

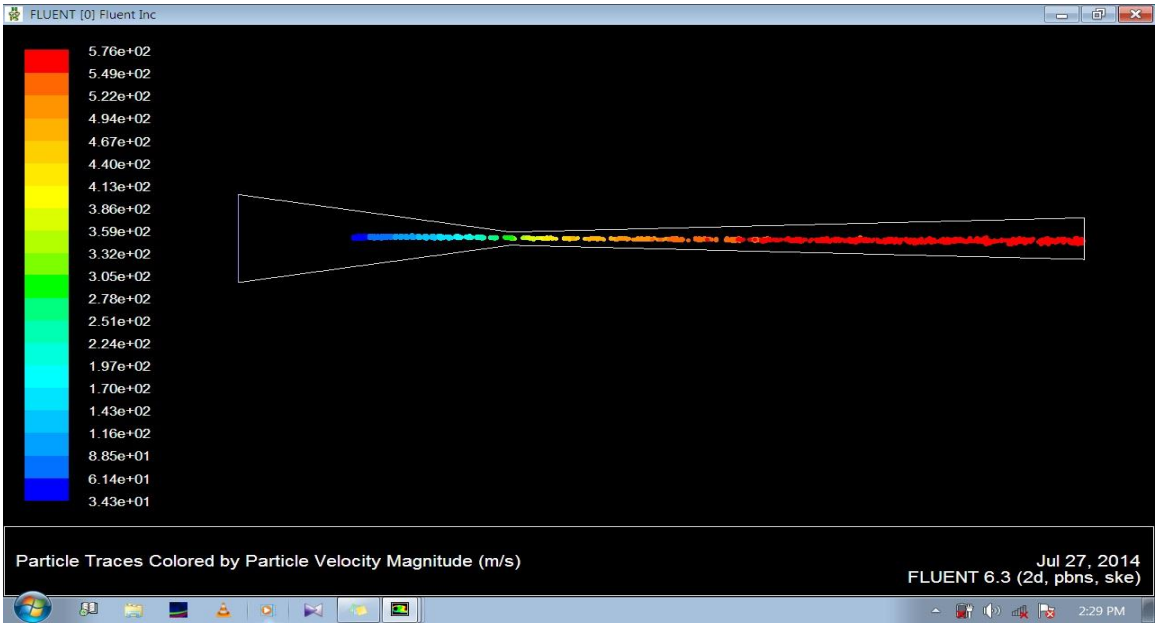

Fig.25a. *Velocity of Particle at outlet of nozzle for the fixed value of* $V_{air,\,in}$ *;*$V_{p,\,in}$ *;* $T_{air,\,in}$ and *Injection Length, which are 370; 30m/sec; 400K and 20 mm respectively*

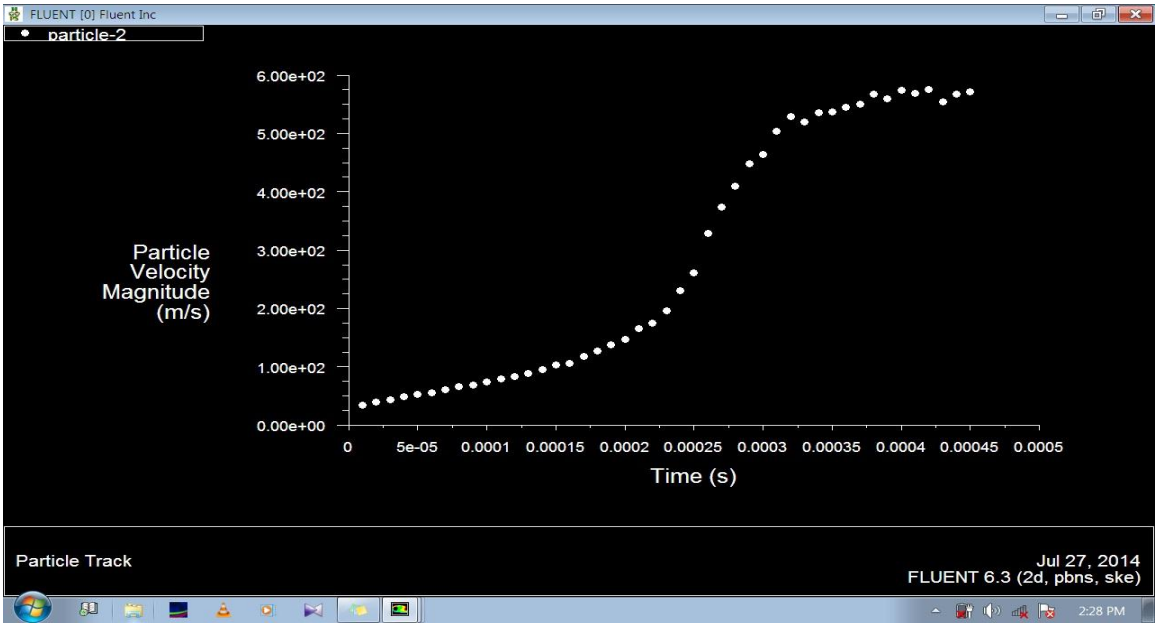

Fig.25b. *Velocity of Particle vs. Time for 20 mm Injector length*

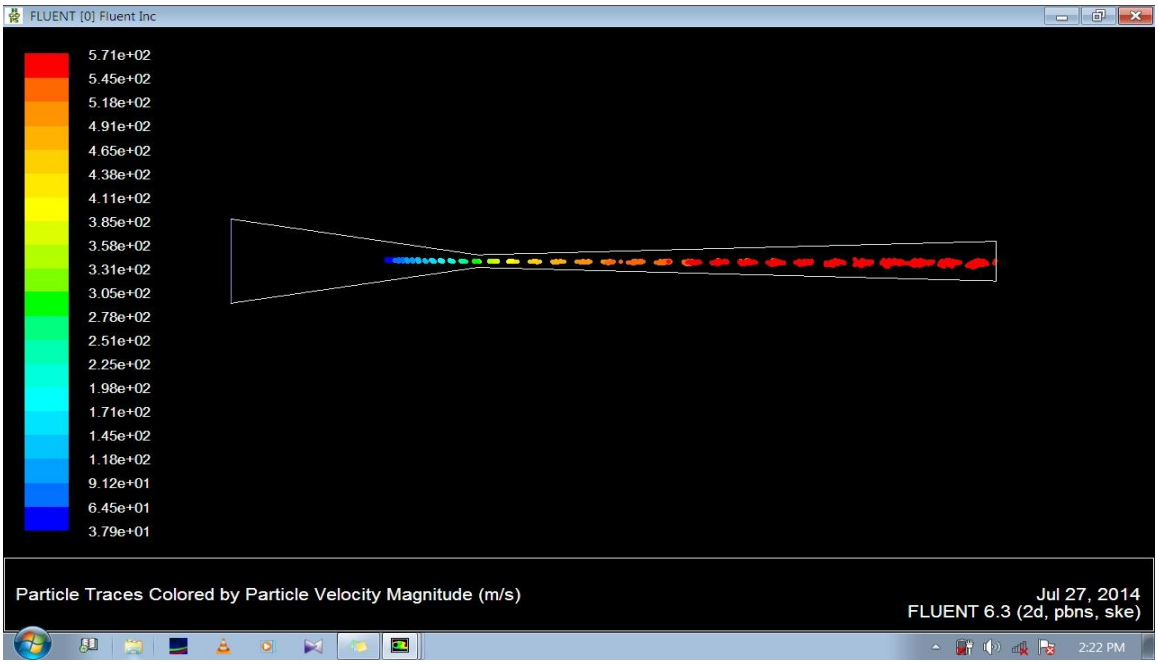

Fig.26a. *Velocity of Particle at outlet of nozzle for the fixed value of* $V_{air,\,in}$ *;*$V_{p,\,in}$ *;* $T_{air,\,in}$ and *Injection Length, which are 370; 30m/sec; 400K and 30 mm respectively*

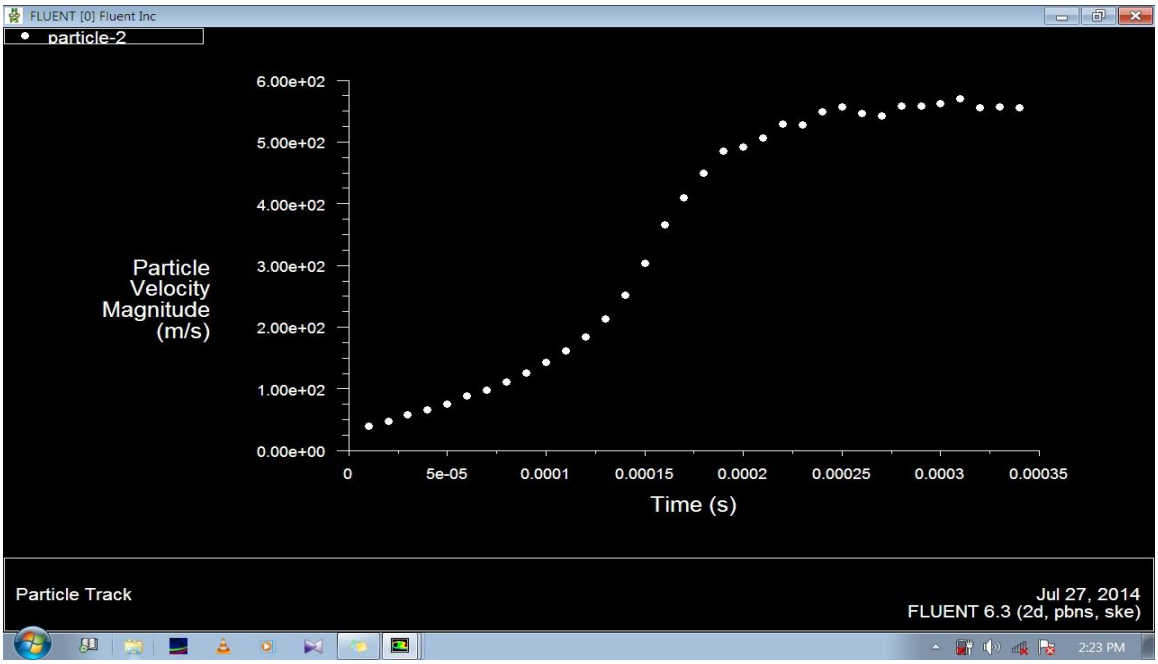

Fig.26b. *Velocity of Particle vs. Time for 30 mm Injector length*

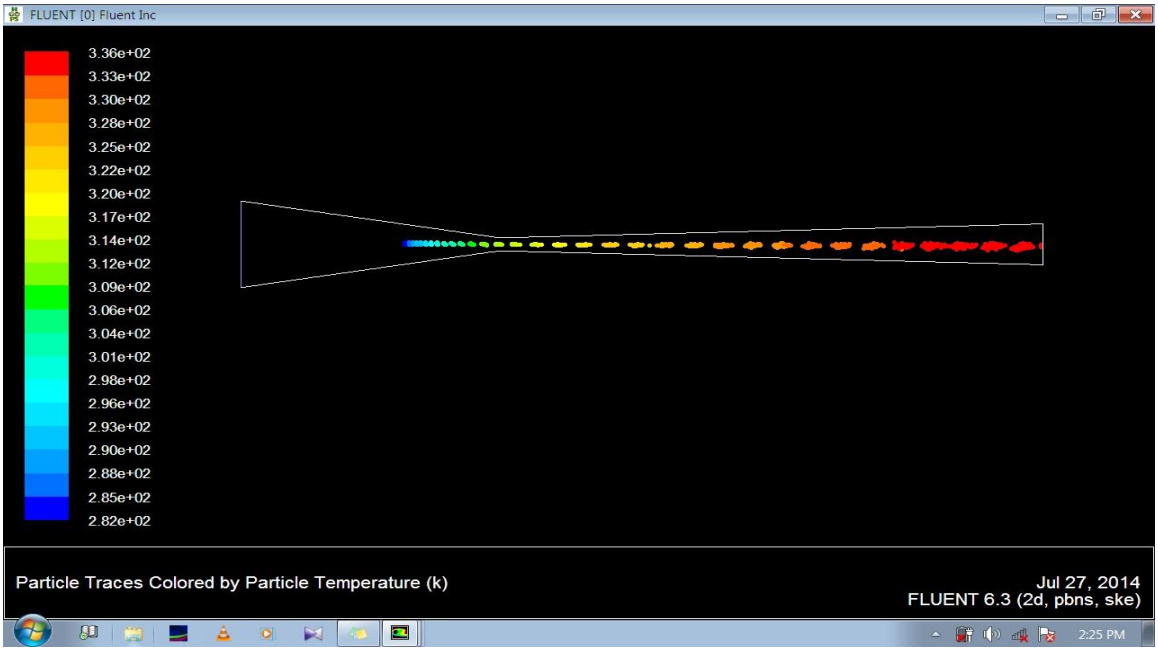

Fig.27a. *Temp. of Particle at outlet of nozzle for the fixed value of* $V_{air,\,in}$ *;* $V_{p,\,in}$ *;* $T_{air,\,in}$ and *Injection Length, which are 370; 30m/sec; 400K and 30 mm respectively*

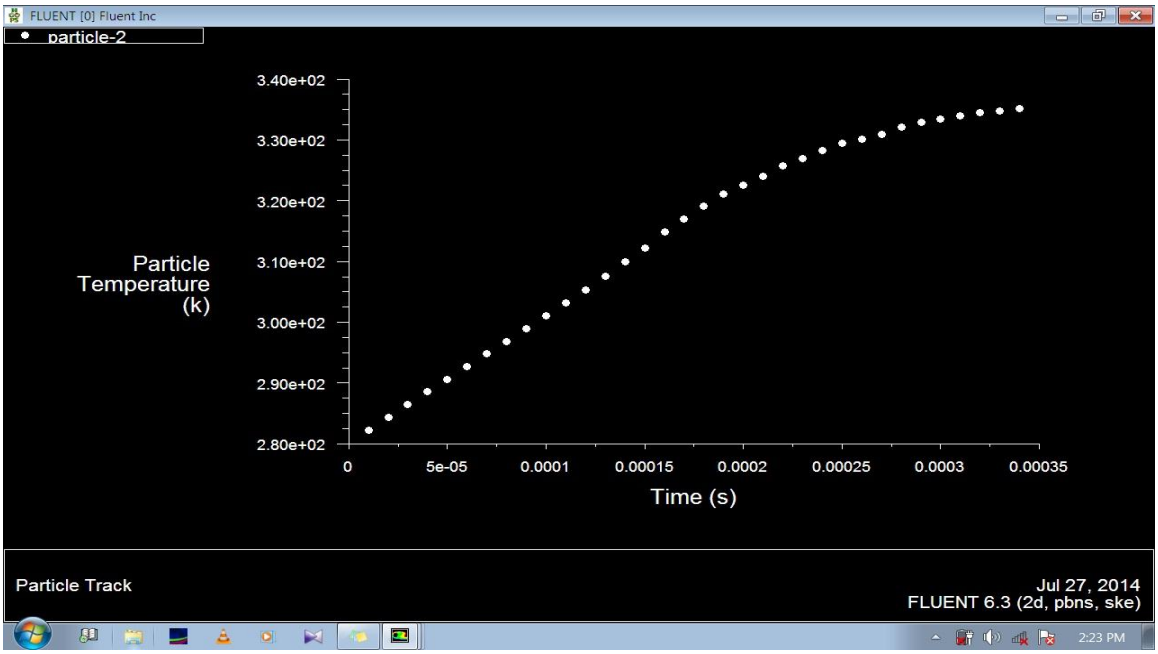

Fig.27b. *Temp. of Particle vs. Time for 30 mm Injector length*

6.1.3. Simulation for 390 m/sec. at 10, 20 and 30 mm Injector length

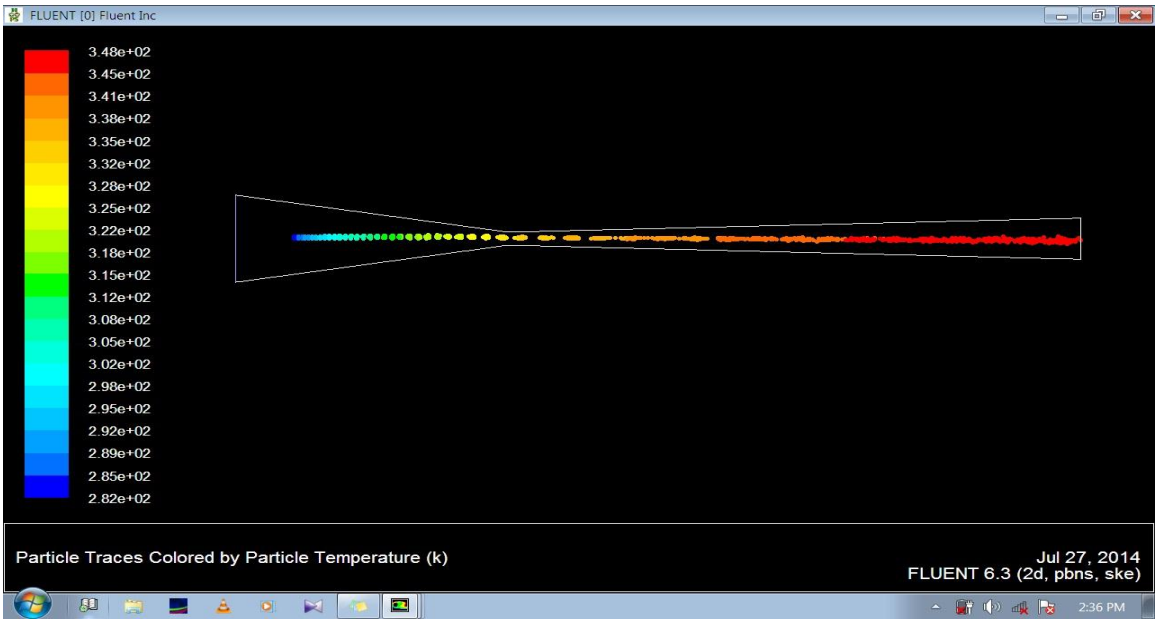

Fig.28a. *Temp. of Particle at outlet of nozzle for the fixed value of* $V_{air,\,in}$ *;* $V_{p,\,in}$ *;* $T_{air,\,in}$ and *Injection Length, which are 390; 30m/sec; 400K and 10 mm respectively*

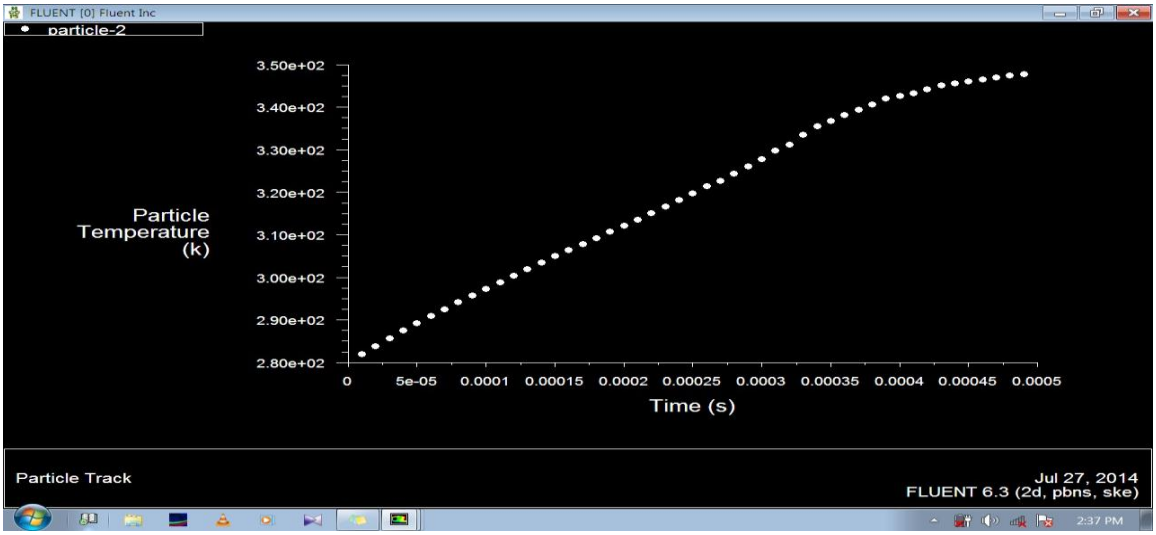

Fig.28b. *Temp. of Particle vs. Time for 10 mm Injector length*

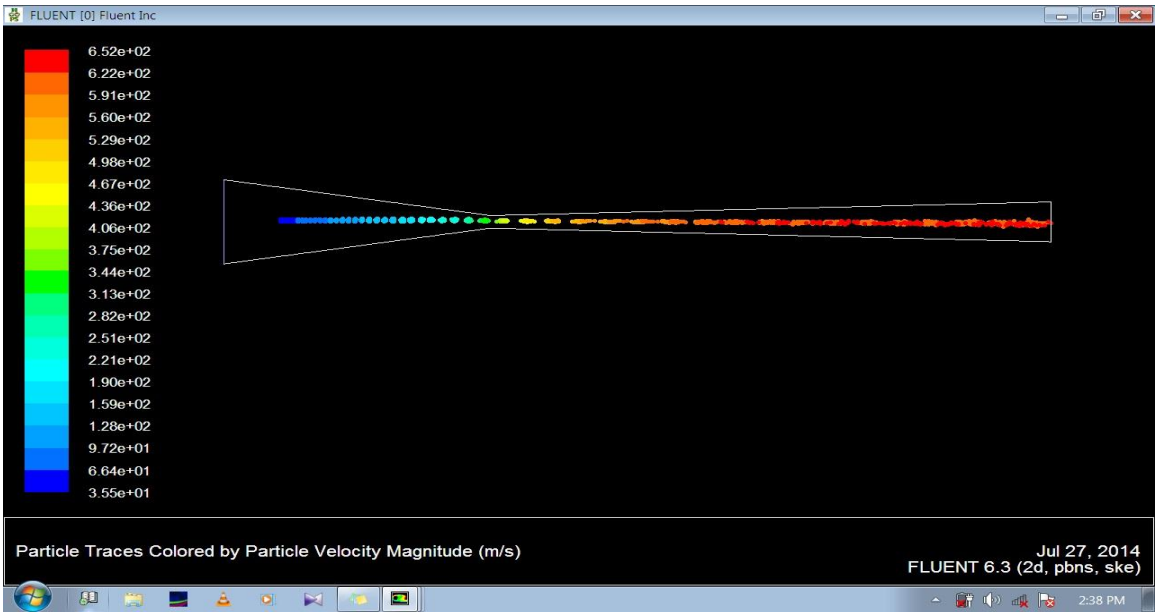

Fig.29a. *velocity of Particle at outlet of nozzle for the fixed value of* $V_{air,\,in}$ *;*$V_{p,\,in}$ *;* $T_{air,\,in}$ and *Injection Length, which are 390; 30m/sec; 400K and 10 mm respectively*

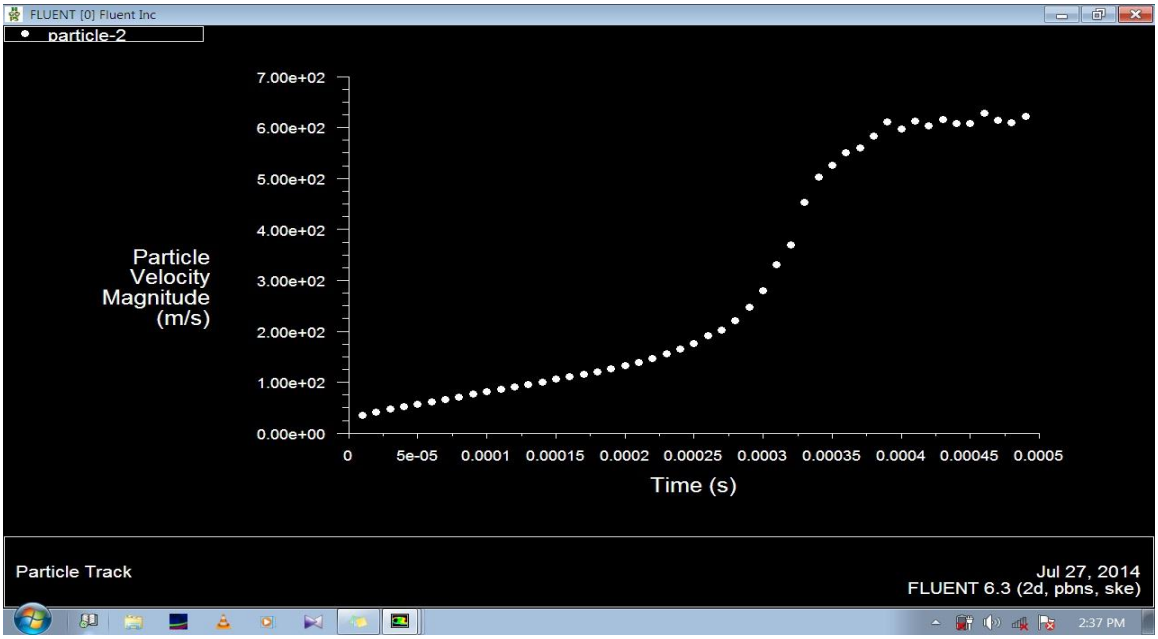

Fig.29b. *velocity of Particle vs. Time for 10 mm Injector length*

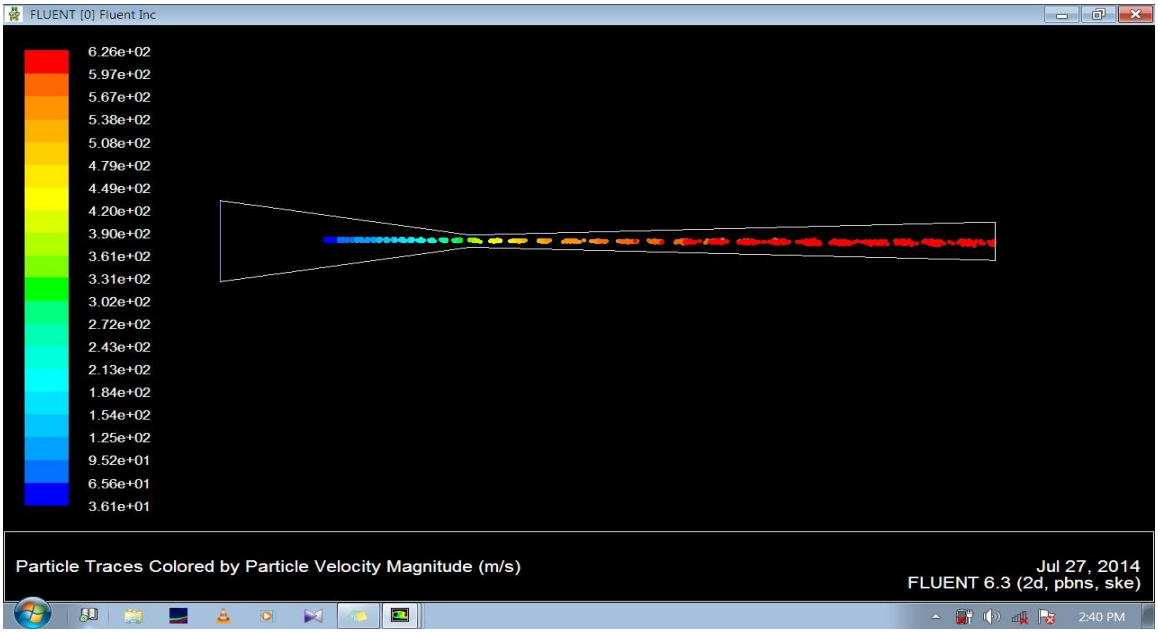

Fig.30a. *velocity of Particle at outlet of nozzle for the fixed value of* $V_{air,\,in}$ *;*$V_{p,\,in}$ *;* $T_{air,\,in}$ and *Injection Length, which are 390; 30m/sec; 400K and 20 mm respectively*

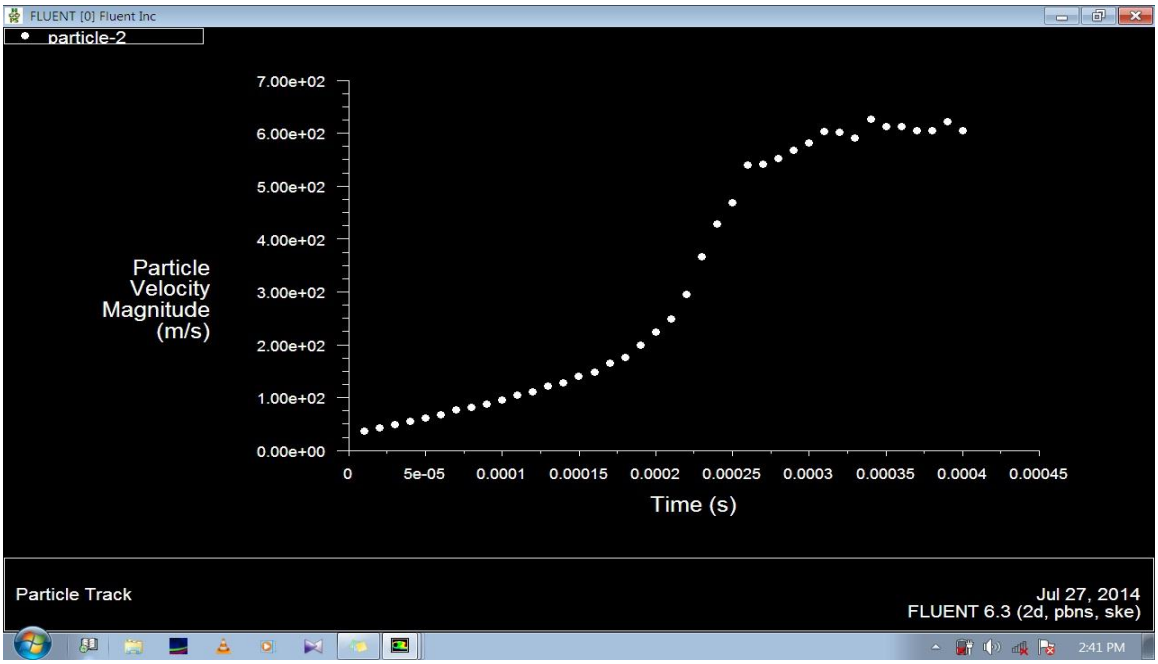

Fig.30b. *velocity of Particle vs. Time for 20 mm Injector length*

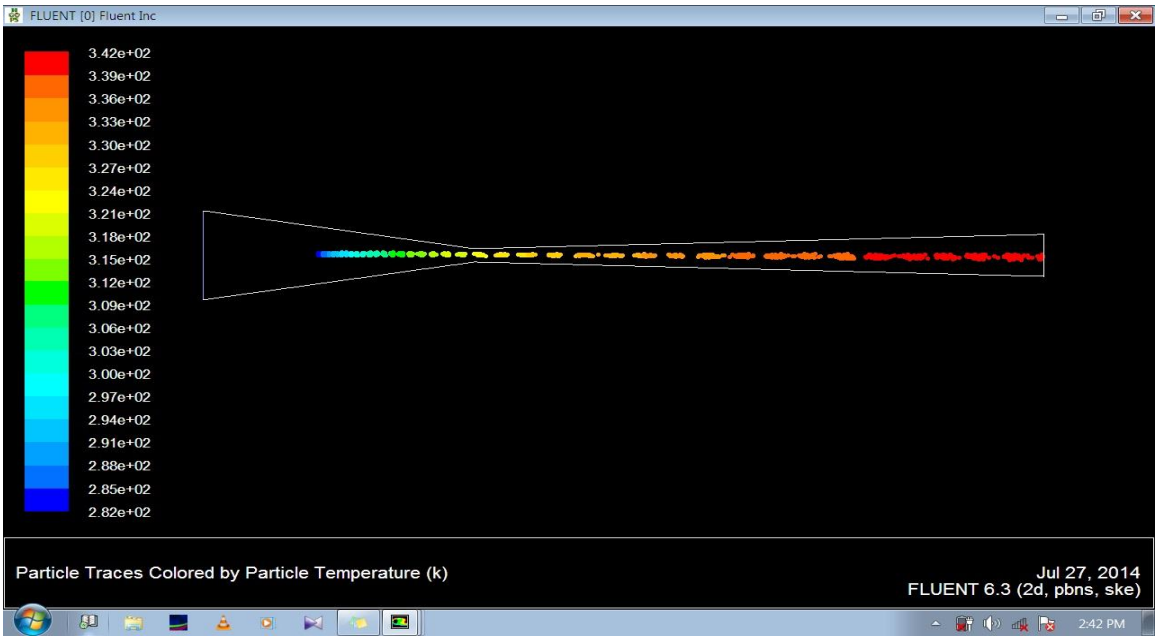

Fig.31a. *Temp. of Particle at outlet of nozzle for the fixed value of* $V_{air,\,in}$ *;* $V_{p,\,in}$ *;* $T_{air,\,in}$ and *Injection Length, which are 390; 30m/sec; 400K and 20 mm respectively*

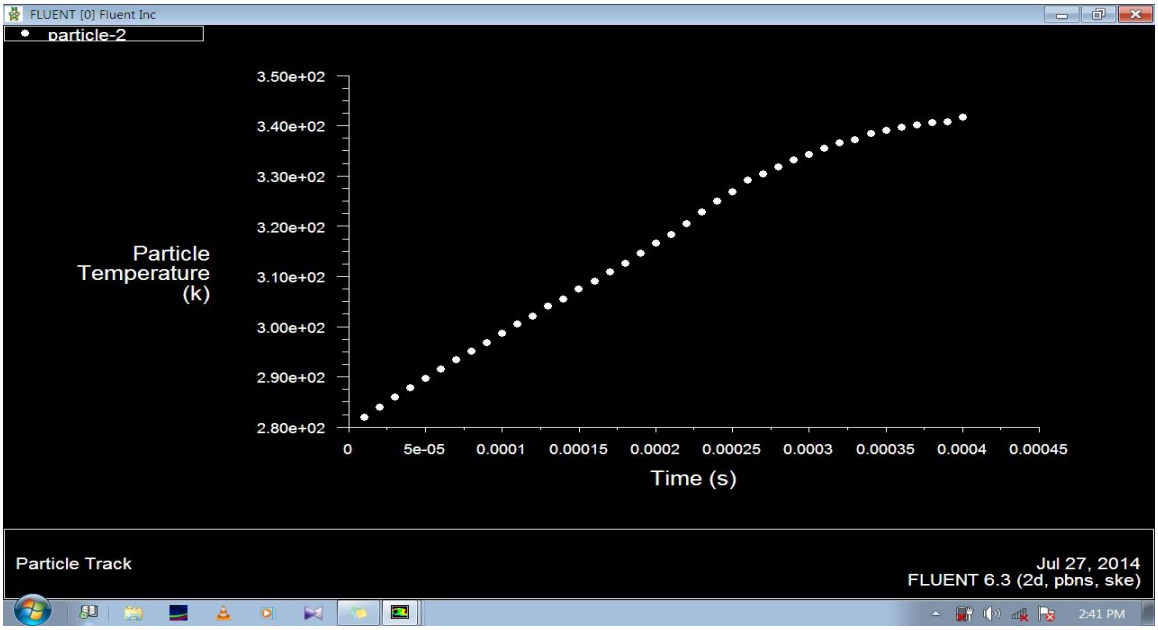

Fig.31b. *Temp. of Particle vs. Time for 20 mm Injector length*

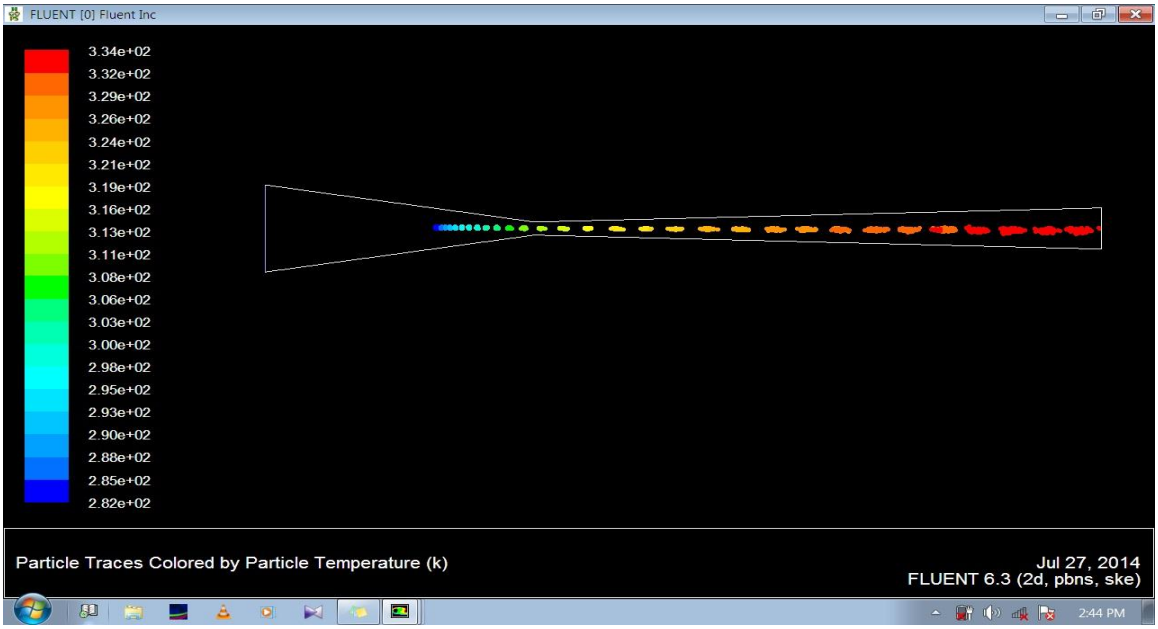

Fig.32a. *Temp. of Particle at outlet of nozzle for the fixed value of $V_{air,\,in}$;$V_{p,\,in}$; $T_{air,\,in}$ and Injection Length, which are 390; 30m/sec; 400K and 30 mm respectively*

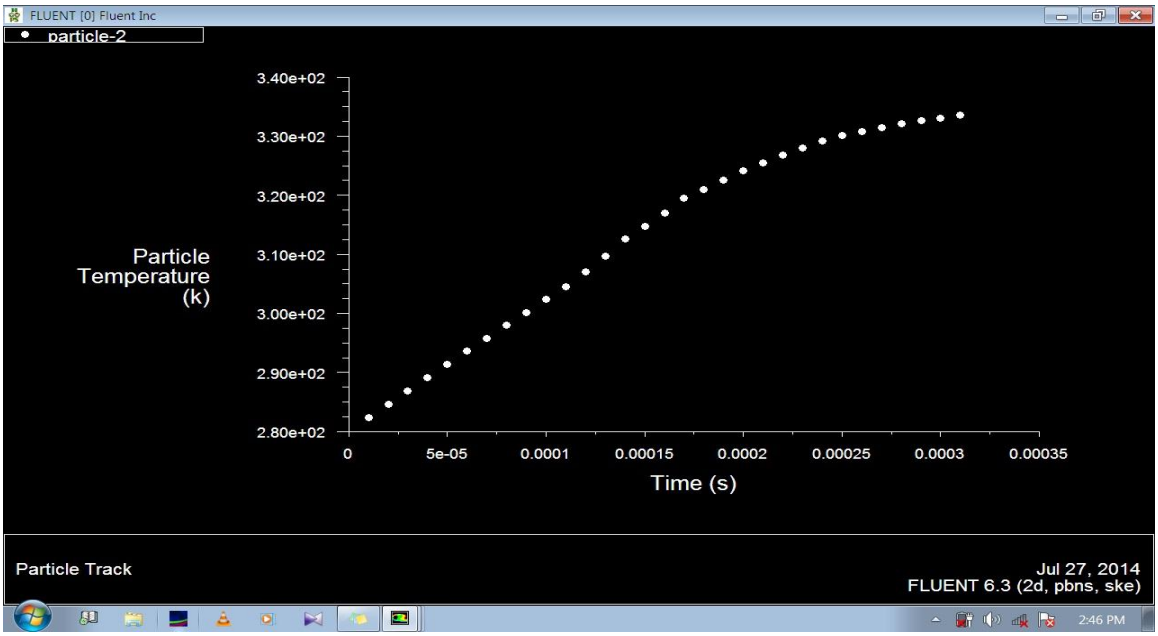

Fig.32b. *Temp. of Particle vs. Time for 30 mm Injector length*

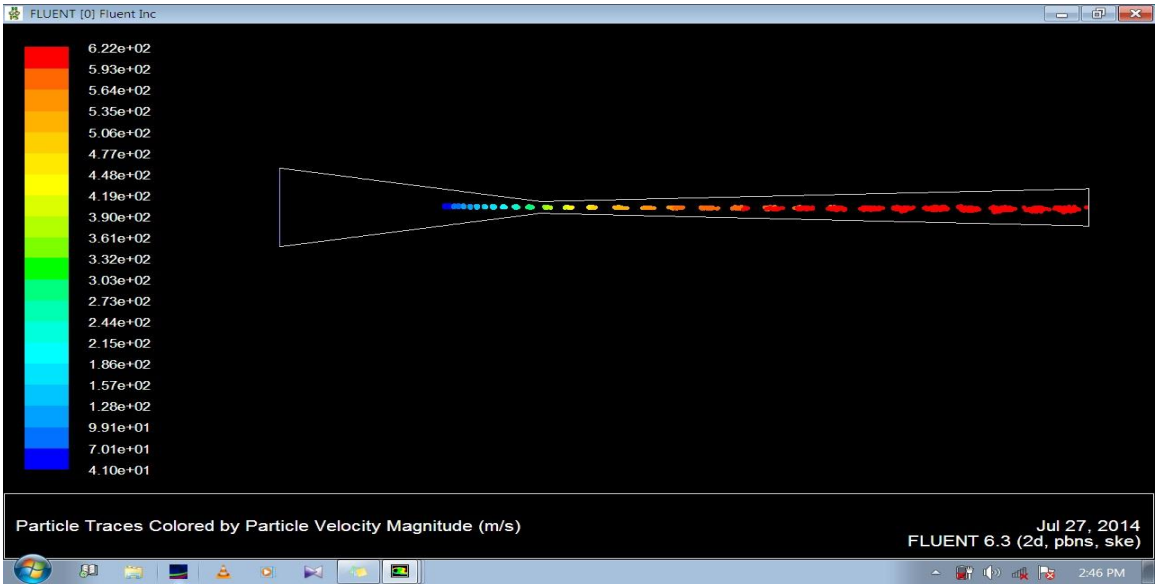

Fig.33a. *Velocity of Particle at outlet of nozzle for the fixed value of* $V_{air,\,in}$ *;*$V_{p,\,in}$ *;* $T_{air,\,in}$ and *Injection Length, which are 390; 30m/sec; 400K and 30 mm respectively*

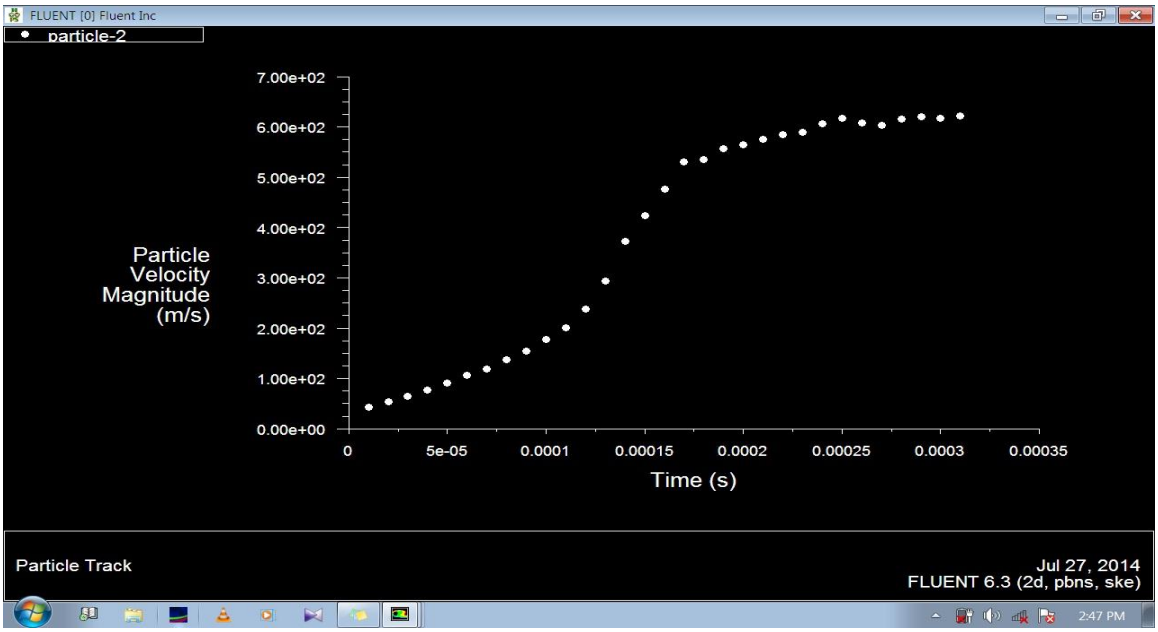

Fig.33b. *velocity of Particle vs. Time for 30 mm Injector length*

6.1.4. Simulation for 410 m/sec. at 10, 20 and 30 mm Injector length

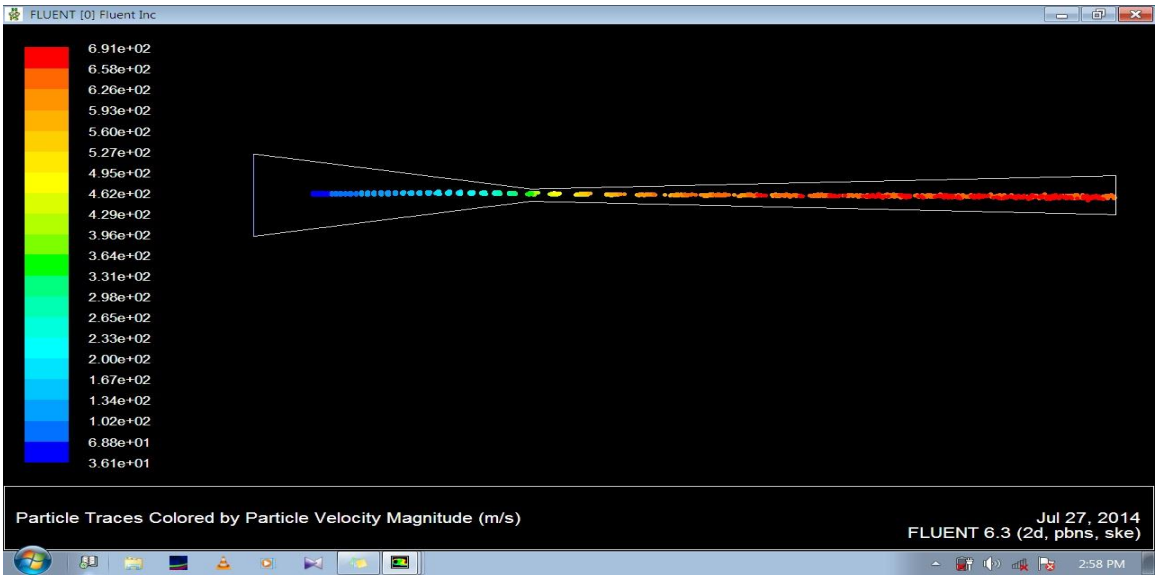

Fig.34a. *Velocity of Particle at outlet of nozzle for the fixed value of* $V_{air,\,in}$ *;*$V_{p,\,in}$ *;* $T_{air,\,in}$ and *Injection Length, which are 410; 30m/sec; 400K and 10 mm respectively*

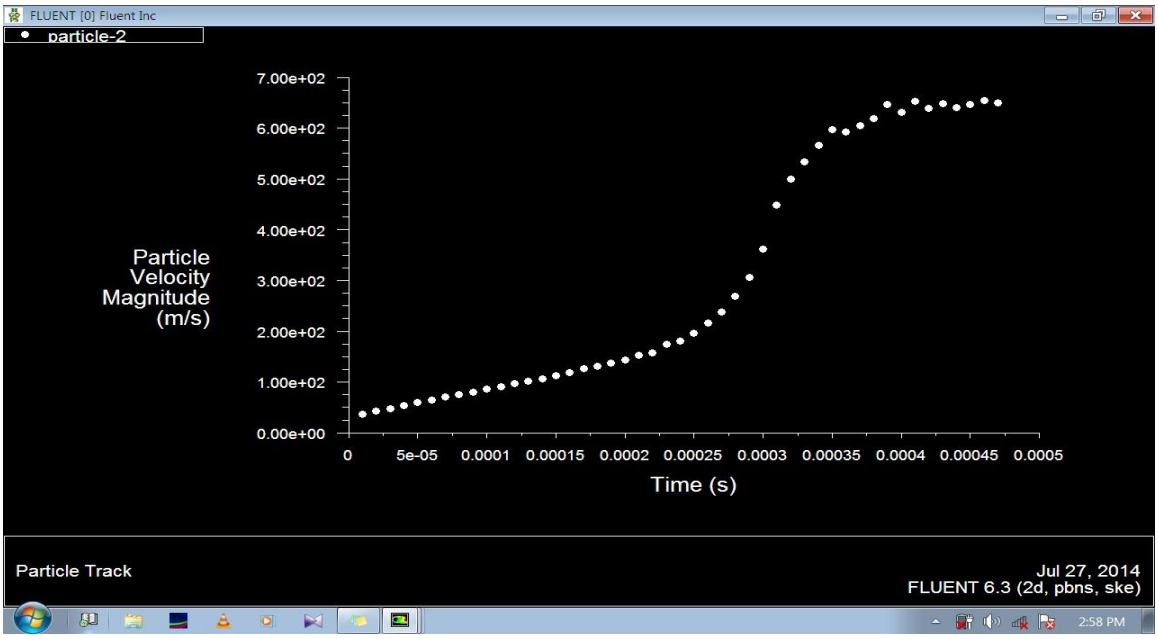

Fig.34b. *velocity of Particle at vs. Time for mm Injector length*

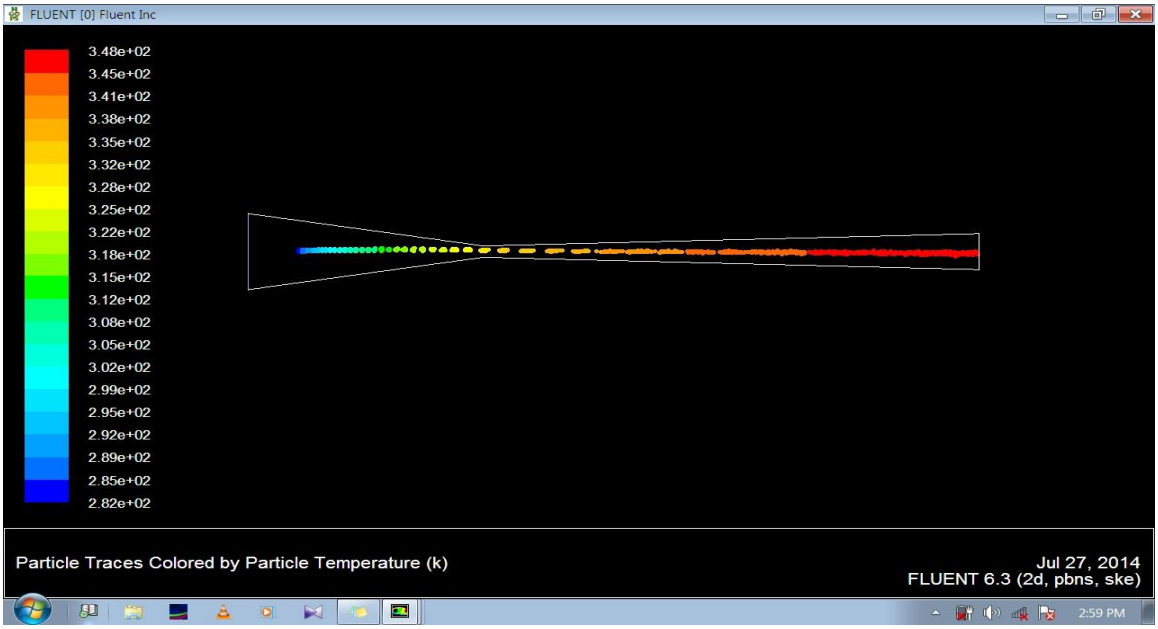

Fig.35a. *Temp. of Particle at outlet of nozzle for the fixed value of* $V_{air,\,in}$ *;* $V_{p,\,in}$ *;* $T_{air,\,in}$ and *Injection Length, which are 410; 30m/sec; 400K and 10 mm respectively*

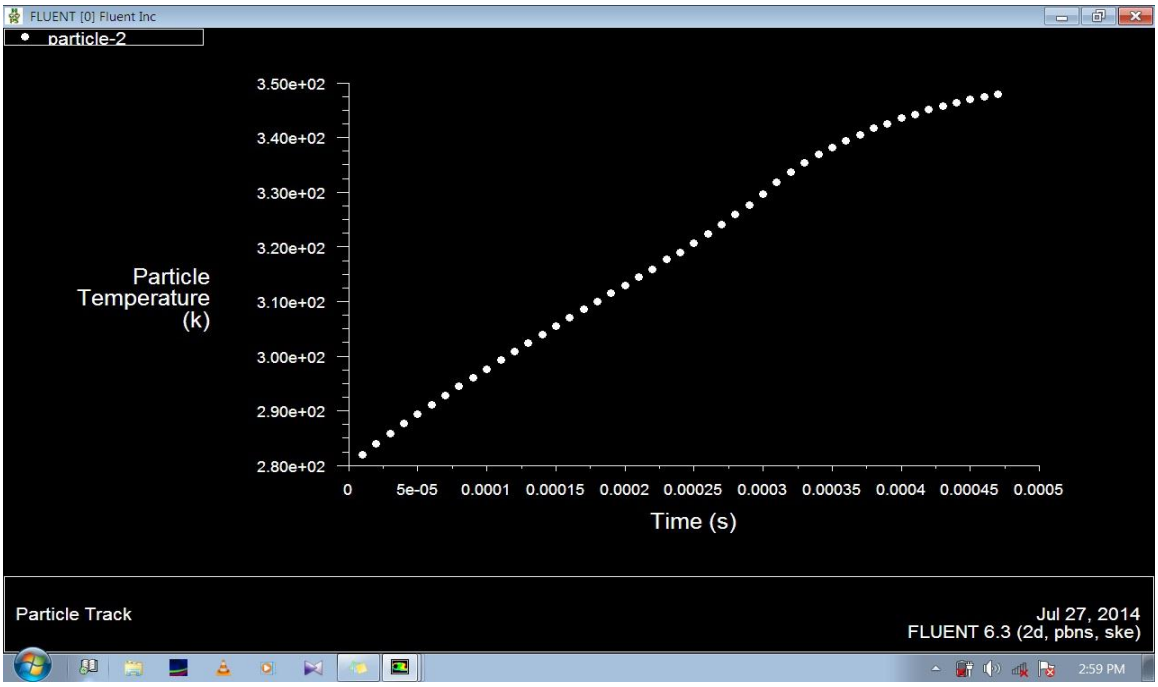

Fig.35b. *Temp. of Particle vs. Time for 10 mm Injector length*

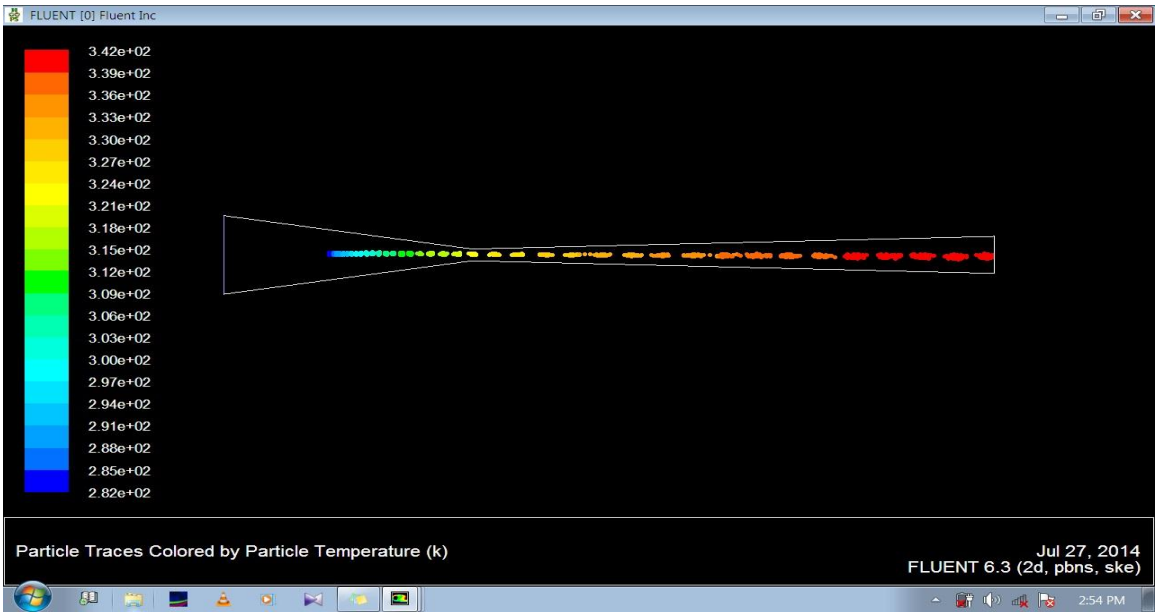

Fig.36a. *Temp. of Particle at outlet of nozzle for the fixed value of* $V_{air,\,in}$ *;*$V_{p,\,in}$ *;* $T_{air,\,in}$ *and Injection Length, which are 410; 30m/sec; 400K and 20 mm respectively*

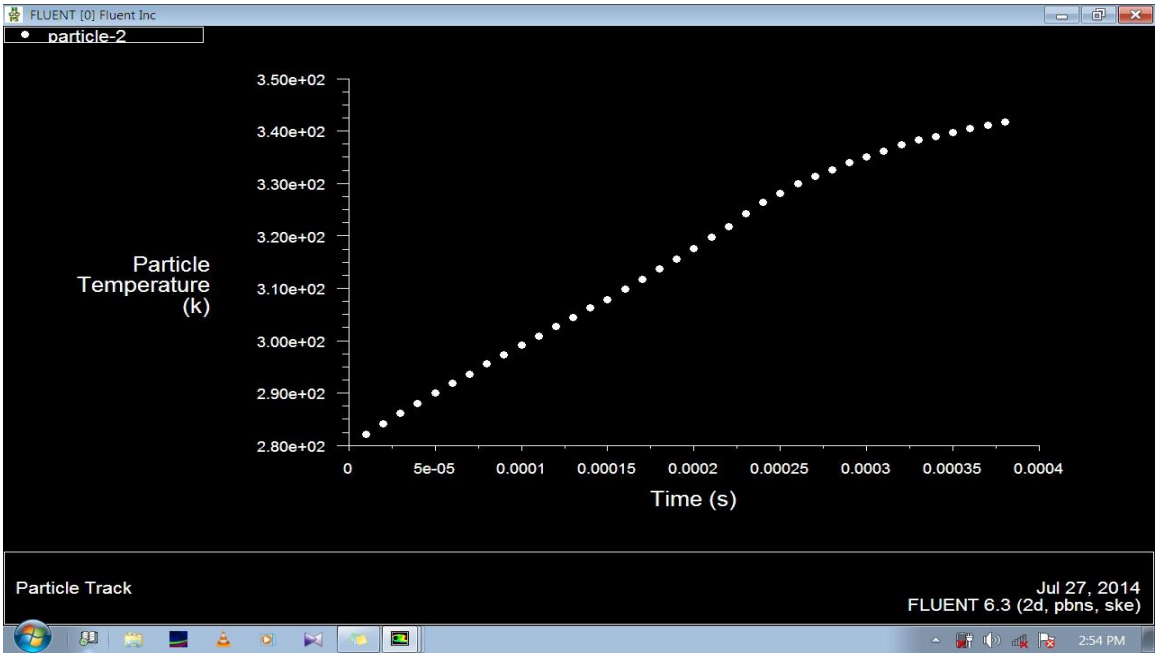

Fig.36b. *Temp. of Particle vs. Time for 10 mm Injector length*

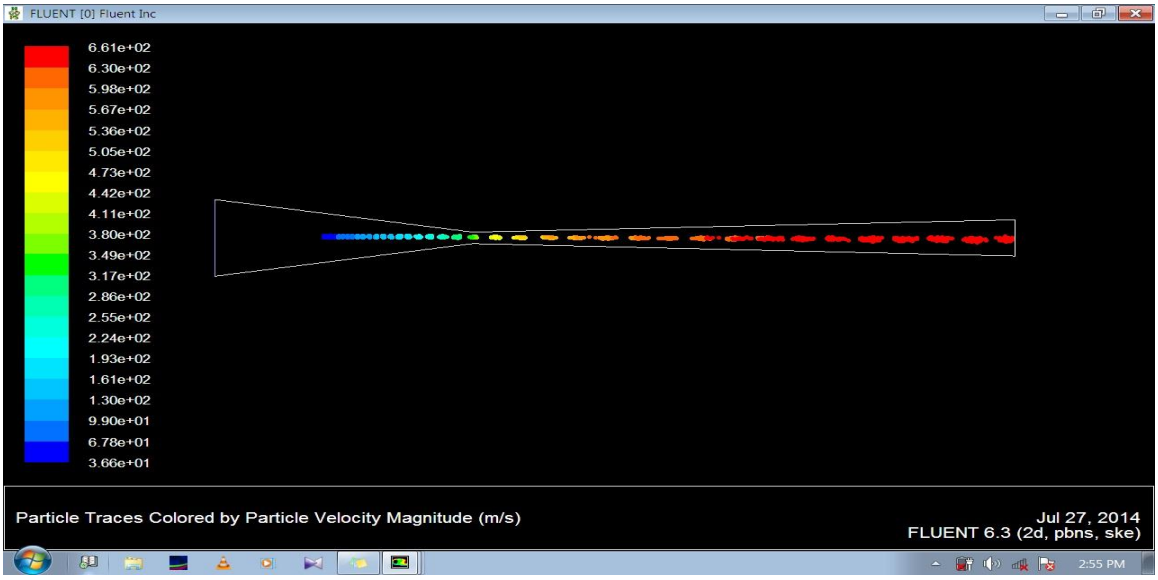

Fig.37a. *Velocity of Particle at outlet of nozzle for the fixed value of* $V_{air,\,in}$ *;*$V_{p,\,in}$ *;* $T_{air,\,in}$ and *Injection Length, which are 410; 30m/sec; 400K and 20 mm respectively.*

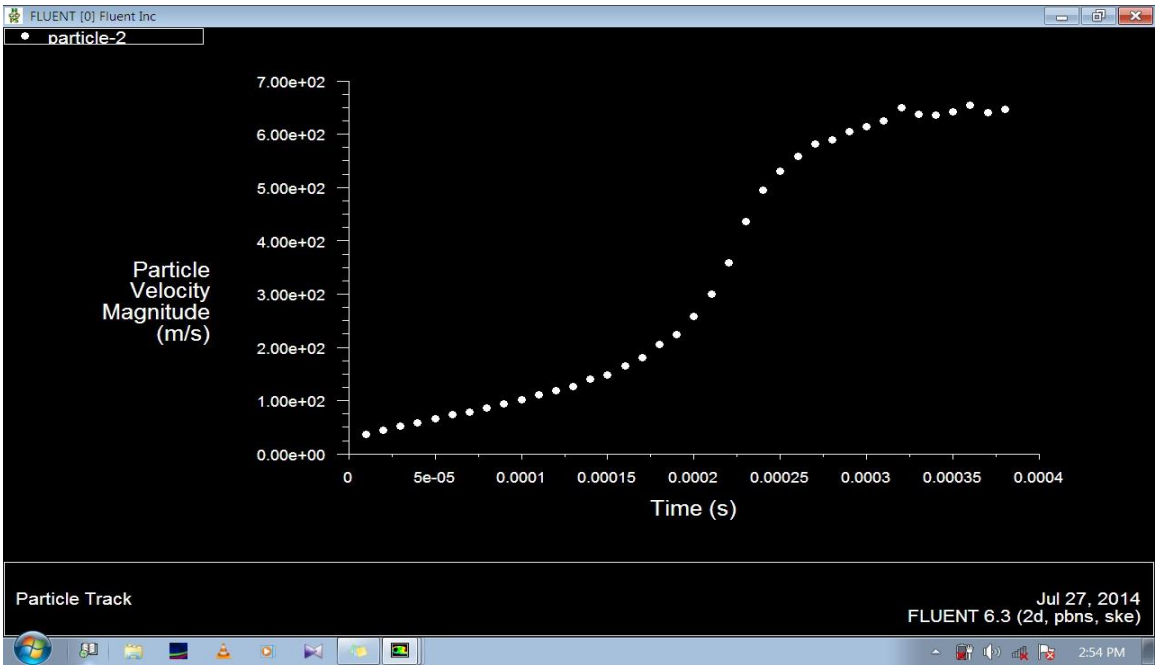

Fig.37b. *Velocity of Particle vs. Time for 10 mm Injector length*

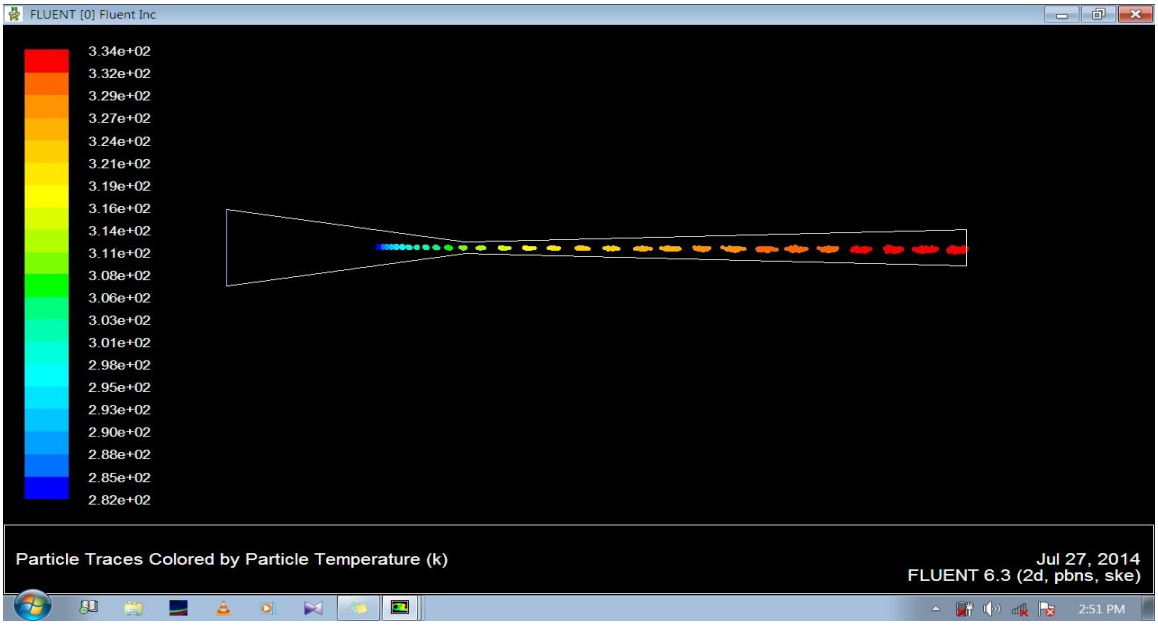

Fig.38a. *Temp. of Particle at outlet of nozzle for the fixed value of* $V_{air,\,in}$ *;* $V_{p,\,in}$ *;* $T_{air,\,in}$ and *Injection Length, which are 410; 30m/sec; 400K and 30 mm respectively.*

This is very clear by the all above Particle velocity Magnitude like Fig. 37 b that velocity of the particles is increase smoothly in approximately linear motion in the divergent section of the nozzle with respect to time and nozzle length while different length of injector to be used.

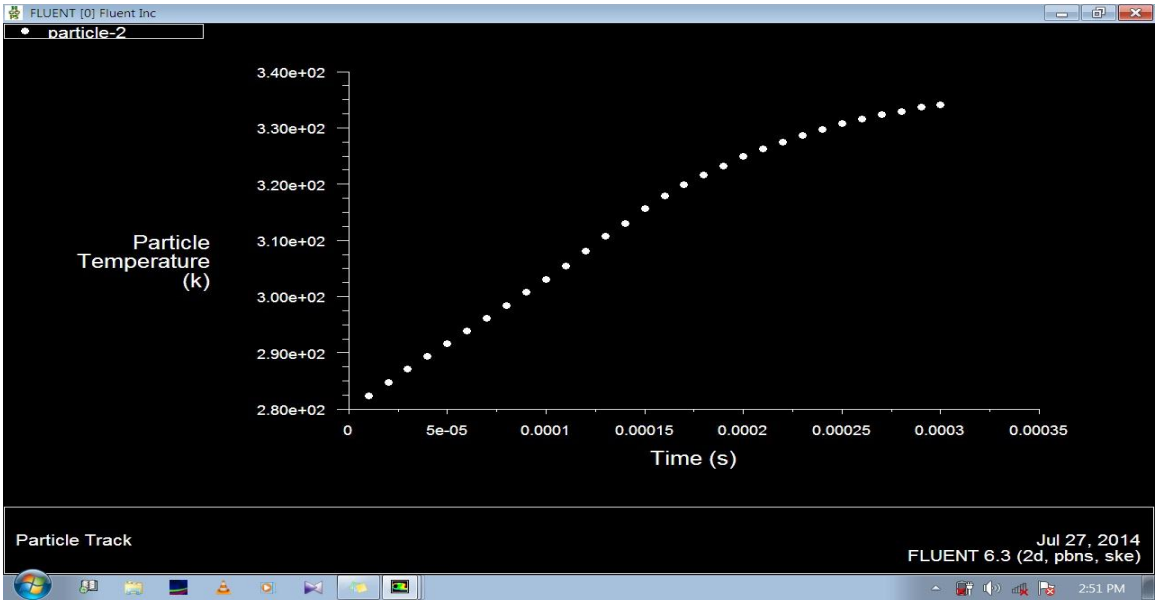

Fig.38b. *Temp. of Particle vs. Time for 30 mm Injector length.*

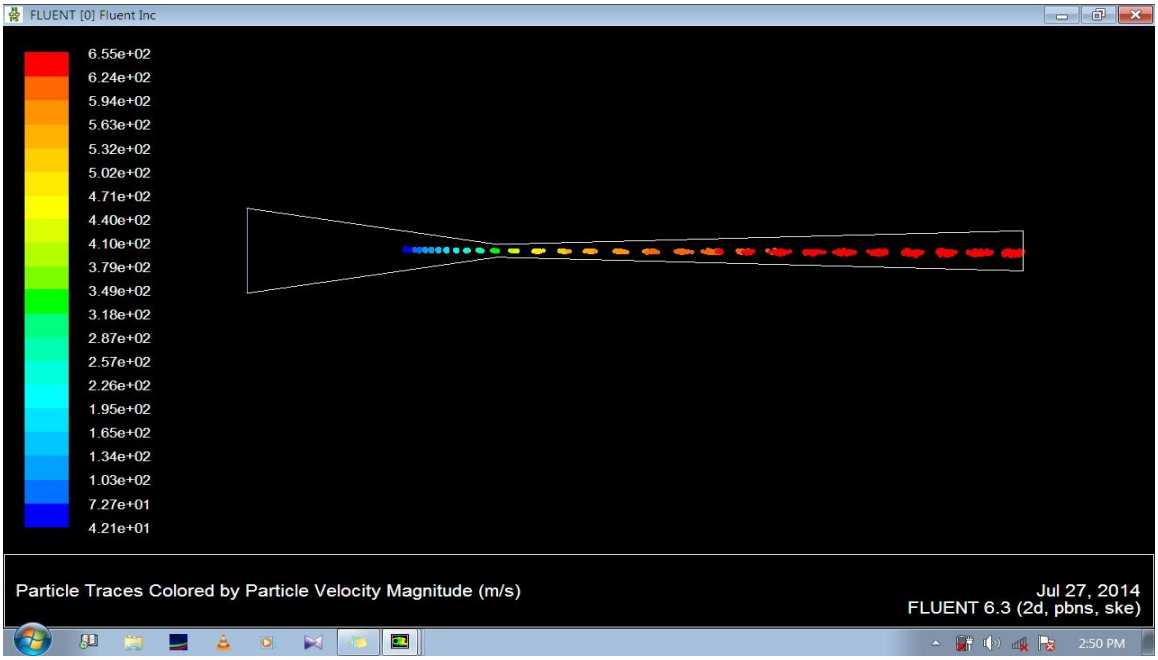

Fig.39a. *Velocity of Particle at outlet of nozzle for the fixed value of* $V_{air,\,in}$ *;*$V_{p,\,in}$ *;* $T_{air,\,in}$ and *Injection Length, which are 410; 30m/sec; 400K and 30 mm respectively.*

This is very clear by the particle velocity magnitude Fig.39.b. that velocity of the particles is increase very rapidly in the divergent section of the nozzle with respect to time and nozzle length while different length of injector to be used.

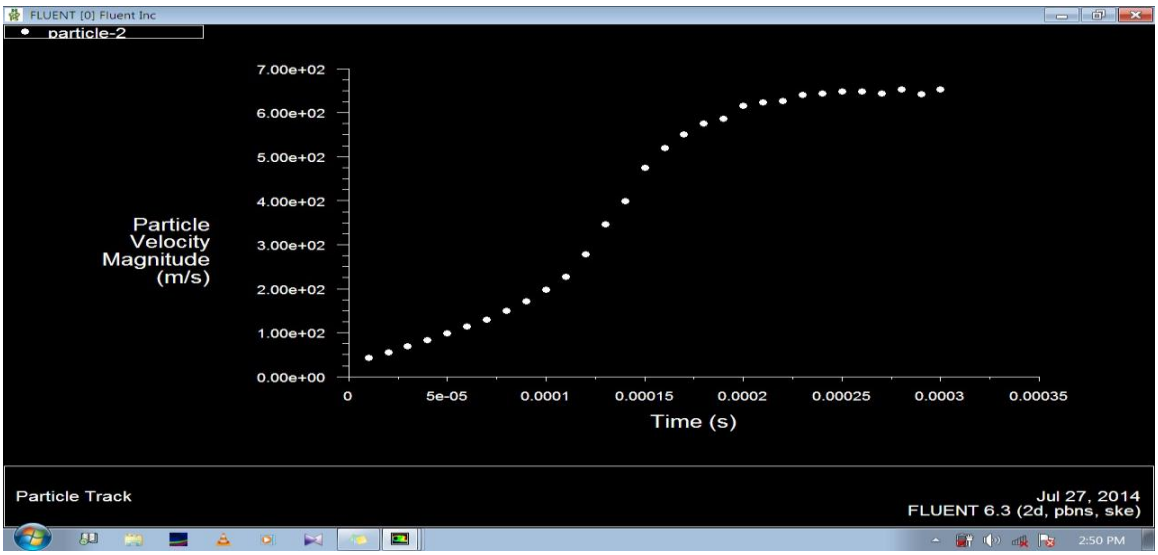

Fig.39b. *Velocity. of Particle vs. Time for 30 mm Injector length*

6.2. Simulation of nozzle at Fixed Inlet air velocity & constant Pressure 1.5

6.2.1. Simulation for 300 m/sec. at 10, 20 and 30 mm Injector length

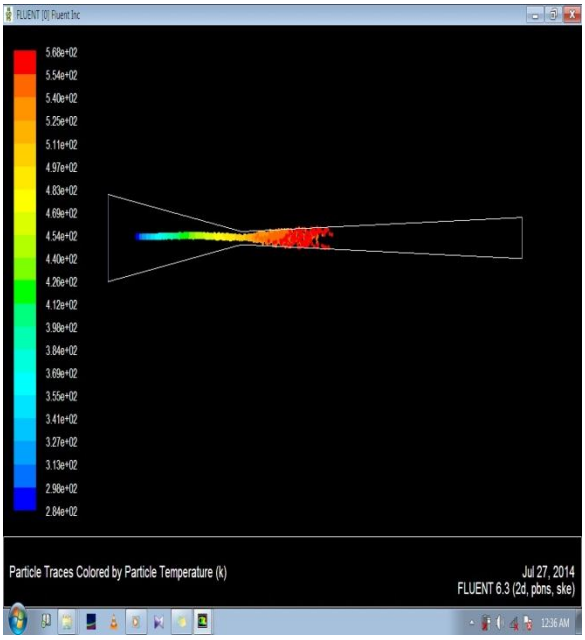

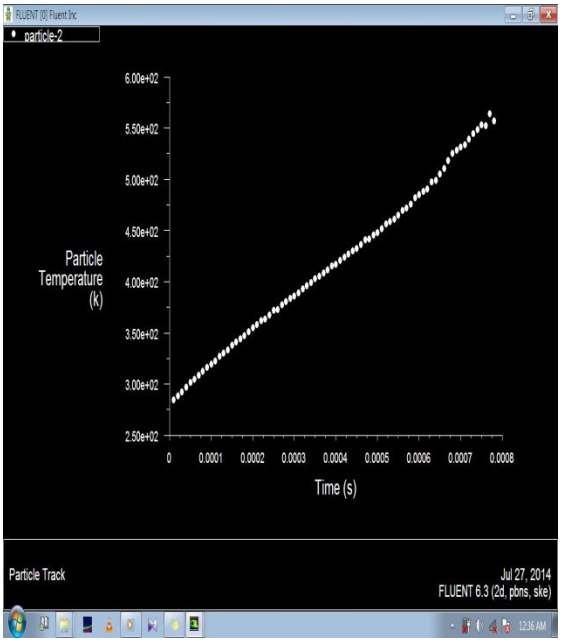

Fig.40a. & Fig.40b. *Temp. of Particle at outlet of nozzle for the fixed value of* $V_{air,\,in}$ *;*$V_{p,\,in}$ *;* $T_{air,\,in}$ and *Injection Length, which are 300; 20m/sec; 300K and 10 mm respectively.* **&** *show graph temp. of Particle vs. Time for 10 mm Injector length.*

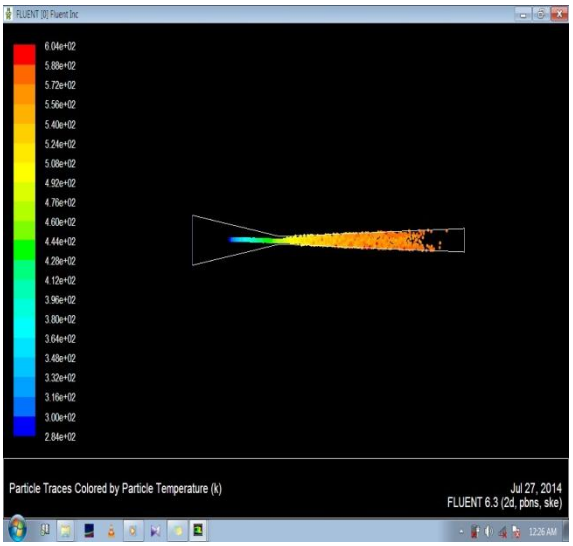

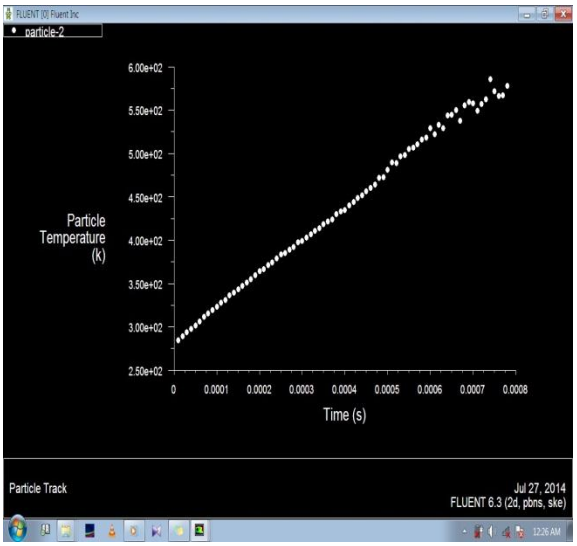

Fig.41a. & Fig.41b. *Temp. of Particle at outlet of nozzle for the fixed value of* $V_{air,\,in}$ *;*$V_{p,\,in}$ *;* $T_{air,\,in}$ and *Injection Length, which are 300; 20m/sec; 300K and 20 mm respectively.* **&** *show graph temp. of Particle vs. Time for 20 mm Injector length.*

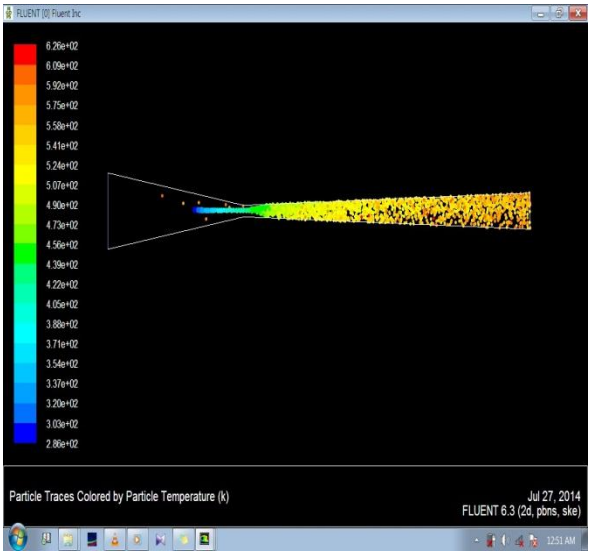

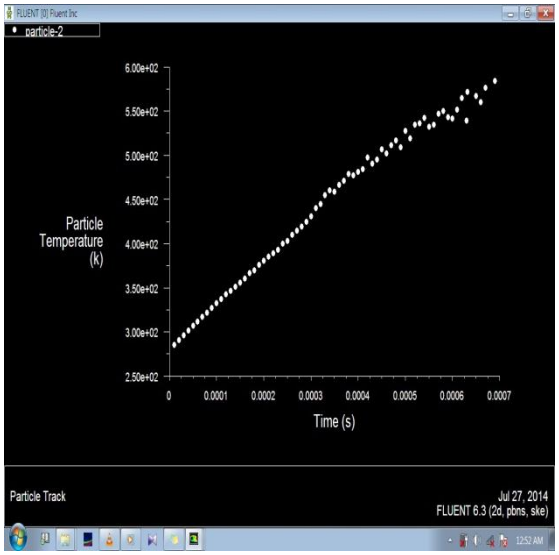

Fig.42a. & Fig.42b. *Temp. of Particle at outlet of nozzle for the fixed value of* $V_{air,\,in}$ *;* $V_{p,\,in}$ *;* $T_{air,\,in}$ and *Injection Length, which are 300; 20m/sec; 300K and 30 mm respectively.* **&** *show graph temp. of Particle vs. Time for 30 mm Injector length.*

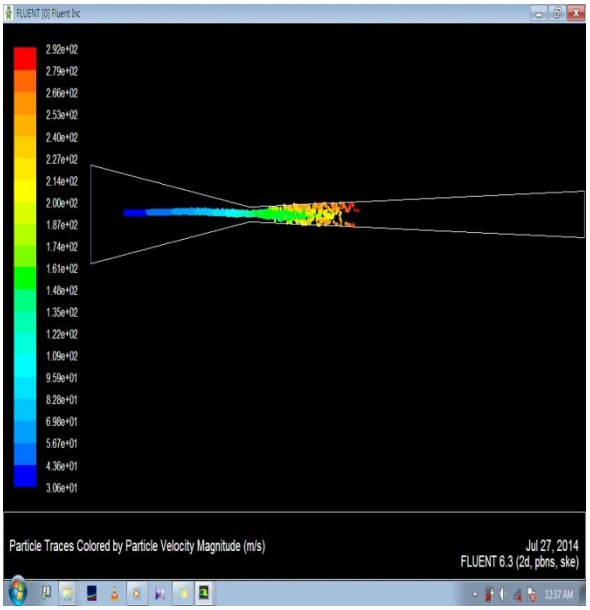

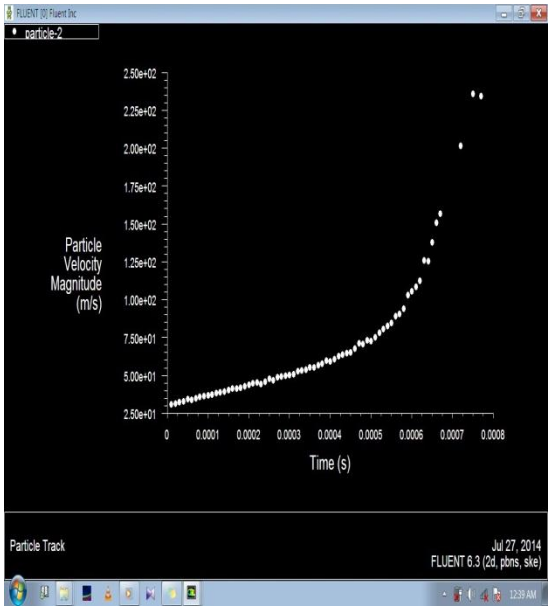

Fig.43a. & Fig.43b. *Velocity of Particle at outlet of nozzle for the fixed value of* $V_{air,\,in}$ *;* $V_{p,\,in}$ *;* $T_{air,\,in}$ and *Injection Length, which are 300; 20m/sec; 300K and 10 mm respectively.* **&** *show graph Velocity of Particle vs. Time for 10 mm Injector length.*

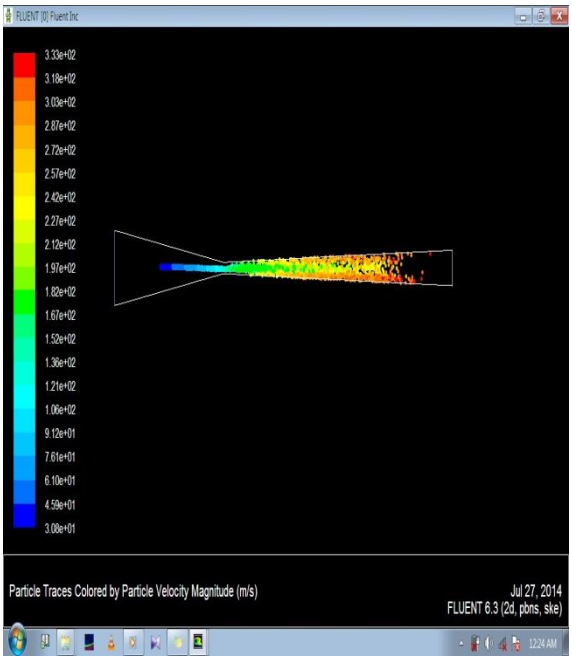

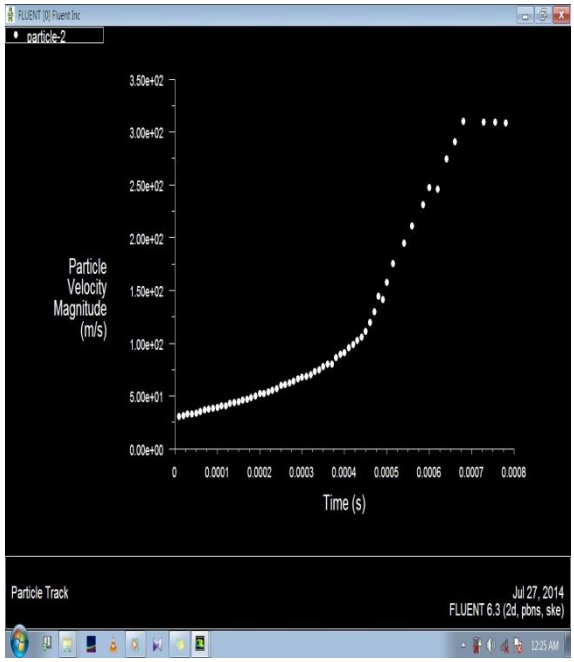

Fig.44a. & Fig.44b. *Velocity of Particle at outlet of nozzle for the fixed value of* $V_{air,\,in}$ *;* $V_{p,\,in}$ *;* $T_{air,\,in}$ and *Injection Length, which are 300; 20m/sec; 300K and 20 mm respectively.* **&** *show graph Velocity of Particle vs. Time for 20 mm Injector length.*

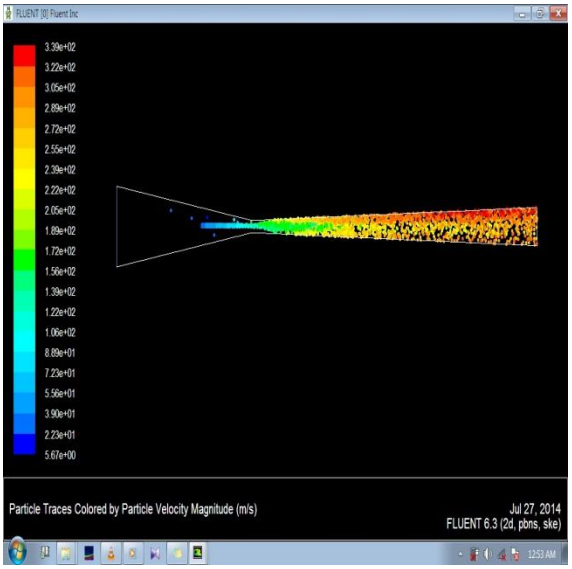

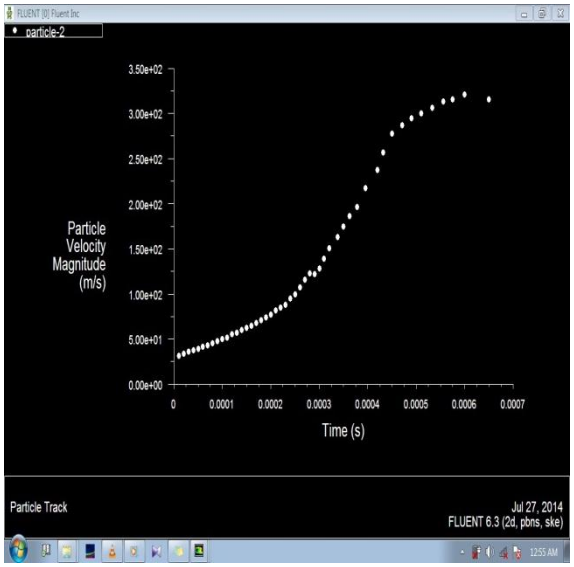

Fig.45a. & Fig.45b. *Velocity of Particle at outlet of nozzle for the fixed value of* $V_{air,\,in}$ *;*$V_{p,\,in}$ *;* $T_{air,\,in}$ and *Injection Length, which are 300; 20m/sec; 300K and 30 mm respectively.* **&** *show graph Velocity of Particle vs. Time for 30 mm Injector length.*

6.3. RESULT

CASE 1

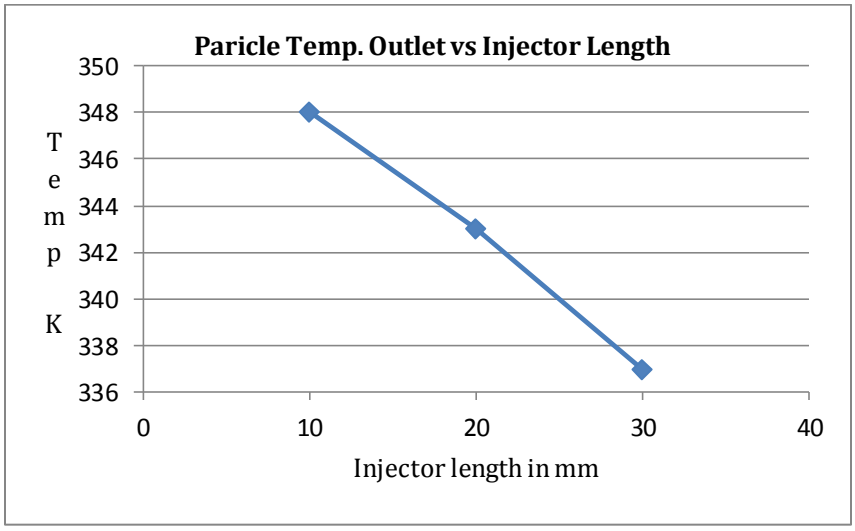

Fig. 46a.

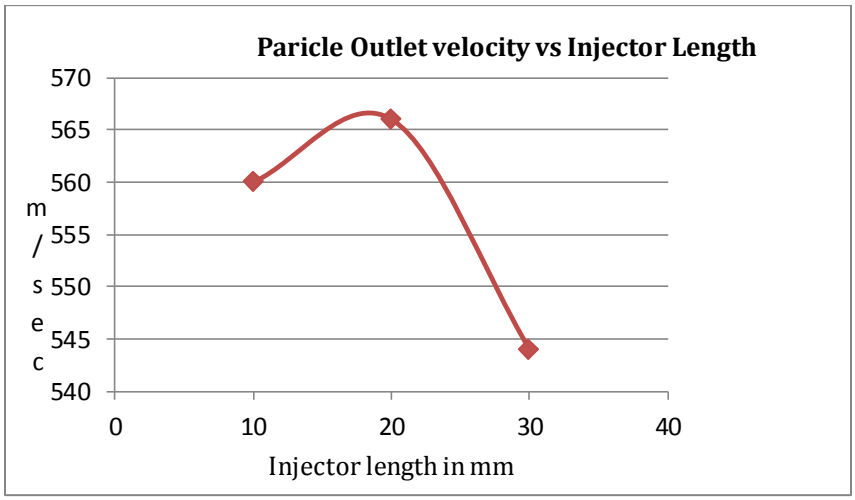

Fig. 46.b.

In that case 1 Vair inlet was taken 350 m/sec and length of injector are 10 mm, 20mm and 30mm respectively increase in the nozzle. The temperature was affected due to the variation of injector length and it was seen that as we have increase the injector length the temperature will be decrease.

In other hand the velocity of particles Firstly increase up to the 20 mm length of injector after that it will be decreases simultaneously.

CASE 2

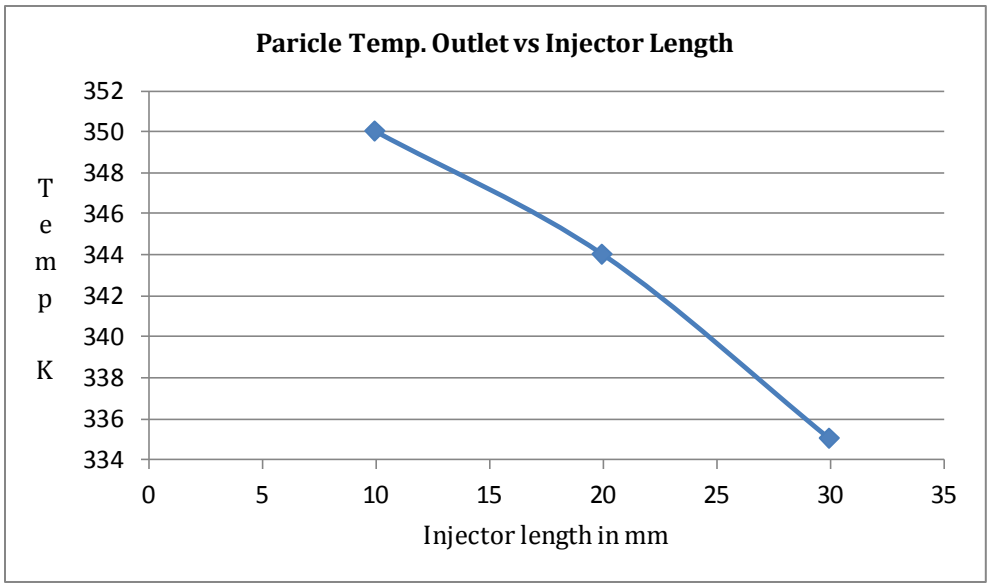

Fig. 47.a.

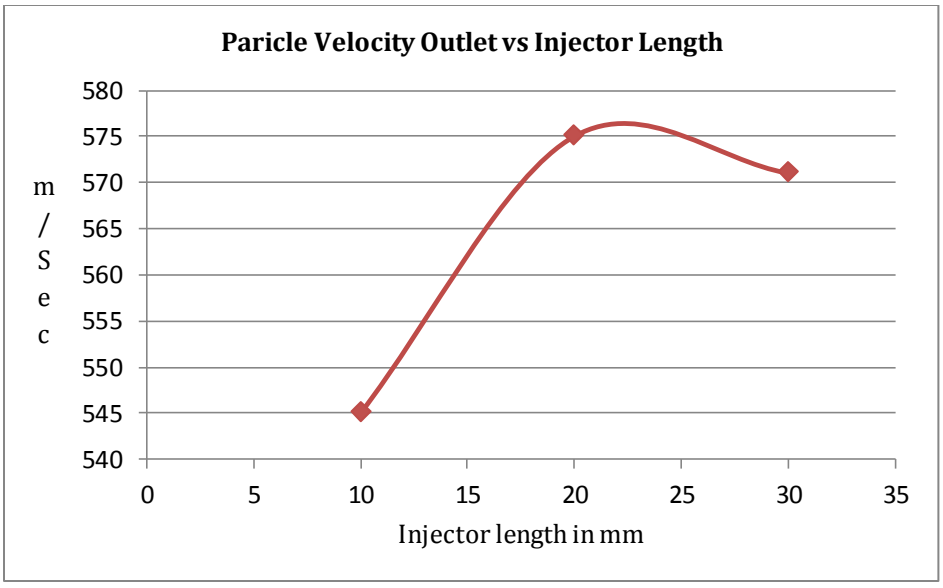

Fig. 47.b.

In that case 2 Vair inlet was taken 370 m/sec and length of injector are 10 mm, 20mm and 30mm respectively increase in the nozzle. The temperature was affected due to the variation of injector length and it was seen that as we have increase the injector length the temperature will be decrease.

In other hand the velocity of particles firstly increase up to the 20 mm length of injector after that it will be decreases simultaneously.

CASE 3

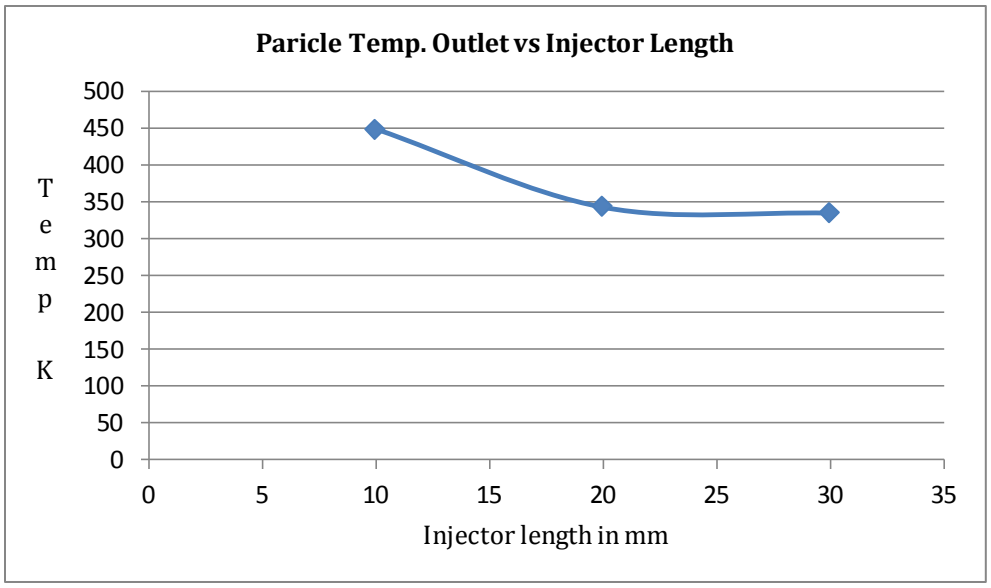

Fig. 48.a

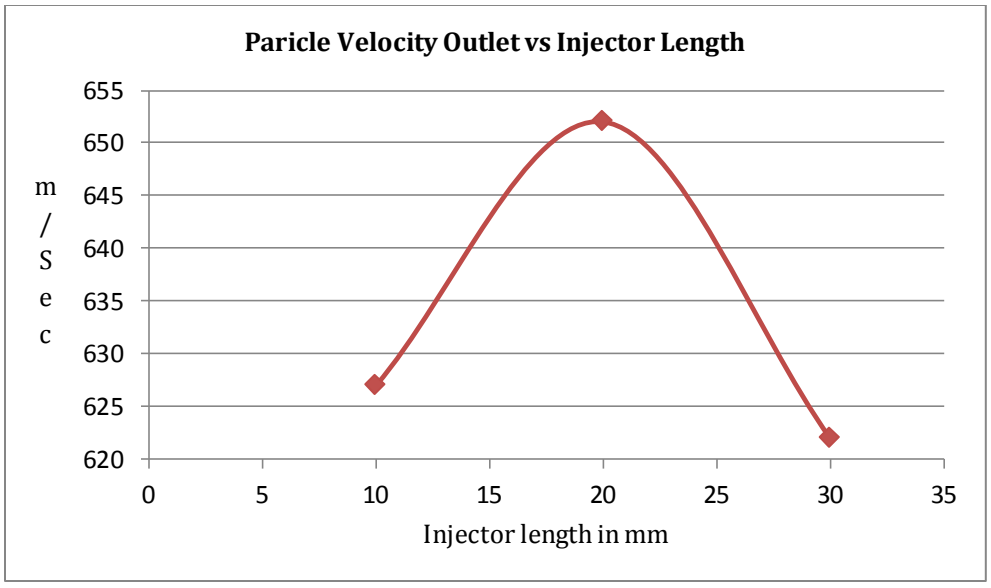

Fig. 48.b.

In that case 3 Vair inlet was taken 390 m/sec and length of injector are 10 mm, 20mm and 30mm respectively increase in the nozzle. The temperature was affected due to the variation of injector length and it was seen that as we have increase the injector length the temperature will be decrease.

In other hand the velocity of particles Firstly increase up to the 20 mm length of injector after that it will be decreases simultaneously.

CASE 4

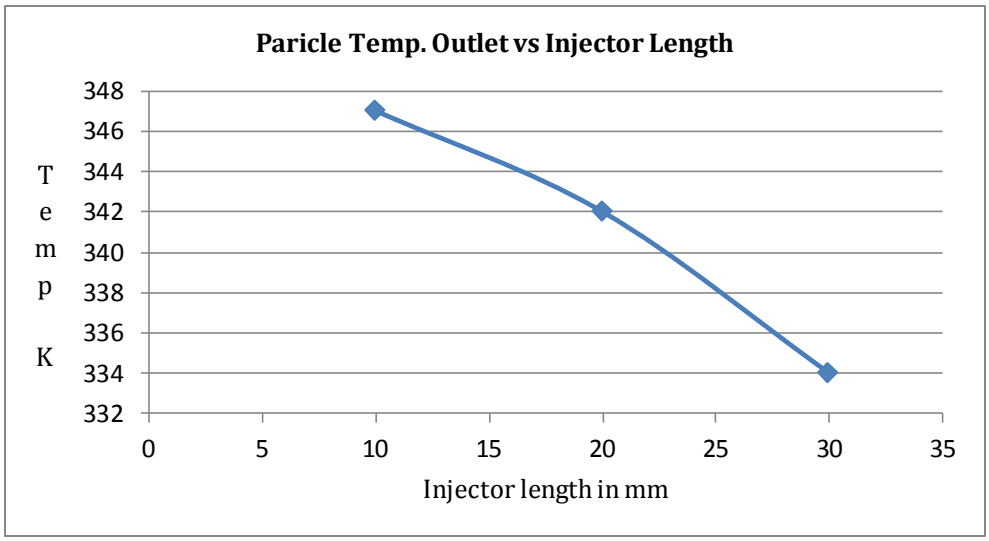

Fig.49.a.

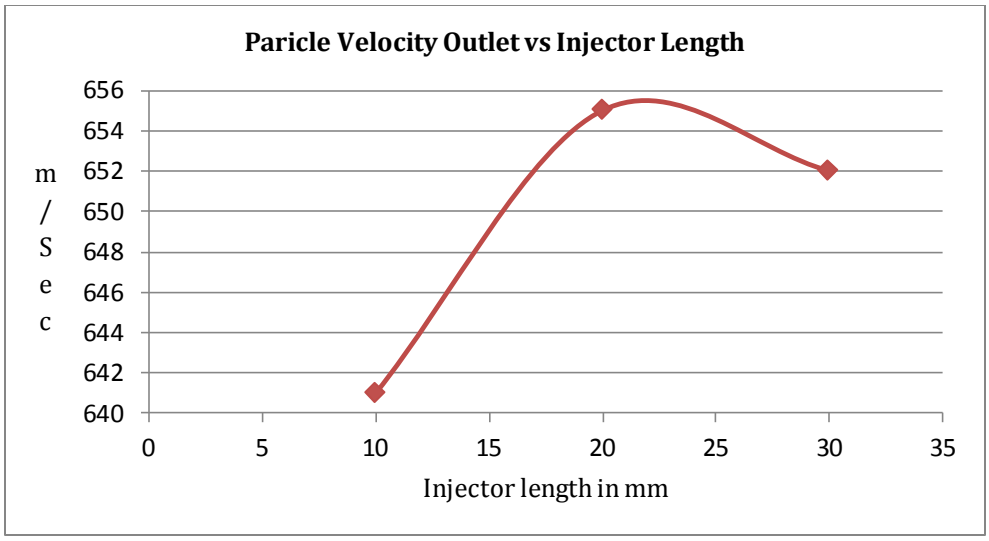

Fig.49.b.

In that case 4 Vair inlet was taken 410 m/sec and length of injector are 10 mm, 20mm and 30mm respectively increase in the nozzle. The temperature was affected due to the variation of injector length and it was seen that as we have increase the injector length the temperature will be decrease.

In other hand the velocity of particles firstly increase up to the 20 mm length of injector after that it will be decreases simultaneously.

That data from case 1 to case 4 have taken from the table 3.

CASE 5

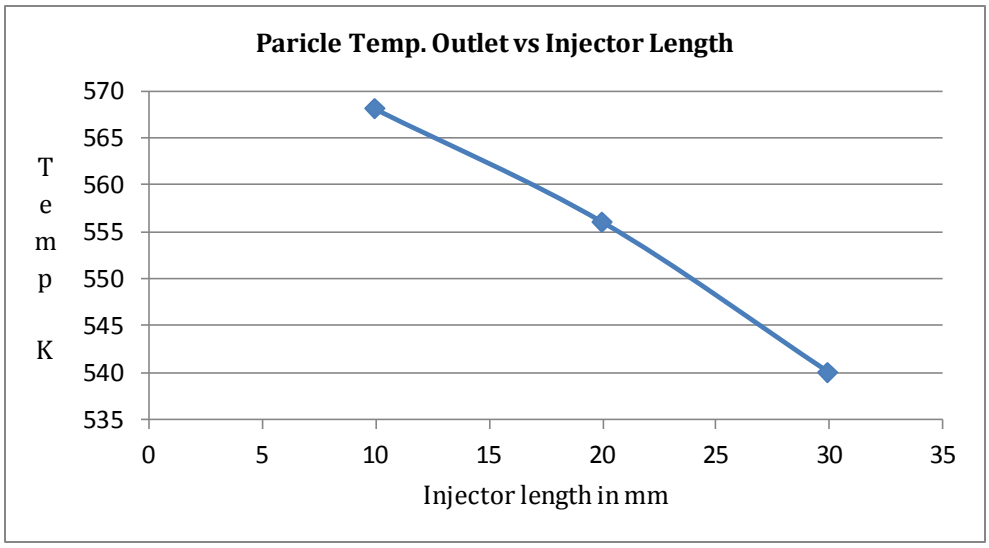

Fig.50.a.

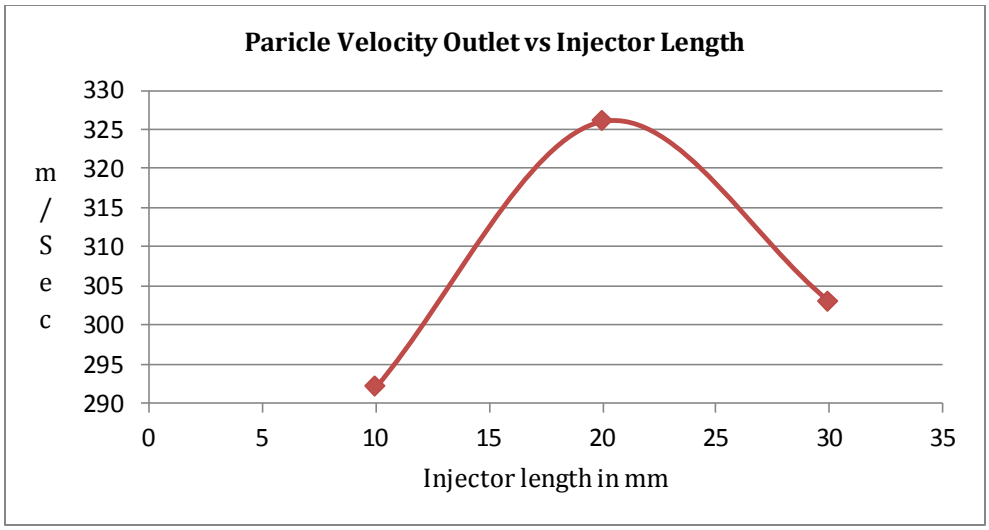

Fig.50.b.

In that case 5 Vair inlet was taken 300 m/sec at 1.5 MPa pressure and length of injector are 10 mm, 20mm and 30mm respectively increase in the nozzle. The temperature was affected due to the variation of injector length and it was seen that as we have increase the Injector length the temperature will be decrease.

In other hand the velocity of particles firstly increase up to the 20 mm length of injector after that it will be decreases simultaneously.

That data has taken from the table 4.

CASE 6

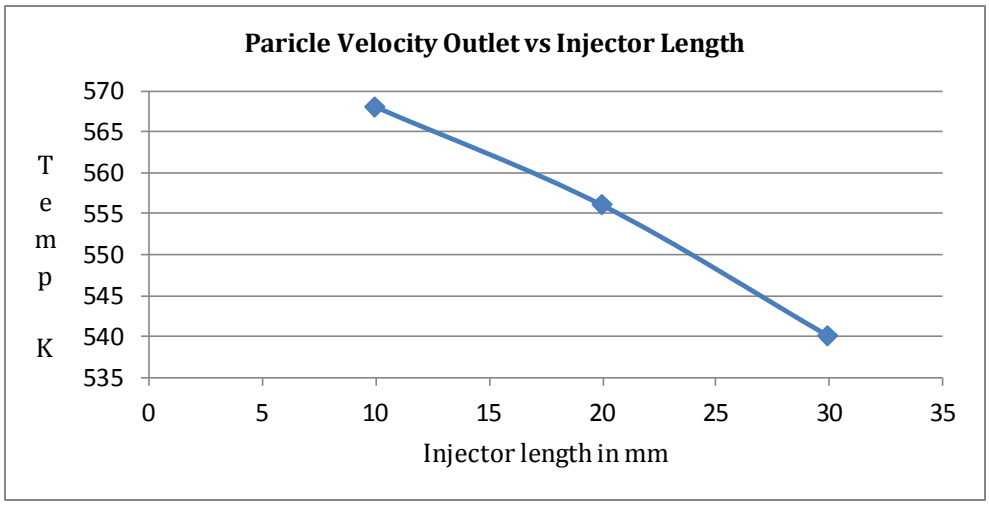

Fig.51.a.

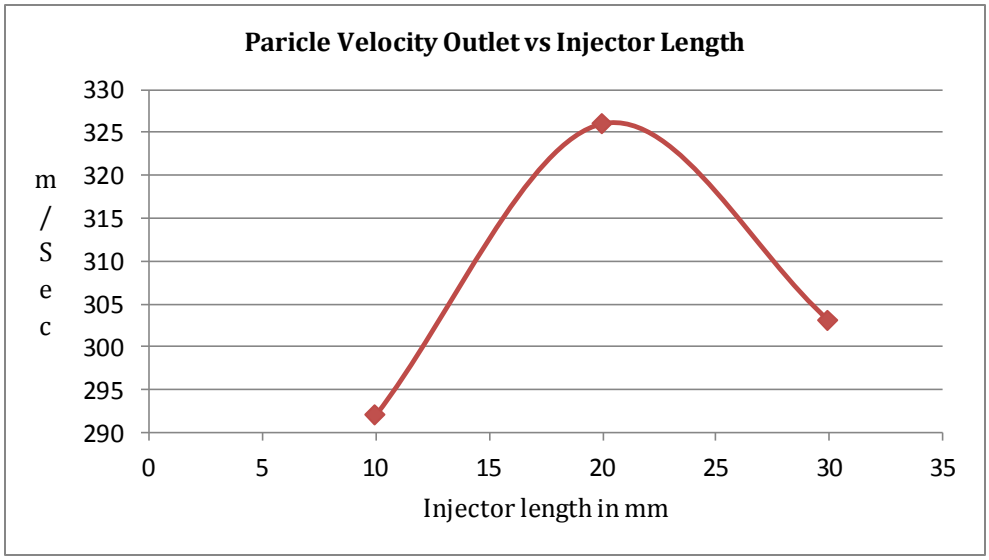

Fig.51.b.

In that case 6 Vair inlet was taken 300 m/sec at 2.5 MPa pressure and length of injector are 10 mm, 20mm and 30mm respectively increase in the nozzle. The temperature was affected due to the variation of injector length and it was seen that as we have increase the Injector length the temperature will be decrease.

In other hand the velocity of particles firstly increase up to the 20 mm length of injector after that it will be decreases simultaneously.

That data has taken from the table 4.

TABLE -4	At 1.5 Mpa					
S.NO	**Vair Inlet**	**V p Inlet (m/sec)**	**Tair inlet (K)**	**Vp outlet (m/sec)**	**Tp Outlet (K)**	**Injection Length (mm)**
1	300	20	300	292	568	10
2	300	20	300	326	556	20
3	300	20	300	303	540	30
At 2.5 Mpa						
4	300	30	300	349	580	10
5	300	30	300	390	578	20
6	300	30	300	360	563	25
7	300	30	300	328	548	30

6.4. CONCLUSIONS

1. This is very clear in the all cases (e.g. Case-1, case-2, case-3, case-4, case-5 and case-6) that the temperature of the particle is highest for the injector length 10mm and lowest for the injector length 30mm.
2. The result also shows that the temperature slightly decreases with increase the length of the injector.
3. While the temperature would be decrease linearly but this thing is not happened with the velocity of particles at the outlet of the nozzle. As well as the length of injector the velocity of particles firstly increase up to the 20mm length after that it would be decrease.
4. This is also found that the optimum result would be getting at the 20 mm length of injection.

REFRENCES

[1]. *H. Fukanuma, R. Huang* Simulation of Cold Spray Nozzle Accompanying a Water cooling Adjustment, *Plasma Giken Co., Saitama, Japan*.

[2]. *A. Papyinyrin* (2006), the Development of the Cold Spray Process, Cold Spray Technology (CST), USA.

[3]. *R. Ghelichi,* (2011) Numerical simulation of cold spray coating, Surface & Coatings Technology 205 5294–5301.

[4]. *Hamid Assadi, Frank Gartner,* (2002) Bonding mechanism in cold gas spraying, *Department of Materials Engineering, Tarbiat Modarres University*.

[5]. *R.C. Dykhuizen and M.F. Smith,* (1998), Gas Dynamic Principles of Cold Spray, JTTEE5 7:205-212 ASM International.

[6]. *Xiaoqian Guo, Yaran Niu, Liping Huang, Heng Ji, and Xuebin Zheng,* (2012), Microstructure and Tribological Property of TiC-Mo Composite Coating Prepared by Vacuum Plasma Spraying, ASM International.

[7]. *Sung-Hwan Jang1, Sung-Han Park1, Jeong-Whan Han1,Chang-Hee Lee2, Hyung-Jun Kim3,* (2006), Factors of Nozzle Design Affecting on Supersonic Flow in Cold Spray Process School of Materials Science and Engineering, Inha University, inchon, 402-751, South Korea, *Trans Tech Publications, Switzerland*.

[8]. *S.V. Klinkov, V.F. Kosarev, A.A. Sova, I. Smurov,* (2008) Deposition of multicomponent coatings by Cold Spray, Khristianovich Institute of Theoretical and Applied Mechanics SB RAS (ITAM SB RAS), 630090, Novosibirsk, Russia.

[9]. *Wen-Ya Li a,*, Hanlin Liao a, Hong-Tao Wang b, Chang-Jiu Li b, Ga Zhang a, C. Coddet*, (2005), Optimal design of a convergent-barrel cold spray nozzle by numerical method State Key Laboratory for Mechanical Behavior of Materials, School of Materials Science and Engineering.

[10]. *Wen-Ya Li *, Hanlin Liao, G. Douchy, C. Coddet*, (2006),Optimal design of a cold spray nozzle by numerical analysis of particle velocity and experimental validation with 316L stainless steel powder, LERMPS-UTBM, Site de Se´venans, 90010 Belfort Cedex, France.

[11]. *Surface Engineering, CSIR*- National Aerospace laboratories, Bangalore.

[12]. *T.Van steenkiste and J.R. Smith*, (2003) Evaluation of coating Produced via kinetic and Cold Spray Processes.

[13]. *V. Champagne*, (2007), the Cold Spray Materials Deposition Process, Fundamentals and Application, Wood head publishing.

[14]. FLUENT 6.3 *User's Guide*, Chapter Modeling Turbulence.

[15]. *A. Amsden, P. J. O'Rourke, and T. D. Butler. KIVA-2*: (1989), A Computer Program for Chemically Reactive Flows with Sprays. Technical Report LA-11560-MS, UC- 96, Los Alamos National Laboratory, Los Alamos, New Mexico.

[16]. *Qasim Murtaza, Joseph Stokes and Malika Ardhaoui*, (2012), Computational fluid dynamics analysis of the production of bio-thermal spray hydroxyapatite powders, Int. J. Computational Materials Science and Surface Engineering, Vol. 5, No. 1, Materials Processing Research Centre (MPRC), Dublin City University

[17]. *Rajesh Bhaskaran, Lance Collins*, Introduction to CFD Basics.

[18]. *J. M. McDonough* (2007), LECTURES in COMPUTATIONAL FLUID DYNAMICS of INCOMPRESSIBLE FLOW: Mathematics, Algorithms and Implementation, Departments of Mechanical Engineering and Mathematics, University of Kentucky.

[19]. *Lecture 4*(2006), Computational engineering Introduction to numerical methods, FVM.